Impact of Synthesis Methods and Oxidizing Agents on the Catalytic Performance of Various Catalysts in the Oxidative Coupling of Methane

vorgelegt von
Master of Science (Chemie)
Kirsten Langfeld
Cottbus

Von der Fakultät II – Mathematik und Naturwissenschaften
der Technischen Universität Berlin
zur Erlangung des akademischen Grades

Doktor der Naturwissenschaften
Dr. rer. nat.

vorgelegte Dissertation

Promotionsausschuss:

Vorsitzender:	Prof. Dr. Regine von Klitzing, TU Berlin
Berichter:	Prof. Dr. Reinhard Schomäcker, TU Berlin
Berichter:	Prof. Dr. Manfred Baerns, TU Berlin
Berichter:	PD Dr. Evgenii V. Kondratenko, LIKAT, Rostock

Tag der wissenschaftlichen Aussprache: 05.03.2012

Berlin 2012
D 83

Danksagung

Die vorliegende Arbeit wurde in der Zeit von Oktober 2007 bis Dezember 2011 im Institut für Chemie der Technischen Universität Berlin angefertigt. Ein Teil der Katalyse-Experimentalreihen wurde im Leibniz-Institut für Katalyse (LIKAT) in Rostock durchgeführt. Die Materialcharakterisierungen wurden im ZELMI der TU Berlin und im Fritz-Haber-Institut (FHI) der Max-Planck-Gesellschaft in Dahlem vorgenommen.

Mein besonderer Dank gilt Herrn Prof. Dr. Reinhard Schomäcker für die Betreuung der Arbeit. Ebenfalls möchte ich Herrn Dr. Evgenii Kondratenko für die Betreuung der Experimente im LIKAT und die wissenschaftlichen Gespräche danken. Bei Herrn Prof. Dr. Manfred Baerns möchte ich mich für die Übernahme der dritten Begutachtung danken.

Desweiteren möchte ich mich bei Claudia Berger-Karin bedanken, die mich tatkräftig beim Durchführen der Experimentalreihen im LIKAT unterstützt hat. Mein Dank gilt ebenfalls Verena Strempel und René Marschner, die mich zeitweise im Labor unterstützt haben. Gisela Weinberg, Dr. Oliver Görke und Dr. Benjamin Frank danke ich für die Unterstützung bei der Charakterisierung meiner Materialien. Für die Unterstützung im Labor und bei Computer-Fragen möchte ich mich herzlich bei Gabriele Vetter und Torsten Otremba bedanken.

Mein weiterer Dank gilt der gesamten Arbeitsgruppe von Herrn Prof. Dr. Schomäcker, die mir stets eine angenehme und produktive Arbeitsatmosphäre ermöglichte.

Mein besonderer Dank gilt meinen Eltern, die mich stets unterstützt und an mich geglaubt haben. Auch meinen Schwiegereltern möchte ich für ihre Unterstützung danken.

Benjamin und Julian Erik danke ich für die Bereicherung meiner Zeit abseits der Arbeit.

Meinen Eltern, Benjamin und Julian

Zusammenfassung

Ziel der vorliegenden Arbeit war es, über templatgestützte Synthesewege Katalysatoren für die Oxidative Kupplung von Methan (OCM) herzustellen und an diesen den Einsatz alternativer Oxidationsmittel für die OCM zu testen. Ausgehend von Mischoxiden des Perowskit-Typs wurde $SrCoO_x$ als Basissystem gewählt und auf verschiedenen Synthesewegen hergestellt. Die Synthese unter Zuhilfenahme von Mikroemulsionen wurde hier mit der Co-Fällung und der Sol-Gel Methode verglichen. Erstere führt zu niedrigeren Phasentransformationstemperaturen und daraus resultierend kleineren Partikelgrößen und höheren spezifischen Oberflächen. In der OCM mit Sauerstoff zeigten jedoch alle Proben eine hohe Verbrennungsaktivität und geringe C_2-Selektivtität, wie aus der Literatur bekannt. Dennoch konnte gezeigt werden, dass die Mikroemulsionsroute zu Katalysatoren mit höherer Aktivität und C_2-Selektivität führen. Als nächstes wurde $SrCoO_x$ über Cellulose-Templatierung hergestellt. Weitere Perowskit-Zusammensetzungen wurden durch schrittweise Substitution der A- bzw. B-Position im $SrCoO_x$-Perowskitgitter vorrangig durch Lanthanoide und seltene Erden synthetisiert. Der Test der Katalysatoren in der OCM zeigte, dass ein Austausch mit La, Nd, Pr und Sm an der A-Position, aber auch von Mn und Fe an der B-Position zu höheren Aktivitäten in der OCM mit O_2 führten. Der Austausch von Sr mit Ca und Ba bzw. der Austausch von Co mit Mo und Cr wirkten sich hingegen negativ auf die Aktivität aus. Leider konnte keine Korrelation mittels Materialanalysen gefunden werden, die diese Trends erklären würden. Die Materialien, die mittels Cellulose-Templatierung hergestellt wurden, wiesen zum Teil hohe spezifische Oberflächen auf und waren sehr aktiv in der größtenteils unselektiven Methanaktivierung. Ein aussagekräftiger Vergleich der erhaltenen Leistungsdaten der Katalysatoren mit den in der Literatur publizierten Werten ist aufgrund variierender Katalysebedingungen generell schwer. Daher wurden aus den vorangegangenen Arbeitspaketen und aus der Literatur die aktivsten und selektivsten Katalysatoren für die OCM herausgesucht. Diese Materialien wurden in der OCM mit O_2, aber auch mit CO_2 und N_2O untersucht und ausgewählte Katalysatoren anschließend detaillierter analysiert. Leider zeigte keiner der Katalysatoren eine nennenswerte Aktivität in der OCM mit CO_2. Dafür stellte sich N_2O als ein sehr gutes alternatives Oxidationsmittel heraus, dass mit fast allen Katalysatoren zu leicht verringerten Umsätzen, aber dafür tendenziell zu höheren C_2-Selektivitäten führt. Allerdings zeigt sich, dass kaum ein Material über 40 h in der Katalyse strukturell stabil ist, was den anhaltenden Forschungsbedarf aufzeigt.

Abstract

Aim of the present work was to prepare catalysts via template-assisted synthesis routes for the Oxidative Coupling of Methane (OCM) and to use these materials for the testing of alternative oxidizing agents for the OCM.

Based on mixed oxides of the perovskite-type, $SrCoO_x$ was chosen as basis system and synthesized with different methods. The microemulsion-assisted synthesis was compared here with the co-precipitation and the sol-gel method. The first leads to lower phase transformation temperatures which results in smaller particle sizes and higher specific surface areas. However, in the OCM with oxygen all samples show a high combustion activity and small C_2-selectivities as described in literature. Anyhow, it could be shown that the microemulsion method produces catalysts with higher activities and C_2-selectivities.

Next, $SrCoO_x$ was synthesized using cellulose-templates. Further perovskite compositions were prepared via stepwise substitution in the A- or B-position in the $SrCoO_x$ lattice, prior by lanthanides and rare earth metals. The test in the OCM showed that an exchange with La, Nd, Pr and Sm at the A-position, but also of Mn and Fe at the B-position leads to higher activities in the OCM with O_2. The exchange of Sr with Ca and Ba or the exchange of Co with Mo and Cr affects the activities negatively. Unfortunately, no correlations were found by material analysis methods, which could explain these trends. The materials synthesized by cellulose-templates partially possess high specific surface areas and are very active in the mostly unselective methane activation.

A significant comparison of the performance data of the catalysts with those data published in literature is generally difficult due to the varying catalysis conditions. Therefore the most active and selective catalysts for the OCM from former work packages and from literature were selected. These materials were examined in the OCM with O_2, but also with CO_2 and N_2O and selected catalysts were subjected to a detailed analysis. Unfortunately, none of the catalysts shows a significant activity in the OCM with CO_2. Instead N_2O turns out to be a good alternative oxidizing agent, which produces higher C_2-selectivites at slightly reduced conversions over almost all catalysts. The fact that none of the materials was structurally stable over more than 40 h on-stream under varying reaction conditions shows the persistent research demand.

1 Motivation

The activation of aliphatic C-H bonds using heterogeneous oxidation catalysis is one of the most demanding challenges in the wide field of catalysis research. In contrast to the relatively stable saturated hydrocarbons the product molecules possess functional groups like oxygen atoms or C-C-multiple bonds, which are usually very active towards oxidation. The interaction of such activated functional groups with excess gas phase oxygen likely initiates the deep oxidation. Therefore a sufficient product selectivity, which would be relevant for an industrial application, is obtained only in a few cases. Nevertheless, a high research effort is raised to chemically convert C_1–C_4-alkanes, which are components in natural gas, in industrially valuable amounts over short process pathways. Butane can be easily converted into maleic anhydride, which is at the moment the only industrially realized process of alkane activation. The yields of the target products in the reactions of propane to acrylic acid or of ethane to ethylene (or acetic acid) are in the academic research still too low regarding the economic reasonability. But with respect to the steady increase of the oil and gas prices an industrial realization seems to be only a doubt of time.

About 600 million tons of methane are annually emitted to the earth atmosphere [1]. Approximately 70.000 to 181.000 billion m^3 natural gas, whose main component is methane, are stored on earth [2]. In addition methane is stored in huge amounts at the sea ground in the form of methane hydrate. Thus it would be very reasonable to convert the methane into higher valued products. Yet it is converted mainly to synthesis gas via the energy-intensive steam reforming and the synthesis gas is afterwards used for numerous processes. An interesting and promising direct process would be the oxidative coupling of methane (OCM) to ethane and ethylene. In 2008 the worldwide ethylene turn-over amounted to more than 160 billion US $. The ethylene in turn is mainly converted into HDPE (high density poly ethylene), followed by LLDPE and LDPE (low density poly ethylene). 11% of the world wide ethylene demand is for ethylene oxide.

Since the first reports dealing with the OCM reaction of Keller and Bhasin in 1982 [3] intensive studies examined optimized catalyst systems and process conditions which lead to higher but still not industrially relevant ethylene yields.

The enormous potential and the relatively simple structure of all participating reactants were the reasons for the decision that the research cluster “UNICAT-Unifying Concepts in Catalysis” chose the activation of methane in general and especially the OCM as a model reaction for a broad fundamental study. Starting with structure-function-analyses of the Li doped MgO catalyst which is one of the best known and most studied catalyst materials, a top-down strategy for developing an optimized catalyst system will take place. Afterwards this material will be tested in mini-plant scale. UNICAT comprises of over 50 research groups with more than 250 co-workers and is funded by the BMBF with up to 7 mio € per year.

The present work with the main topic OCM is a part of this ambitious research project. Instead catalyst optimization this work focuses on the comparison of different oxidizing agents. Besides the usually used oxygen the oxidizing agents nitrous oxide and carbon dioxide will be tested. Both are environmentally harmful exhaust gases from the chemical industry so that the usage and consumption of these exhaust gases would be a win-win situation. The usage of carbon dioxide in chemical processes is not expected to reduce its amount significantly because the anthropogenic carbon dioxide emission numbers in the area of gigatons. In contrast the nitrous oxide, which is the much more harmful greenhouse gas, is produced in smaller amounts at numerous chemical processes such as the adipic acid production. Due to the lower oxidation capability of nitrous oxide and carbon dioxide compared to molecular oxygen a lower overall activity but a significant higher C_2-selectivity is expected. This trend was already observed in other reactions and will now be tested for the OCM. In addition the use of carbon dioxide or nitrous oxide would be also advantageous regarding safety aspects. Both gases are non toxic and inflammable.

The catalyst systems will be selected from the best catalysts described in literature. These systems won’t be optimized regarding their composition but it will be tried to find new innovative synthesis strategies. An enhanced specific surface area can, e.g., be achieved by applying a microemulsion or cellulose template in the synthesis whereas the catalysts in literature are mostly synthesized by co-precipitation or wet-impregnation. The combination of optimized catalyst synthesis and a more selective oxidizing agent could be an important contribution in the enhancement of the ethylene yield in the OCM for an industrial usage of this reaction.

2 Theoretical Background

2.1 Oxidative Coupling of Methane

2.1.1 Methane

Methane, the simplest hydrocarbon molecule, is the main component of natural gas, whose reservoirs on earth are still huge. It can also be obtained from organic wastes as a component of biogas, which is produced by anaerobic alkaline fermentation. Furthermore, methane can be synthesized via CO hydrogenation from synthesis gas using nickel catalysts at temperatures about 573–873 K. The reaction is exothermic ($\Delta_R H$ = - 207 kJ mol^{-1}) and can be carried out in a fixed-bed or fluidized-bed reactor at 20–50 bar. However, current efforts are focused on hydrogenation of CO_2 as an environmental strategy to convert this greenhouse gas being produced in huge amounts in power plants. Methane produced this way can be used as chemical energy storage.

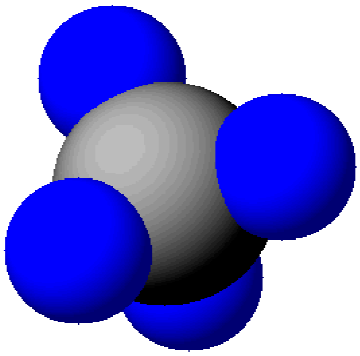

Figure 1. Scheme of a methane molecule (carbon: grey; hydrogen: blue).

The hydrogen atoms of the highly symmetric methane molecule are tetrahedrally coordinated around the carbon atom as shown in Figure 1. The C-H bond of methane (434 kJ mol^{-1}) is the strongest of the alkane series and therefore it is very demanding to selectively activate and convert methane. At present methane is mainly used as combustion gas for the energy production. Only a small fraction is used for chemical applications, which are summarized in Figure 2.

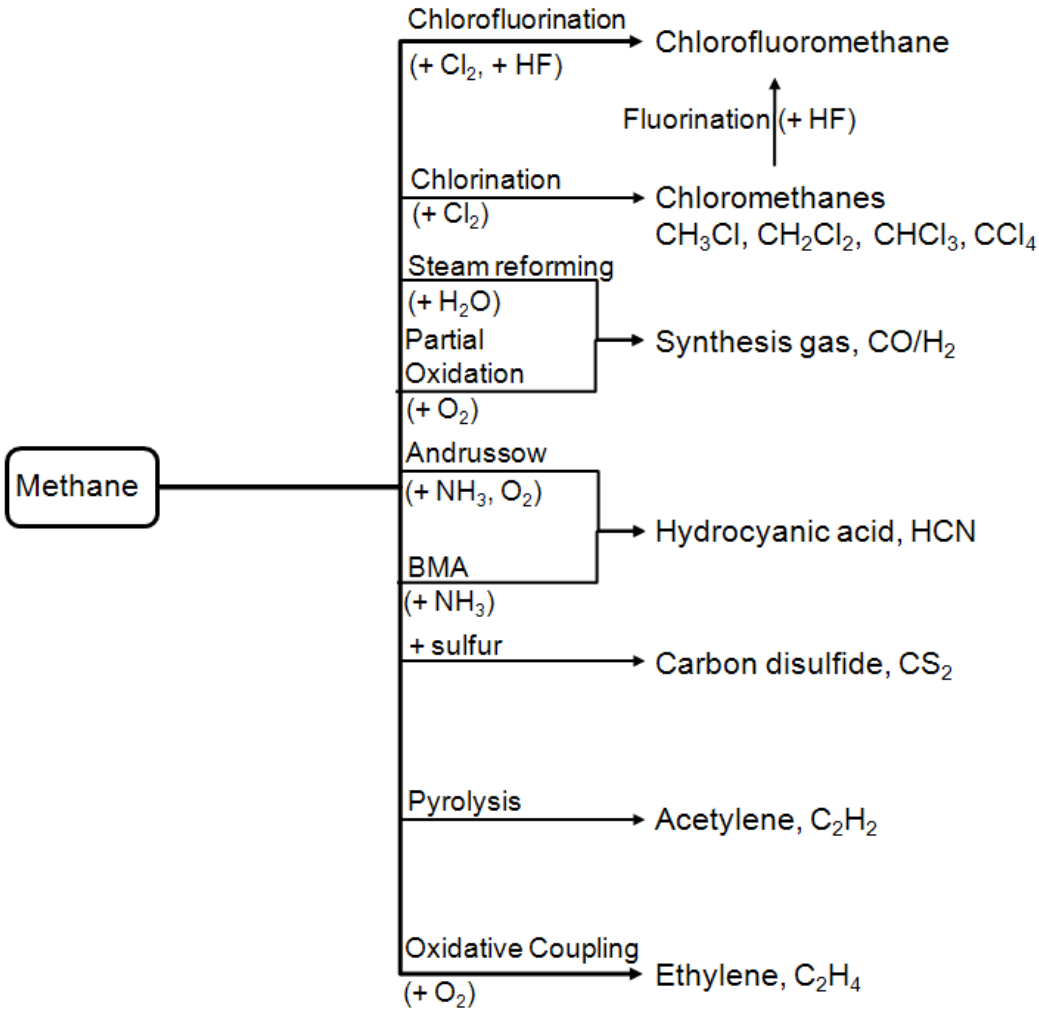

Figure 2. Overview over the different chemical uses for methane.

Chlorination of methane occurs via radical pathways at 400–500℃ without catalyst and yields a mixture of chloromethanes, which are used as solvents, refrigerants, or for the syntheses of silicones and fine chemicals.

Another important use for methane is the chemical conversion to hydrocyanic acid, which can proceed via two different processes, the Andrussow and the Degussa process [4]. The Andrussow process is the catalytic oxidation of methane with ammonia and air (Eq. 1) using rhodium doped platinum grids at about 1273–1473 K. In this process the reaction gases are quenched behind the reactor and the excess of ammonia gets edulcorated using sulfuric acid. Hydrocyanic acid is absorbed in water and subsequently obtained in high purity by distillation. The Degussa process is the catalytic dehydrogenation of methane without addition of oxygen at 1473–1573 K

(Eq. 2). The endothermic process occurs in ceramic tubes, which are coated with platinum.

Large amounts of methane are industrially converted to synthesis gas via steam reforming [5]. Here, methane and steam are converted over a Ni/Al_2O_3 catalyst to a mixture of carbon monoxide and hydrogen (synthesis gas) (Eq. 3).

Furthermore, methane reacts with sulfur at 923 K over silica gel to carbon disulfide, which is mainly used for cellulose reclaim fibers, according to Eq. 4.

Acetylene can be synthesized from methane in an electric arc at about 2273 K (Eq. 5) or via the Sachsse-Bartholomé process (Eq. 6) by the partial combustion of methane with pure oxygen and the formation of water.

$$CH_4 + NH_3 + 1.5\ O_2 \rightarrow HCN + 3\ H_2O \quad (1)$$

$$CH_4 + NH_3 \rightarrow HCN + 3\ H_2 \quad (2)$$

$$CH_4 + H_2O \rightarrow CO + 3\ H_2 \quad (3)$$

$$CH_4 + 4\ S \rightarrow CS_2 + 2\ H_2S \quad (4)$$

$$2\ CH_4 \rightarrow C_2H_2 + 2\ H_2 \quad (5)$$

$$2\ CH_4 + 1.5\ O_2 \rightarrow C_2H_2 + 3\ H_2O \quad (6)$$

$$CH_4 + 0.5\ O_2 \rightarrow CO + 2\ H_2 \quad (7)$$

$$CH_4 + CO_2 \rightarrow 2\ CO + 2\ H_2 \quad (8)$$

$$2\ CH_4 + O_2 \rightarrow C_2H_4 + 2\ H_2O \quad (9)$$

The partial catalytic oxidation of methane (POM, Eq. 7) and the conversion of methane with carbon dioxide to synthesis gas (dry reforming, Eq. 8), respectively, are reactions with a great potential for industrial application. However, due to low CO selectivity and catalyst deactivation problems they are not realized so far.

Another challenging route to convert methane is the oxidative coupling of methane (OCM) to ethane and ethylene (Eq. 9). Due to the strong C-H bond high temperatures of 1073–1173 K are needed. The low C_2-yields prevented an industrial application so far for economic reason.

Also the direct oxidation of methane to formaldehyde and methanol, which is examined in lab scale, is irrelevant for an industrial application so far due to the low yields.

2.1.2 Reaction Mechanism of OCM

The heterogeneously catalyzed OCM is a promising route to directly produce ethylene from methane but the C_2-yields are not sufficient for industrial realization so far. One of the most and best investigated catalysts for OCM is Li/MgO. Numerous characterization techniques such as XRD, XPS, EXAFS and XANES have been applied [6] to understand the origin and nature of active sites for this reaction. The bulk crystallinity of the catalyst is reduced at low lithium concentrations (< 2.5%) due to the entering of lithium into the bulk of MgO. After the reaction defects in the environment near the surface of MgO and Li/MgO were detected. The Li doped MgO shows a much higher activity in the OCM than the pure MgO. It is concluded that the Li-induced defects are responsible for the activity and a maximum activity is observed at very low lithium concentrations in the catalyst (Figure 3) [7].

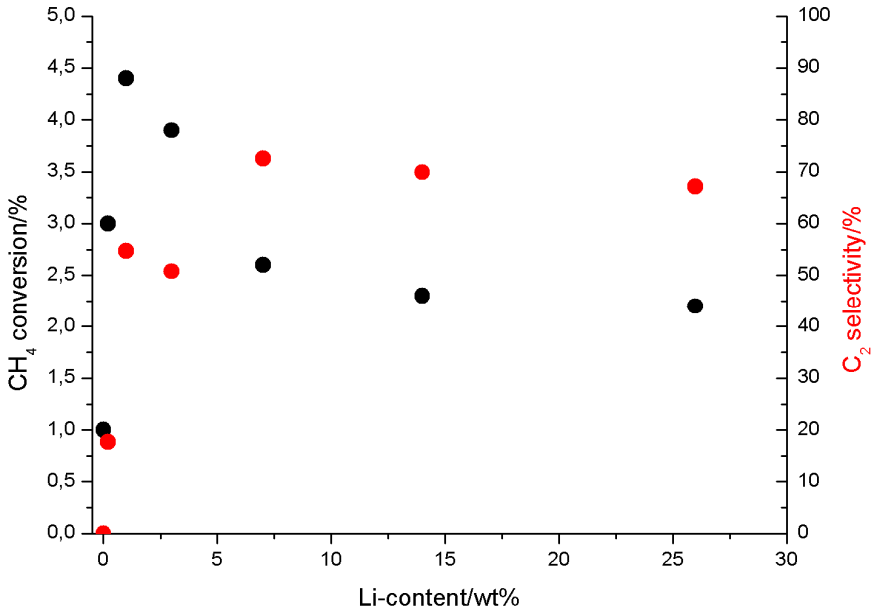

Figure 3. Dependence of the methane conversion and the C_2 selectivity on the Li content of Li doped MgO [8].

The apparently related catalyst system Na_2O/CaO was also studied in the OCM and via conductivity and contact potential difference methods it was proven that anionic vacancies in the CaO lattice are induced by Na_2O. These vacancies, which are localized at and near the catalyst surface, lower the C_2-selectivity [9]. However, a low degree of saturation of the Na_2O/CaO surface with oxygen resulted in an increased selectivity as proven by Kondratenko *et al.* by means of TAP experiments [10].

A broad variety of oxygen species (O^{2-}, O_2^-, O_3^{2-}, $O_2^{\delta-}$, and O^-) formed during OCM was detected by means of Raman spectroscopy of Nd_2O_3, BaO, and BaX_2 (with X = F, Cl, and Br) catalysts [11]. This agrees with other reports about the formation of oxygen species such as O^-, O_2^{2-}, O_2^-, and O_3^- on metal oxide surfaces [12–14] which are important for the selective oxidation of methane. The O_2^-, O_2^{2-} and O_3^{2-} ions are stabilized in anionic vacancies. It is supposed that there are electron donor sites at the catalyst surface from which oxygen molecules receive electrons to form ions like O^- and O^{2-} [15, 16]. Direct observation of O^-, O_2^-, and O_3^- succeeded when Li/MgO was quenched from 923 K in O_2 by liquid nitrogen [17]. These radical anions were also found over LaOF and BaF/LaOF catalysts in the OCM using *in situ* IR spectroscopy [18]. O_2^- ions, which are formed in the presence of oxygen, activate methane to form methyl radicals. Thus O_2^- ions were suggested to be the active sites in the OCM, in contrast to O^- ions, which could not be detected.

The cleavage of the C-H bond remains the most critical step in converting the methane molecule. The C-H breaking was suggested as homolytic or heterolytic mechanism. However, there is agreement that the OCM proceeds via methyl radicals formed at the catalyst surface and their recombination to form C_2-products takes place in the gas phase [19–21]. The formation of methyl radicals from methane via a methoxy radical was directly observed on an O/Mo (110) surface [22]. Here, oxygen was injected on a Mo (110) surface resulting in the formation of a two- or three-dimensional oxide layer. CH_3O- fragments were subsequently established after injection of methane vapor and a two-dimensional layer was formed up to 473 K. Three-dimensional layers resisted up to 703 K. At higher temperatures the fragments decomposed to H_2 and $CH_3\cdot$ radicals.

The importance of gas phase reactions was shown by Campbell *et al.* [23] over a Li/MgO catalyst. It could be shown that more than 40% of the C_2H_6 produced was

derived from the coupling of methyl radicals in the gas phase. In addition, for a Sr/La_2O_3 catalyst, Gutman *et al.* [24] showed that even 75% of the C_2H_6 resulted from the coupling of $CH_3\cdot$ radicals in the gas phase. Methyl radicals were shown to participate in a network of reactions, heterogeneous or gas-phase ones, which lead to a broad spectrum of reaction products. Numerous scientific publications dealt with the modeling of this homogeneous-heterogeneous reaction system [25–38] with modest success although the process schemes are very similar in all reports. A simplified reaction scheme of the OCM reaction network comprising parallel and consecutive reactions is shown in Figure 4.

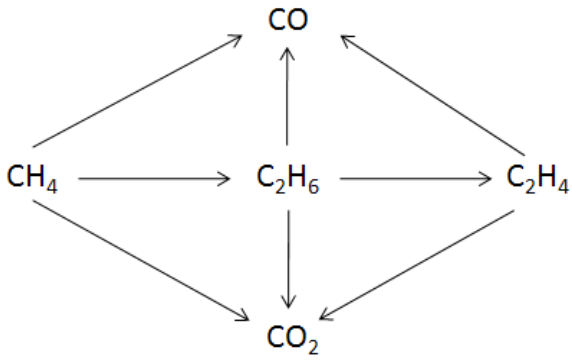

Figure 4. Simplified reaction scheme of OCM.

Once the methyl radicals enter the gas phase they may couple to form ethane which can be converted via homogeneous or heterogeneous dehydrogenation to ethylene. Methyl radicals can also participate in chain branching reactions with already formed C_2 products. However, hydrocarbon molecules with more than two carbon atoms formed this way usually decompose to CO_x under rough OCM reaction conditions. Of course, the methyl radicals can also react with gas-phase oxygen forming $CH_3O_2\cdot$ which was found by Jones *et al.* by means of ESR spectroscopy [39]. This $CH_3O_2\cdot$ species is most likely a precursor for CO_x formation [40], which is supported by the fact that its formation decreases with increasing temperatures. According to this the C_2-selectivity is enhanced at elevated temperatures.

Typically the C_2-selectivity decreases with increasing CH_4-conversion because primary and secondary C_2-products oxidize to CO_x as favored by the kinetics within the reaction network. These pathways (Figure 4) account for the inherently limited

yield of the overall OCM process [35, 36, 41, 42]. The minimum required yield of higher hydrocarbons for an industrially viable process has been estimated to be around 20 to 25% [43].

As noted previously, ethane is the initial C_2-product since the direct formation of ethylene by for example coupling of CH_2 would be a minor pathway. However small amounts of C_2H_4 were observed even at short residence times [44].

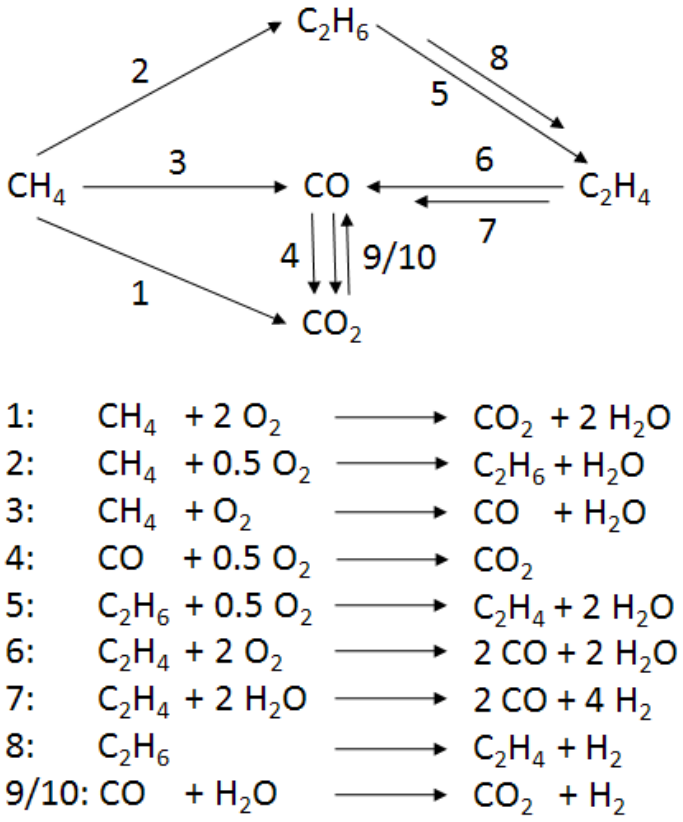

Figure 5. Reaction scheme of OCM over a La_2O_3/CaO catalyst [45].

Figure 5 represents a reaction network which was suggested by Baerns *et al.* for a La_2O_3/CaO catalyst. It is applicable for a broad range of reaction conditions (temperature range of 973–1223 K, methane to oxygen ratio of CH_4/O_2 = 2.5–10 and p_{tot} ca. 0.1 MPa). Methane reacts via different pathways. It can suffer the undesired total oxidation to carbon dioxide (Eq. 1), it might form ethane via the OCM (Eq. 2), or it can form carbon monoxide by the partial oxidation of methane (Eq. 3) with the subsequent oxidation of carbon monoxide to carbon dioxide (Eq. 4). Carbon monoxide can also be oxidized to carbon dioxide with *vice versa* via the water-gas

shift reaction (Eqs. 9 and 10). Ethane can heterogeneously react to ethylene via its oxidative dehydrogenation (ODH, Eq. 5) or can follow the homogeneous non-catalytic thermal dehydrogenation to ethylene (Eq. 8). Ethylene can undergo the oxidation to carbon monoxide (Eq. 6) or the steam reforming (Eq. 7). All reaction pathways are heterogeneously catalyzed except the thermal dehydrogenation of ethane.

It has been tried to model the OCM via a Langmuir-Hinshelwood kinetic model using the assumption that methyl radicals couple on the surface [46] or that adsorbed methane reacts with surface oxygen [37]. Later, using transient methods it was approved that in the required temperature range no methane is adsorbed on the catalyst surface [47–49]. However, the formation of methyl radicals from gaseous methane and surface oxygen species via an Eley-Rideal mechanism was approved by Baerns *et al.* over Sm_2O_3 by means of TAP-experiments [20].

Although the principal reaction details are well established, much more research work has to be done with regard to the kinetics, as well as to the reactor design, reaction conditions [45], or catalyst design with the ultimate goal to fully understand the OCM reaction and to make it attractive for an industrial application.

2.1.3 Catalysts

Since the pioneering studies on OCM by Keller and Bhasin [3], Hinsen and Baerns [50] as well as Ito and Lunsford [51] in the early 1980's numerous studies on the introduction of new catalysts for the OCM reaction were published. A huge number of catalytic materials have been investigated and optimized in order to enhance the C_2-yield. A plausible classification is the systematic division of OCM catalysts into four classes [52, 53]: (A) reducible metal oxides, (B) non-reducible metal oxides, (C) halogen-containing oxide materials, and (D) solid electrolytes.

Materials of group (A) have to be very stable towards oxidative or reductive conditions especially at high temperatures. They have to supply large amounts of lattice oxygen and they have to rapidly reoxidize because these materials are preferentially used in periodic mode of OCM with alternating CH_4 and O_2 feed streams. In this so-called redox OCM the oxidized catalyst forms C_2-products in a stream of CH_4 on the cost of its lattice oxygen. After a certain period of reaction the

gas stream is switched to O_2 in order to reoxidize the catalyst. With regard to the above mentioned requirements it is not surprising that perovskites are superior catalysts for the redox mode. For example $Sr_{0.75}Na_{0.25}NiO_{3-x}$ and $SrNi_{0.75}Li_{0.25}O_{3-x}$ (Table 1) are reported to achieve C_2-yields of 17.3% and 22.4%, respectively [54]. $SrMnO_x$ and $SrCoO_x$ based perovskite-type mixed oxides were also identified to be selective catalysts for the redox OCM [55].

Table 1. Overview over catalysts for the OCM reaction.

Catalyst	*T* [K]	CH_4:O_2:inert	GHSV [h^{-1}]	*X*(CH_4) [%]	*S*(C_2) [%]	Ref.
$Sr_{0.75}Na_{0.25}NiO_{3-x}$	973	[a]	2000	17.4	99.8	[56]
$SrNi_{0.75}Li_{0.25}O_{3-x}$	973	[a]	2000	22.5	99.7	[56]
$Bi_{1.5}Y_{0.3}Sm_{0.2}O_{3-x}$	1173	[b]	4900	55	68	[57]
BaF_2(95 mol%)/Y_2O_3	1023	2.47:1:11.4	6000[c]	36.1	62.1	[58]
Li(0.2 wt%)/MgO	923	10:5:85	6000[c]	3	17.7	[8]
Na(0.32g)/$BaSrTiO_3$	1073	4:2:4	6000	47	51	[59]
$NaWO_4$/SiO_2	1123	4.5:1	2000	44	52	[60]
$RbWO_4$/SiO_2	1123	4.5:1	2000	32	78	[60]
Sr(1 wt%)La_2O_3	1023	30:5:65	37500	20.9	63.6	[61]
$NaMnO_4$(12 wt%)/MgO	1198	5:1:4	9600	25	70	[62]
La/CaO	1073	8:1	51360[c]	19.8	67.2	[63]
Nd/CaO	1073	8:1	51360[c]	19.5	70.8	[63]
Li/Ce/MgO	1073	5:1:4	6000[c]	21.6	64	[64]
$LiCa_2Bi_3O_4Cl_6$	993	20:10:70		41.7	46.5	[65]
Mn(2 wt%)/Na_2WO_4(5 wt%)/SiO_2	1073	45:15:39	36000[c]	36.8	64.9	[66]

[a] alternating feed mode; [b] membrane reactor; [c] unit: mL g^{-1} h^{-1}.

The non-reducible metal oxides (B) are very active materials for the co-feed mode, where the gas stream comprises oxygen and methane in parallel. The best performing non-reducible metal oxides are those of rare earth and alkaline earth metals. The selectivity to C_2-products can even be improved by doping with alkaline earth and alkali metal oxides [67, 64, 68]. Some of the best performing non-reducible OCM catalysts are listed in Table 1. Li/MgO is probably the most extensively studied catalysts of class (B) [8, 69–74]. Matsuura *et al.* obtained one of the highest C_2-yields ever reported (21.1%) with a 3 mol% Li/MgO at 973 K in an atmosphere comprising CH_4 and O_2 in the ratio 3:1 without any inert diluting gas [69]. However, even for this well investigated system Arndt *et al.* recently disclosed contradictions and open questions from a thorough literature review [75]. One of the biggest problems of Li/MgO is the deactivation due to the loss of lithium as volatile LiOH. In common laboratory reactors made of quartz glass this volatile compound irreversibly forms Li_2SiO_3 at the reactor walls [70, 76, 77]. Another very general problem in catalytic sciences is the lack of directly comparable data due to the broad variety of reaction conditions.

Another non-reducible oxidic high performance OCM catalyst reported in literature is Mn(2 wt%)/Na_2WO_4(5 wt%)/SiO_2 showing a C_2-yield of 23.9% at 1073 K [66]. Jiang *et al.* proposed tetrahedral WO_4 surface species as the OCM active sites with manganese oxide enhancing the exchange between gaseous and lattice oxygen. Later on this model was expanded with a redox mechanism with a W^{6+}/W^{5+} couple and lattice oxygen ions [78]. Wang *et al.* investigated the same catalyst and suggested a Na-O-Mn species being responsible for activation of methane [79]. In advanced kinetic studies they found that the catalyst was inert towards methyl radicals even at temperatures around 1063 K [80]. This property was concluded to be responsible for its superior OCM performance. The same catalyst was also studied by XRD, XPS/XAES, TPR, and microreactor testing by Palermo *et al.* [81]. They identified the silica support, especially the α-cristobalite, to be necessary to form highly selective catalysts. An addition of Na is important for the phase transformation of the silica support at low temperatures, which they assumed to be critically important to form highly active and selective catalysts. Contrarily, they found that the presence of Mn is less important for the formation of well-performing OCM catalysts. Consequently, they investigated catalysts incorporating different ions including Na

and Rb among others with WO_4 supported on SiO_2 [60]. In this study C_2-yields of 22.88% over $NaWO_4/SiO_2$, 20.1% with K_2WO_4/SiO_2 and 24.96% over $RbWO_4/SiO_2$ are reported at 1123 K in an atmosphere with the composition of methane: oxygen = 4.5:1.

As described before alkali metal promoted catalysts such as Li/MgO show a good activity in the OCM but at high temperatures the alkali metals tend to evaporate, which leads to catalyst sintering and deactivation. The use of high melting promoters such as alkaline earth or rare earth metal oxides could avoid this problem. A number of publications dealt with the use of calcium-based catalysts for the OCM [82–86]. For instance, a lanthanum-calcium oxide catalyst was tested in the OCM in a micro-catalytic fixed-bed reactor at 973–1013 K by Becker and Baerns [83]. They reported that the catalytic performance of materials with different composition is more affected by the composition of the surface then of the bulk. The authors suggested that a catalyst leads to high C_2 selectivities if it possesses a basic nature and acidic sites. Choudhary *et al.* found La/CaO to be an active and selective catalyst with a long life-time under OCM reaction conditions [87]. Rane *et al.* studied rare earth metal promoted calcium oxide catalysts for the OCM [63]. They found a variety of active catalysts, e.g., La/CaO, Nd/CaO, and Yb/CaO, with C_2-yields of 13.3, 13.8, and 13.3%, respectively (Table 1). They suggested that the stronger the basic sites are the more active and selective is the catalyst.

Another example of class (B) catalysts, which was found to be highly active for the OCM, is $NaMnO_4$(12 wt%)/MgO [62]. At 1123 K this catalyst shows a C_2-yield of 8.8% and at 1198 K the C_2-yield reaches even 15.7%. The authors explain the activity of the catalyst material with the ability of Mn to promote odd number of electron oxygen centers in the catalyst. A significantly enhanced catalytic performance with a C_2 yield of 31% at 1023 K was reported by Otsuka *et al.* over manganese oxide, which was promoted with lithium chloride [88]. In general, the halogen-containing oxide materials of catalyst class (C) show high C_2 selectivities at high methane conversions. Shigapov *et al.* reported the improvement of the OCM performance of CaO via promoting with $CaCl_2$ [89]. The enhanced catalytic performance of various oxides by doping with chlorides was also reported by Burch *et al.* [90] and Warren [91]. It is supposed that small amount of chlorine is formed

which initiates gas-phase reactions. This assumption, however, would indicate a limited life-time of the active catalyst.

Y_2O_3-based materials are catalytic systems of high interest. When Y_2O_3/CaO was studied for the OCM an increasing Y_2O_3 content enhanced the C_2 selectivity [92], which was referred to the formation of interstitial superoxide ions O_2^-. Furthermore, the incorporation of Sr^{2+} into the Y_2O_3 lattice was found to substantially enhance methane conversions and C_2 selectivities [93]. Hence, Au *et al.* investigated BaF_2/Y_2O_3 and found a C_2-yield as low as 7.8% over pure Y_2O_3 [58]. However, after addition of 30 mol% BaF_2 the C_2-yield is 19.5% and over a BaF_2(95 mol%)/Y_2O_3 catalyst the C_2-yield reaches even 22.4%. O_2 adsorption and TPR experiments show that the BaF_2/Y_2O_3 catalyst has a higher ability to activate O_2 than the undoped Y_2O_3. The authors suggest that the ionic exchange between BaF_2 and Y_2O_3 generates active defects. By means of EPR spectroscopy they disclosed that trapped electrons were generated and during OCM the BaF_2/Y_2O_3 catalyst was reduced by hydrogen, which was dissociated from methane. The trapped electrons were furthermore supposed to act as active sites for activation of O_2.

The last group of OCM catalysts consists of solid electrolytes (D). The most important applications for solid electrolytes are membrane reactors [94, 95]. For instance, $SrCe_{0.9}Yb_{0.1}O_x$ shows a very high C_2-yield of 31.6% at 1023 K, which was related to the proton conductivity of the catalytic material. However the instability of the membranes due to carbonate formation is a basic disadvantage of this kind of catalyst materials.

2.2 Perovskites

2.2.1 Structure and Composition

Perovskites were first discovered in 1839 by the German mineralogist Gustav Rose (Figure 6a) in rock cuttings from Achmatowsk (Russia). He examined the mineral and described its cristallinity, Mohs hardness (5.5), density, and analyzed the chemical composition. In general linguistic usage the mineral with the composition $CaTiO_3$ is named perovskite after the Russian politician and mineralogist Lew Alexejewitsch Perowski (Figure 6b).

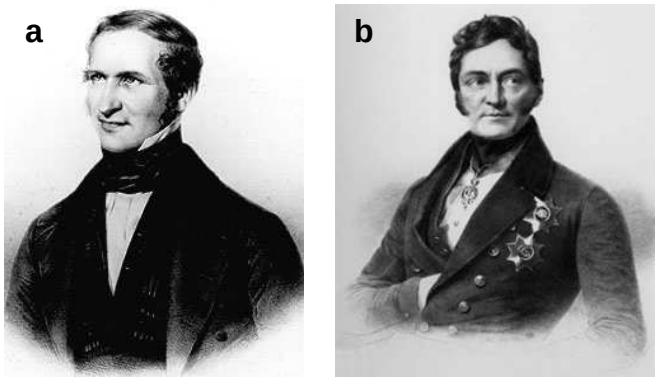

Figure 6. (a) Gustav Rose (1798-1873) and (b) Lew Alexejewitsch Perowski (1792–1856), discoverer and eponym of Perovskites, respectively.

However, the formation of the Perovskite structure is not limited to the elemental composition comprising Ca and Ti. It is generally described by the formula ABO_3, where A and B are usually alkaline earth, rare earth, and transition metal cations, and the A cation is larger than the B cation. Their catalytic properties are closely related to the nature of the B-site cation [96, 97]. The oxygen nonstoichiometry and mobility inside the Perovskite lattice are affected by the A-site cation [98].

The crystal system of the $CaTiO_3$-perovskite (Figure 7) is orthorhombic due to the small Ca cations, which distort the ideal cubic structure [99]. In contrast $SrTiO_3$ forms an ideal cubic structure due to the larger diameter of Sr^{2+}. The degree of deformation of the crystal system for each ABO_3 system correlates with the Goldschmidt tolerance factor *t* (Eq. 10) [100].

$$t = \frac{r_A + r_O}{\sqrt{2}(r_B + r_O)} \qquad (10)$$

With r_A being the radius of the cation A, r_B the radius of the cation B and r_O the radius of the anion which is usually oxygen. Selected perovskites based on Sr and Co with corresponding tolerance factors based on empirical ionic radii given in literature [96] are assembled in Table 2.

Table 2. Perovskite-type mixed oxides based on $SrCoO_x$ and corresponding tolerance factor according to the Goldschmidt equation.

Formula	*t*	*Formula*	*T*	*Formula*	*t*	*Formula*	*t*
$SrCoO_x$	1.03	$SrFeO_x$	0.98	$LaSrCoO_x$	1.01	$SrFeCoO_x$	1.01
$CaCoO_x$	1.00	$SrMgO_x$	0.95	$CeSrCoO_x$	1.00	$SrMgCoO_x$	0.99
$CeCoO_x$	0.98	$SrMnO_x$	1.01	$PrSrCoO_x$	1.00	$SrMnCoO_x$	1.02
$LaCoO_x$	0.99	$SrMoO_x$	0.98	$NdSrCoO_x$	0.99	$SrMoCoO_x$	1.00
$PbCoO_x$	1.05	$SrNiO_x$	1.03	$CaSrCoO_x$	1.01	$SrNiCoO_x$	1.03
$PrCoO_x$	0.98	$SrPbO_x$	0.92	$PbSrCoO_x$	1.04	$SrPbCoO_x$	0.97
$NdCoO_x$	0.97	$SrPdO_x$	0.96	$SrAlCoO_x$	1.04	$SrPdCoO_x$	0.99
$SrAlO_x$	1.04	$SrSbO_x$	1.00	$SrCrCoO_x$	1.02	$SrSbCoO_x$	1.02
$SrCrO_x$	1.00	$SrSnO_x$	0.96	$SrCuCoO_x$	0.98	$SrSnCoO_x$	0.99
$SrCuO_x$	0.94	$SrZnO_x$	0.94	$SrYCoO_x$	0.95	$SrZnCoO_x$	0.98

Red: Substitution of A-site cation Sr^{2+}; blue: substitution of B-site cation Co^{4+}; dashed: partial substitution of respective cations.

Although most compounds with a perovskite structure are oxides some carbides, nitrides, halides, and hydrides also form this structure. The Goldschmidt relation is based on the system at room temperature. The ideal undistorted cubic structure of $SrTiO_3$ has a tolerance factor of 1. The range of $0.75 < t < 1.02$ corresponds to a distorted perovskite structure which can transform to an ideal cubic structure at high temperatures. About 90% of all natural metals of the periodic system of elements are known to form a stable perovskite-type oxide. The unit cell of a $CaTiO_3$ perovskite is shown in Figure 7. Typically, the B-site cation is 6 fold and the A-site cation is 12 fold coordinated with O^{2-} ions.

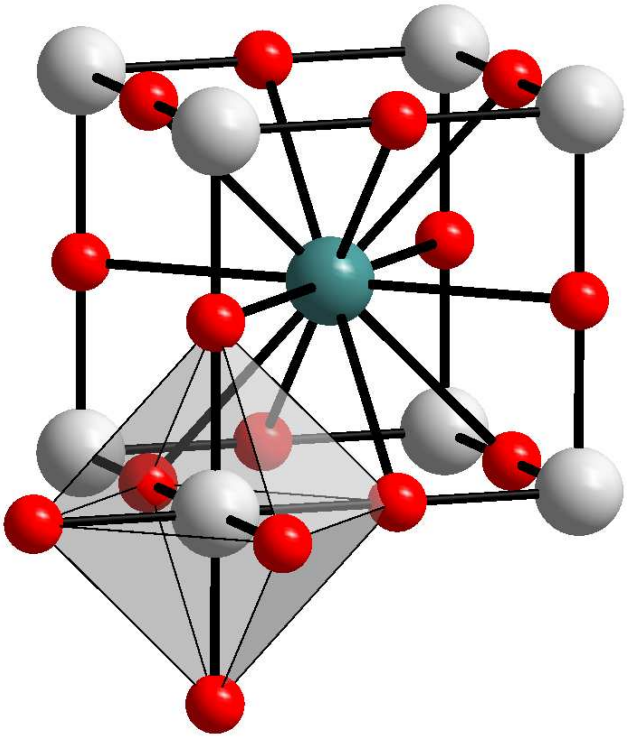

Figure 7. Scheme of the orthorhombic crystal system of a $CaTiO_3$ perovskite [101].

Besides the tolerance factor also the charges of the A and B cations have to balance the oxygen anion charge. It means that perovskites of different charge distribution are possible, e.g, $A^{1+}B^{5+}O_3$, $A^{2+}B^{4+}O_3$ or $A^{3+}B^{3+}O_3$. Also the partial substitution of the A or B ion is possible considering these conditions which offer a huge amount of different compositions. Defects of cations and anions result in frequently observed non-stoichiometry of the system. Here, the oxygen deficiency is more common than the cationic vacancies. Examples of perovskites with anion vacancies are the brownmillerite-type like $Ca_2Fe_2O_5$ [96] or $La_2Ni_2O_5$ [102], which are highly oxygen deficient perovskites with one of six anion positions being vacant. Contrarily, the oxygen excess nonstoichiometry in perovskite oxides is less frequently observed due to the fact that interstitial oxygen in the perovskite lattice is thermodynamically unfavored. However, $LaMnO_x$ is a common representative, which shows an exact composition of $LaMnO_{3.12}$ [103].

Moreover, perovskites of the ABO_3 type possess several interesting physical properties such as ferroelectricity ($BaTiO_3$), ferromagnetism ($SrRuO_3$), weak ferromagnetism ($LaFeO_3$), superconductivity ($YBa_2Cu_3O_7$), large thermal conductivity

due to exciton transport ($LaCoO_3$), and transport properties for high temperature thermoelectric power (La_2CuO_4).

2.2.2 Application in Heterogeneous Catalysis

Due to their variable and broad range of chemical compositions but also because of the well controllable physical and chemical properties and a very good thermal stability perovskites are excellent model compounds in chemical research especially in catalysis. Perovskites have been successfully used in numerous heterogeneously catalyzed reactions such as the removal of environmental toxins via NO_x decomposition [104], exhaust treatment [105–107], hydrogenation and hydrogenolysis reactions like the hydrogenation of carbon oxides (CO [108, 109] and CO_2 hydrogenation [110]), for photocatalysis to decompose water [96], as chemical sensors for gases [111], and in electrocatalysis for oxygen reduction [112] and solid oxide fuel cells [113]. The good performance of perovskites in oxidation catalysis is closely related to the surface defects being generated by cation and anion deficiencies or by defects generated by partial substitution of the cations [96]. These sites are preferential points for O_2 adsorption and step-wise charge transfer to generate catalytically active oxygen species. Oxidation reactions such as the CO oxidation or the oxidation of hydrocarbons, e.g., the oxidation of paraffins, olefins, aromatics, and oxygenate compounds [96] are common applications for perovskites. Due to the good thermal stability at least below 1300 K and their high catalytic activity perovskite oxides are good combustion catalysts. The combustion of propane over Sr- or Ce-doped $LaMO_3$ with M = Fe, Co and the combustion of propylene and isobutene on $LaBO_3$ with B = Cr, Mn, Fe, Co, Ni were examined. The correlation between O_2 adsorption and catalytic activity in the propylene and isobutene combustion suggests that these reactions occur via a mechanism in which adsorbed oxygen is the dominant species [114–116].

Methane combustion over $LaBO_3$ with B = transition metals and over Sr-substituted $La_{1-x}Sr_xBO_3$ with $0 < x < 0.4$ was examined by Arai *et al.*, who found high activities comparable to those of Pt/Al_2O_3 combustion catalysts [117]. In $La_{1-x}A'_xBO_3$ with B = Co, Fe, Ni perovskites the type of substitution of the A-site cation has a strong influence on the performance in the methane combustion [118]. A bivalent cation (A'

= Sr, Eu) leads to a decreased and a tetravalent one (A'=Ce) leads to an increased catalytic performance. The bivalent cations cause higher oxidation states of Co but because Co^{4+} is unstable, an oxygen release takes place so that oxygen vacancies are formed. In contrast the tetravalent cations lead to a reduction of the cobalt so that many active sites for oxygen adsorption from the gas phase are formed [118]. The partial oxidation of methane to syngas [119–122] as well as the dry reforming of methane with carbon dioxide [123–125] was also studied in literature.

OCM was successfully performed over perovskite-type oxides, however, only in membrane reactors or in alternating feed mode. C_2-selectivities of up to 70% at a methane conversion as low as 3% were obtained with a $La_{0.6}Sr_{0.4}Co_{0.8}Fe_{0.2}O_3$ membrane applying oxygen partial pressures in the range of 0.01 to 1 bar [126]. For this reaction in a membrane reactor it is important to limit the oxygen flux by reaction kinetics because otherwise the membrane would be reduced with subsequent decrease of the selectivity. A membrane reactor was also tested using $BaCe_{0.8}Gd_{0.2}O_{3-x}$ [127]. Typically, methane is passed over one side and oxygen over the other side of the membrane, which leads to high C_2-yields. This implicates that the mobile oxygen species, which migrate to the hydrocarbon-sided surface of the membrane, are more selective for OCM than adsorbed species formed in the presence of pure gaseous oxygen. Wang *et al.* [128] derived a mathematical model for the oxygen transport through thin O^{2-} ion conducting yttria-stabilized zirconia (YSZ) membranes with regard to the diffusion of the charged species of the solid and the surface reactions at the membrane-gas barrier. They showed that higher C_2-yields are possible if a highly permeable ceramic membrane, which is active for the OCM, is used instead of a packed bed reactor. The parameter window for selective OCM in a membrane reactor, however, is very small.

$SrCe_{0.95}Yb_{0.05}O_x$ was used as solid electrolyte in an electrochemical cell, in which OCM was examined [129]. High C_2-selectivities were obtained due to the fact that no gaseous oxygen was present. The same perovskite was used in several catalytic reactors and the yield was the highest in a membrane reactor [130].

A well-studied perovskite system is $SrCoO_x$ [131–136]. This perovskite system is known for its wide range of oxygen nonstoichiometry. The strontium cobaltate was successfully used as cathode material for intermediate-temperature solid oxide fuel

cells [137], as oxygen separation membranes [138] and for complete methane oxidation [139] and for the oxidative coupling of methane (OCM) [140, 54]. $SrCoO_x$ was synthesized by various methods. In general, it is formed through the orthorhombic brownmillerite phase $SrCoO_{2.5}$ [141], which possesses ordered oxygen vacancies layers of corner-sharing CoO_4 tetrahedra and CoO_6 octahedra. It should be stressed that physico-chemical and catalytic properties of $SrCoO_x$ are strongly influenced by the synthesis method [142–144].

2.3 Oxidizing agents

2.3.1 Oxygen

The standard oxidizing agent for oxidative catalytic reactions is molecular oxygen, which can be used as component of air or as a pure gas isolated by fractional distillation after liquefaction of air in the Linde process. Pure oxygen is very reactive and some catalytic transformations are impossible to perform without it. Heterogeneous oxidation catalysis is one of the most important fields of catalysis. For instance, in catalytic purification systems the deep oxidation of toxic compounds is very important. Also the selective oxidation of organic compounds is fundamental for synthesizing important chemical intermediates such as aldehydes, acids, or nitriles.

By interacting with the catalyst surface the oxygen molecule is activated via the following steps: coordination, electron transfer, dissociation and incorporation into the oxide lattice of the catalyst. The weaker the oxygen binding at the catalyst surface is, the more active is the catalyst for complete oxidation. In addition, experimental data show that weakly bound oxygen, which is different from lattice oxygen, is present on the catalyst surface of complete oxidation catalysts. During the O_2 activation process peroxides are generated, which are usually unselective in catalytic reactions. For selective oxidation catalysis this type of oxygen is usually unwanted [145, 146] as it is highly electrophilic and attacks the carbon chain of hydrocarbon molecules, which mostly initiates the total oxidation of the substrate molecule. Using radiospectroscopic methods the oxygen radicals O^- and O_2^- were discovered [147–149] and it was shown that O^- possesses an extremely high oxidative activity and O_2^- has a lesser but still rather high activity. These experiments were all carried out at

significantly lower temperatures compared to those typical for catalysis, therefore the participation of these oxygen radicals in catalysis stays yet unclear.

Depending on the catalyst and reaction conditions, the reaction between methane and oxygen can also end up in partial oxidation of methane (Eq. 7) to synthesis gas [150, 120, 121, 119].

$$CH_4 + 0.5\ O_2 \rightarrow CO + 2\ H_2 \qquad (7)$$

The formation of the unselective by-products CO_2 and H_2O decreases with increasing conversion. However, the POM is not industrially realized so far. Synthesis gas is mainly produced by steam reforming. Here, the POM is often applied in a downstream reformer. The slightly exothermic POM reaction is advantageous over the steam reforming reaction because less heating energy is needed. Therefore the POM reaction is discussed as an alternative to the steam reforming. The main problems are catalyst coking and a demanding reaction engineering to avoid the runaway of the POM reaction [151].

2.3.2 Nitrous Oxide

Nitrous oxide N_2O is non toxic and commonly used as anesthetic but it is also the most hazardous of the greenhouse gases with a by 310 times higher potential than CO_2 to degrade ozone [152]. It is less reactive than oxygen but offers a substantial advantage over molecular O_2: N_2O possesses only one oxygen atom, thus the formation of surface peroxides, which lower the selectivity, is substantially suppressed. The high stability of the N-O bond requires high temperatures and an appropriate catalyst to activate this oxidizing agent. In all catalytic oxidations using N_2O only N_2 would be produced as by-product, which is harmless.

Kondratenko *et al.* examined the use of nitrous oxide in the oxidative dehydrogenation of propane (ODP) over supported vanadia catalysts [146, 153–155] and also in the OCM over SrO [156]. In all cases the selectivity was remarkably enhanced as compared to the reactions with O_2. By means of EPR spectroscopy they found that the active oxygen species with O_2 as oxidizing agent is electrophilic O^-, which is highly reactive with propene to initiate its combustion. In contrast the active oxygen

species with nitrous oxide as oxidizing agent is nucleophilic O^{2-} which is less active in total oxidation, what substantially enhances the propene selectivity [154].

2.3.3 Water and Carbon Dioxide

Another approach is the use of water in terms of steam as oxidizing agent. Water is cheap and non toxic. It is less active than oxygen but similar to N_2O the presence of only one isolated oxygen atom should result in the formation of more selective surface oxygen species, because the formation of peroxides is avoided. After its reduction during OCM water would leave H_2 as exhaust, which is a valuable by-product for other chemical processes.

The use of water as oxidant in the OCM over Li/MgO was already investigated. LiOH is formed by the reaction of H_2O with $LiCO_3$ and the activity of C_2 hydrocarbon formation was enhanced [157]. Perovskites were also used for OCM with water and they showed an increased activity towards C_2 hydrocarbons [158–160].

However, from a general point of view, H_2O cannot directly be regarded as an oxidizing agent in the OCM reaction, as the oxygen atom recombines with hydrogen atoms from methane molecules and the net reaction in this case would be the non-oxidative coupling of methane. But it appears plausible that the addition of steam to the reactant mixture affects the catalyst properties or influences thermodynamic equilibria of gas phase and surface species. In numerous catalytic processes, steam is added to the reaction, mostly to reduce catalyst deactivation by coking. It is also clear that, with regard to downstream refining processes, steam is by far easier to separate from the product gas mixture than inert gases like N_2.

Carbon dioxide is a greenhouse gas which is globally produced in high amounts and locally concentrated in chemical industry and numerous power plants. Thus it is a cheap gas and available in sufficient amounts but it is less reactive in chemical reactions than oxygen. It has a C-O bond strength of about 532 kJ mol^{-1} making it relatively inert, thus high temperatures are required to activate this potential oxidizing agent. There are several possible reactions using CO_2 but only a few are industrially realized. For instance, it is used for the synthesis of urea, salicylic acid, methanol, inorganic carbonates, and pigments. In addition it is used for refrigerating, for

beverages, air conditioning, or fire extinguishers. This industrial usage cannot significantly lower the CO_2 concentration in the atmosphere but still possesses a great potential in chemical synthesis.

Similar to N_2O and H_2O the formation of peroxide species, which could lower the selectivity in OCM, is not that easy with carbon dioxide. In addition no reaction occurs between carbon dioxide and gas phase methyl radicals. Thus it is supposed that carbon dioxide acts more selective in oxidation catalysis than molecular oxygen. The application of carbon dioxide in OCM would generate carbon monoxide as exhaust, which is a useful gas for further synthesis steps. Isotopic studies showed that carbon dioxide is converted to CO and the C_2-hydrocarbons yielded from methane [161].

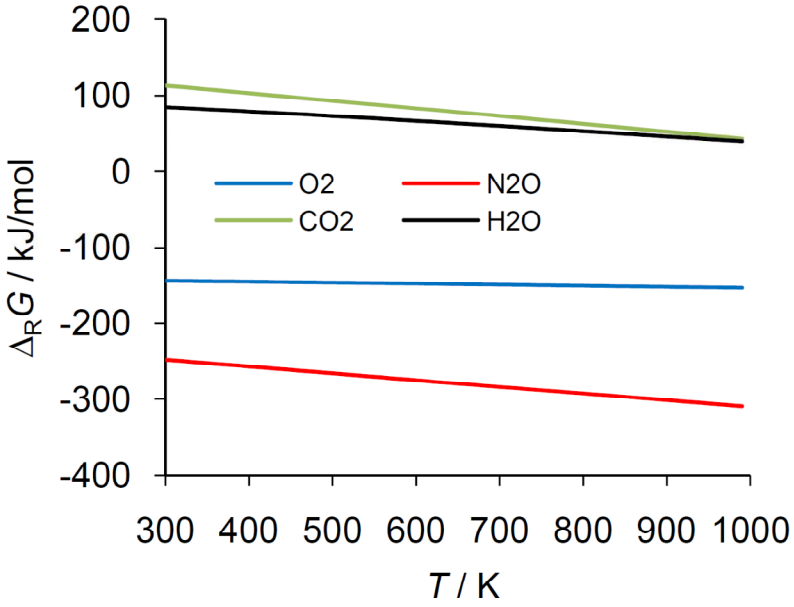

Figure 8. Gibbs enthalpies of OCM with different oxidizing agents.

For the OCM with carbon dioxide different metal oxides were already examined (Y, La, Sm, Ti, Zr, Hf, Nb, Cr, Mn, Fe, Co, Cu, In, Al, Si, Bi, Ge). The reaction between methane and carbon dioxide is the best at a CO_2/CH_4 ratio of 2 [162]. The selective catalyst must attack the carbon dioxide first and selectively break the CH_3-H bond (Eqs. 17 and 18). Y_2O_3 showed the best results and rare earth metals are generally good. Nevertheless the C_2-yields are too low for an industrial use so far. Thermodynamic calculations showed that at 1073–1173 K, 1 atm and equimolar CH_4/CO_2 ratio an equilibrium methane conversion of 15–35% is possible [162]. Also

in Figure 8 it can be seen that the OCM with CO_2 and H_2O requires high reaction temperatures, whereas the reaction has no measurable thermodynamic limitation when O_2 or N_2O is used as the oxidizing agent. Figure 9 exemplifies the resulting limitations of methane conversion as a function of temperature and initial CH_4:CO_2 molar ratio.

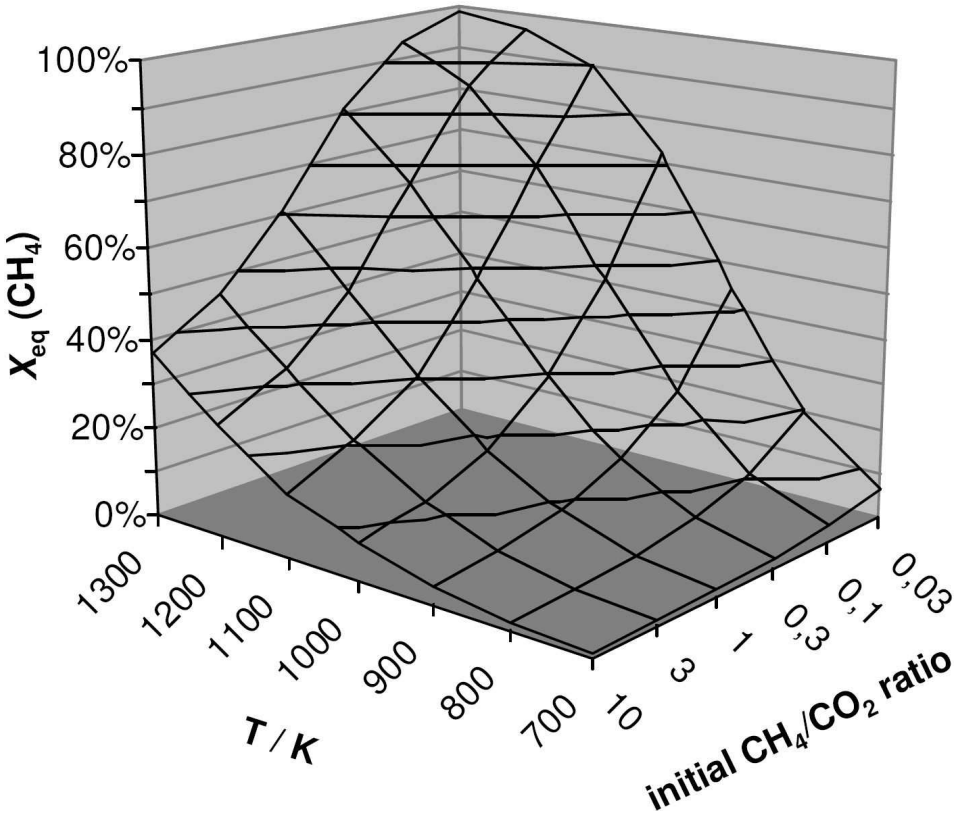

Figure 9. Thermodynamic limitation of CH_4 conversion to C_2H_4 with CO_2 as the oxidizing agent ($CH_4 + CO_2 \leftrightarrows 0.5\ C_2H_4 + H_2O + CO$). Equilibrium conversions are calculated for 1 bar total pressure and without dilutant as a function of temperature and initial molar ration of the reactants.

The OCM using carbon dioxide as oxidant is a challenging alternative but more research is required to identify active catalysts.

2.3.3.1 Steam Reforming of Methane

Steam reforming of methane (Eq. 14) is the dominating pathway of chemical use of natural gas to produce hydrogen or synthesis gas, thus listed in this work for the sake of completeness.

$$CH_4 + H_2O \rightarrow 3\ H_2 + CO \quad (3)$$

$$CO_2 + H_2 \rightarrow CO + H_2O \quad (11)$$

The reaction is endothermic (206 kJ mol^{-1}) and highly energy demanding due to the reaction temperature of 700-1100 °C. The steam reforming is typically performed over Ni-based catalysts. To achieve high hydrogen yields CO is further converted with steam via the water-gas shift reaction (Eq. 11).

2.3.3.2 Dry Reforming of Methane

In principle several reactions between methane and carbon dioxide are possible (Eqs. 8, 12–14). However, from the thermodynamic point of view, only methane dry reforming (Eq. 8) appears to be a realistic option for gas phase transformations (Figure 10). The reaction becomes favorable at temperatures > 900 K. Dry reforming of methane is an interesting way to produce synthesis gas out of greenhouse gases. Synthesis gas is an important feedstock for numerous large scale chemical reactions such as the methanol or ammonia synthesis. During the dry reforming of methane the unwanted water-gas shift reaction (Eq. 11) is usually catalyzed by the same catalyst. As a result, in high-temperature catalytic processes dry reforming, water-gas-shift, and steam reforming (Eq. 3) often occur simultaneously and a kinetic analysis or reactor design is rather difficult.

$$CH_4 + CO_2 \rightarrow 2\ H_2 + 2\ CO \quad (8)$$

$$CH_4 + CO_2 \rightarrow CH_3OH + CO \quad (12)$$

$$CH_4 + CO_2 \rightarrow CH_3COOH \quad (13)$$

$$CH_4 + CO_2 \rightarrow CH_3COCH_3 + H_2O \quad (14)$$

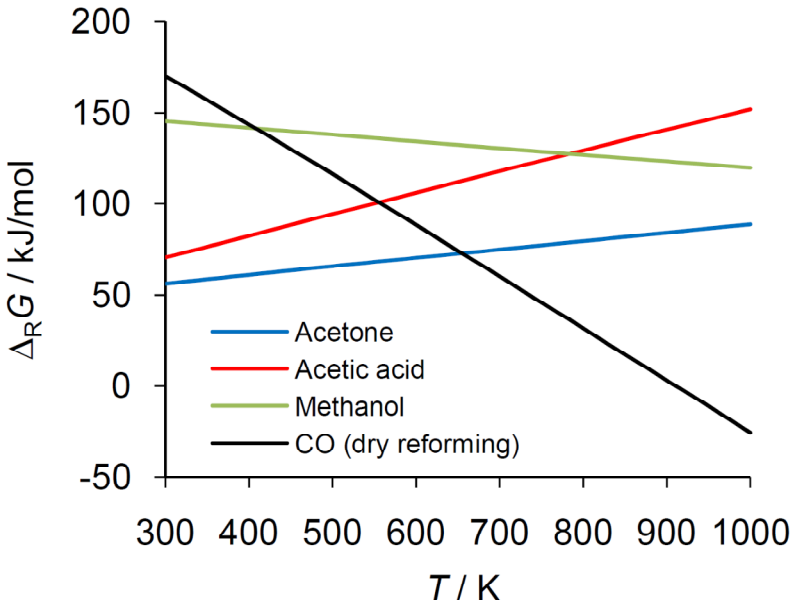

Figure 10. Gibbs enthalpies of gas phase reactions of methane with carbon dioxide.

Noble metals were widely investigated in the dry reforming reaction but they are too expensive. Ni was also found to be very efficient but catalysts based on nickel usually deactivate rapidly due to carbon deposition. Currently, a Ni-Ce-ZrO_2 catalyst system has been developed as a promising dry reforming catalyst, which is active at 1073 K and carbon deposition is minimized [163].

Carbon deposition is a major problem during dry reforming. Methane adsorbs on the catalyst surface and dissociates under release of hydrogen while the adsorbed CH_x-species remain on the catalyst surface. Above 400 K the CH_x species further dehydrogenate due to the pronounced stability of the carbon-catalyst bond, which results in the formation of a coke layer. Over noble metal catalysts such as Rh the CH_x-species were found to favorably react with CO_2 rather than decompose to carbon [164, 165], resulting in a longer life-time. The C-H bond activation in methane is the only kinetically relevant step in the dry reforming reaction because the reactions of carbon dioxide with the adsorbed species at the catalyst surface are fast. Pt was also examined for dry reforming and it was found that small crystallites being rich in coordinatively unsaturated Pt are more active than larger ones. Here, CH_x-species are bounded stronger, which lowers the C-H bond activation energy. This results in enhanced methane activation rates for dry reforming, which were reported to be dependant only on the Pt cluster sizes [44]. It can be concluded that not only

the chemical composition of the catalyst but also its synthesis and crystallite sizes play an important role.

2.4 Catalyst Synthesis Methods

The world demand for catalysts used in chemical synthesis, petroleum refining and polymerization will rise 6.3% per year to $17.2 billion in 2014 [166]. Hence the synthesis of catalysts, especially the optimization of the existing methods is of permanent interest. The performance of a catalyst namely the stability, activity and selectivity is strongly influenced by its synthesis [143, 134, 144].

The larger volumes of produced catalysts in industry are heterogeneous catalysts. This chapter will therefore focus on the synthesis of heterogeneous catalysts, especially on those methods used in this work for OCM catalysts because there is a broad variety of synthesis methods, which cannot be covered here.

2.4.1 Co-Precipitation

Co-precipitation and precipitation of single components are technically important synthesis methods [167], which are used for synthesizing several catalysts necessary for industrial processes as for example Al_2O_3 for the Claus process, the SiO_2 support for hydrogenation reactions, Fe_2O_3 for Fischer-Tropsch reaction, ZrO_2 for methanol synthesis and methanol steam reforming, $AlPO_4$ for polymerization, Sn-Sb-oxides, Bi-molybdates and $(VO)_2P_2O_7$ for selective oxidation reactions. The main difference to the also important sol-gel method is that here a clear phase separation occurs.

The co-precipitation requires a precise control of the synthesis conditions and therefore also demanding equipment. The surface area of the resulting particle is determined during the precipitation process by agglomeration of primary and secondary particles. Also the particle size, shape, the porous structure and other characteristics of the resulting particles are determined in this step that’s why the realization of the co-precipitation is very demanding. The process conditions as temperature, feed rate, pH value, mixing and stirring strongly affect the properties of the material so precision equipment is needed to control these conditions. An

overview over the most important influencing parameters of the co-precipitation is given in Figure 11.

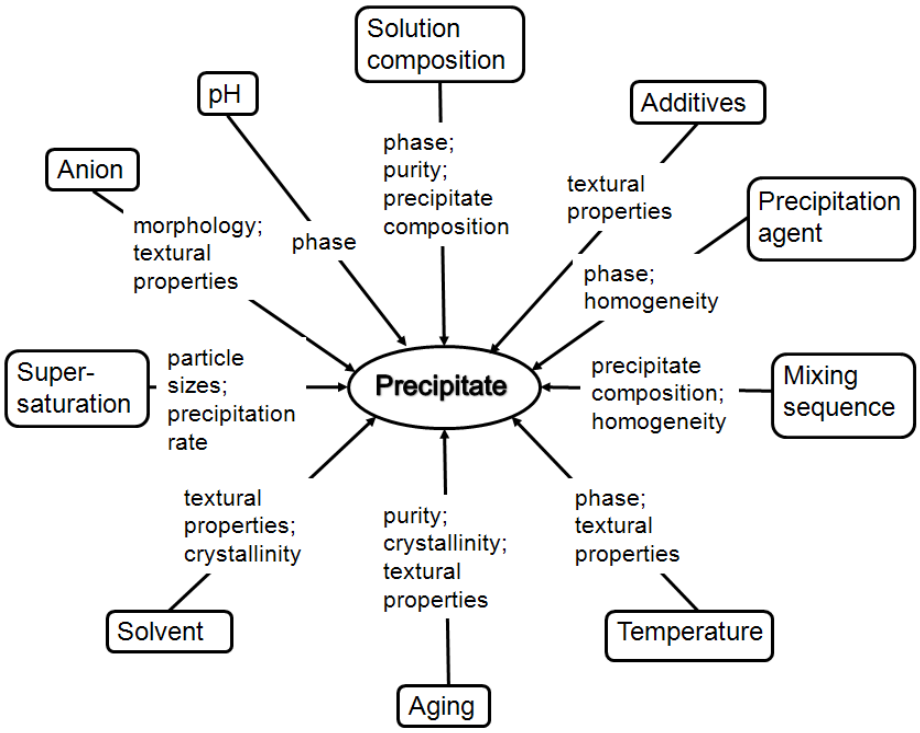

Figure 11. Overview over the main influencing parameters and their effects on the resulting precipitated material [168].

The main steps of the co-precipitation are precipitation, filtration, washing, shaping, drying, calcination and sometimes also the activation of the catalyst. Figure 12 shows a preparation scheme with the main steps in the co-precipitation. As mentioned above the precipitation is the most crucial step because many properties are determined thereby. The precipitation takes place in 3 steps: the liquid mixing, nucleation and crystal growth to form the primary particles which subsequently aggregate. The nucleation and the crystal growth proceed in parallel. First clusters are formed in the nucleation period whereby smaller clusters redissolve and bigger ones grow.

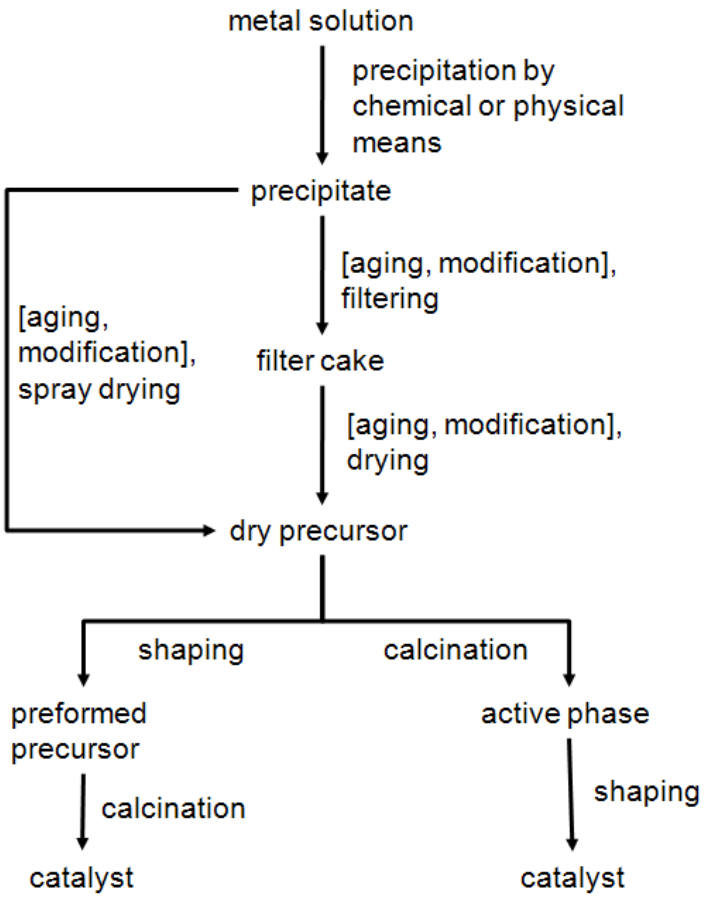

Figure 12. Preparation scheme for the formation of a catalyst by the co-precipitation method (optional steps in parentheses) [168].

For the nucleation which is strongly dependant on the concentration and the temperature also an energy barrier has to be overcome similar to a chemical reaction, therefore a supersaturated solution is needed. The best situation is a homogeneous nucleation where the solid is formed in the bulk of the solution which is initially free of any solid particles. But in practice this is usually not the case. A simplified scheme to describe the formation of solid particles from a solution is shown in Figure 13. The most important curve is the precursor concentration curve which shows the change of the concentration with time. The precipitation starts at the critical saturation concentration and only above this value particle formation takes place. If the concentration is lowered by the consumption of the e.g. metal ions in the solution via particle growth and the concentration is below the nucleation threshold then no further nucleation will take place and only existing particles will continue growing. If the concentration is over the nucleation threshold the solution is called

supersaturated. If the concentration is very high above the threshold the nucleation period will be longer and therefore the particle size distribution will be very wide. In addition high supersaturation levels favor the precipitation of highly dispersed materials and low supersaturation will favor the formation of less but larger crystals. The size of the particles strongly depend on the size of the shaded area under the precursor concentration curve. The bigger this area is the smaller (and the more) the resulting particles are. When multicomponent systems like perovskites are synthesized by co-precipitation, it is very important to work at high levels of supersaturation so that all components precipitate and nucleate at the same time and no undesired gradients will exist in the resulting material.

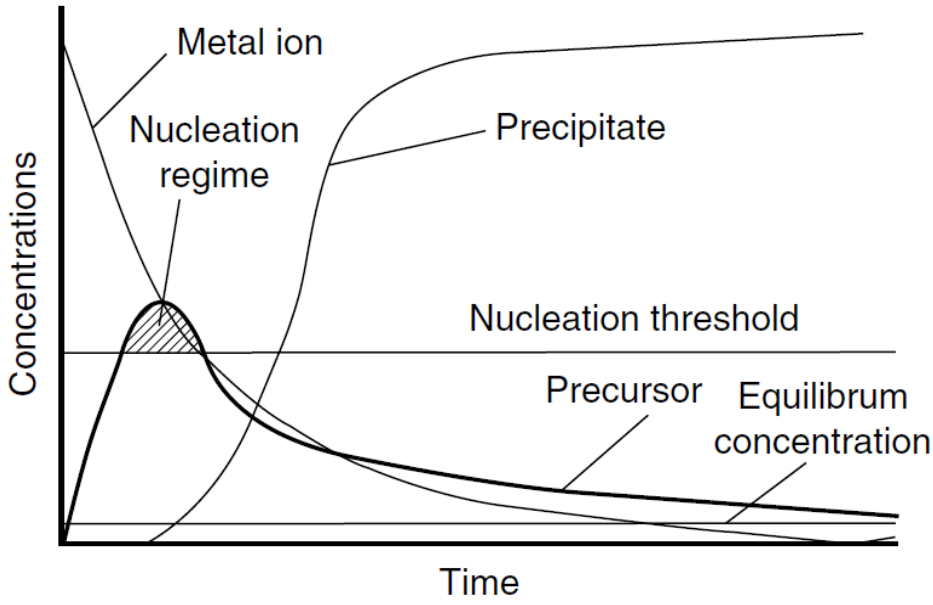

Figure 13. Simplified scheme for the formation of particles from solution. From the metal ion a precursor species is formed (e.g. via hydrolysis or by rising of the pH). When the concentration of the precursor species reaches the nucleation threshold the precipitation of the product starts while consuming the precursor by nucleation and growth. New nuclei are only formed in the shaded area.

Supersaturation can be achieved by physical changes like cooling of the solution or the evaporation of the solvent but also by chemical changes like the addition of a precipitation agent or the direct reaction of the ions to form an insoluble salt, metal or oxide. The precipitation agent changes the pH value, oxidizes or reduces the

precursor if necessary and leads to condensation and precipitation as hydroxide or oxide.

The solvent of the solution is most frequently water, not only because its non-toxic and cheap but also because the solubility of most desired salts is best in water. The solubilities are very important so that no undesired gradients or wrong stoichiometries are formed. The solubilities are very different it is advisable to work at high levels of supersaturation. The salt precursors should be chosen in a way that all undesired counter ions can be removed in the calcinations step like nitrates, carbonates or ammonium which decomposes to volatile products during calcination. For synthesizing catalysts the salts are very often precipitated as hydroxides, oxohydrates or oxides. For spinel-type oxides the precipitation of oxalates is also described to produce good results [169]. In general the catalytic activity can be affected by changing the precipitation conditions.

A big advantage of the co-precipitation method is the high metal loading of up to 60 wt% sometimes even up to 80 wt% or more in contrast to e.g. the impregnation method were only 30 wt% metal loadings can be achieved. Hence the co-precipitation catalysts are also described as bulk or self-supporting catalysts. Also due to the high achievable metal dispersion the co-precipitation catalysts possess a high weight and volume related activity. This precipitation method produces very pure materials with a high flexibility with respect to the final solid products. It is convenient for producing catalysts with a homogeneous distribution of the components and for precursors with well defined stoichiometry which can be easily converted to active catalysts.

The co-precipitation possesses of course also drawbacks. It is very difficult to assure a constant quality of the precipitation products during the whole process. In addition there is no optimal process condition which is the best for all particle characteristics. So the process conditions have always to be adjusted to the properties the resulting particles should possess. Another disadvantage is the large volume of salt solution which is needed and the material has to be separated from the solution after precipitation which is mostly done by filtration. For an industrial application another drawback is that the final product is a powder with particle diameters of 5 to 30 µm.

The powder can be shaped but the calcinations conditions have to be milder than with pre-shaped catalysts in order to avoid sintering effects.

2.4.2 Sol-Gel Methods

The sol-gel method is a suitable way to synthesize all kinds of catalytic materials but also support materials. It was originally developed as a tool for controlling the texture of pure metal-oxide phases and it became a common method to produce all kinds of porous materials out of a solution. Its application but also its principals are well described in literature [170, 171]. To form a material out of a solution of molecular precursors requires different actions as chemical reactions and physical processes like phase separation, dissolution, evaporation, phase transition and others.

In the first step the “sol” is formed by producing a stable colloidal solution followed by an anisotropic condensation of the colloids (micelles). Thereby polymer-chains are formed in which by-products of the condensation are entrapped. If no external solvent is used a gel is formed. The by-products and the solvents are removed and an aero- or xerogel is formed depending on the drying method. The resulting primary particles possess a well-defined structure and a typical texture [172, 173]. Further detailed information about the principals and the physical and chemical basics of the single steps are given in literature [171, 174, 173]. In Figure 14 an overview over the single steps of the formation of a material by the sol-gel-method in given.

After the starting reagents are mixed the first two steps occur in parallel so they are hard to distinguish in practice. The precursor determines the proceeding reactions in the sol-gel synthesis, the additives (solvent, reagents, catalysts) and the needed conditions (pH, reaction time, concentration, temperature, drying method) to control the properties of the resulting material. But also other factors (rates of the activation or condensation, costs, availability and compatibility of the reagents or physical properties as viscosity, stability) affect the planning of the process and its course.

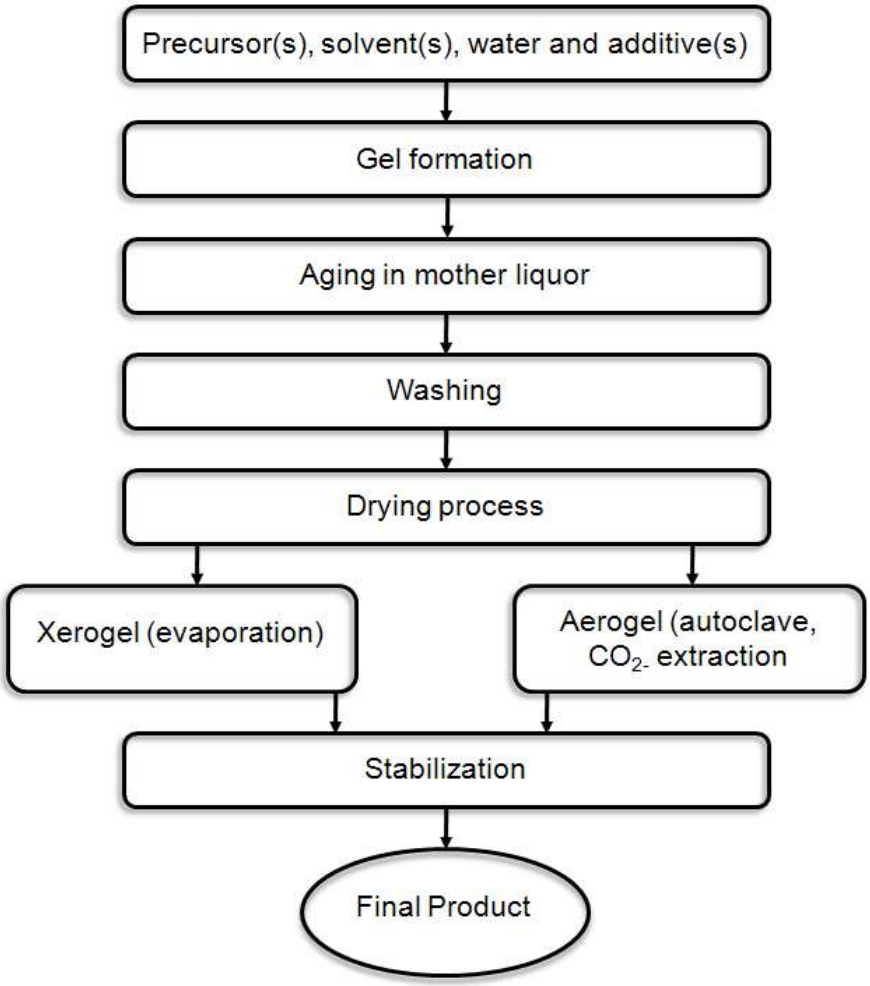

Figure 14. Scheme for the sequence of process steps in the sol-gel method for synthesizing porous solid catalytic materials [173].

A colloidal solution is formed only in the sol-gel synthesis so it has to be distinguished from other synthesis methods performed in solution like precipitation, expansion of supercritical solvents or crystallization. In addition polymer chains are formed here due to the interaction of the reactive groups caused by the mixing of the particles. Also the flocculation is avoided due to the isotropic micelle aggregation.

Thanks to the characteristics of the sol-gel method three different kinds of materials can be formed:

i) Bulk uniphasic materials (mono- or multimetallic gels)

ii) Bulk multiphasic materials (the molecular part and the condensed phase is entrapped between the polymer chains)

iii) Porous uni- and multiphasic coatings and nanometric films (formed by the gel as thin film or the gel directly on the support)

The sol-gel process is a universal synthesis for the full spectrum of modern catalytic materials from multimetallic composite oxide phases to organic-inorganic hybrid interphase catalysts, heterogenized enzymes and catalytic coatings and films. It offers the possibility for the chemical functionalization of porous materials and the control of the texture. The fact that the material is a viscous liquid before it is solidified offers the opportunity to control the shape and the size of the material. It can be nanosized, formed as a thin film or it can be inserted into a matrix.

2.4.3 Template Methods

For the preparation of heterogeneous catalysts the template methods is an essential synthesis tool which is not only used in lab-scale, it is also an important widely applied industrial tool. This is not at least due to the simplicity of this method. No complicated and expensive equipment is needed. Furthermore every kind of metal gradient distribution can be realized reaching from a homogeneous to an eggshell like distribution.

The synthesis of molecules with the assistance of templates especially the synthesis of sterically demanding or cyclic molecules is known since the 1960s. There exist any different kinds of templates such as metal ions, neutral molecules or covalent bound templates. One of the first chemists who used template-synthesis was Busch who defined a template as following: “A chemical template organizes an assembly of atoms with respect to one or more geometric loci in order to achieve a particular linking of atoms.” [175].

Metal ions and neutral molecules can coordinate ligands or guest-molecules. Thereby particular conformations are formed, which are suitable for the formation of the desired product. All intermolecular forces which exist in host-guest pairs stabilize binary and ternary complexes. Metal cations are chelated permanently or temporarily e.g. as copper-phthalocyanine [176] or by crown ethers [177].

Neutral molecules support electrostatic interactions and hydrogen bonds. The driving force of the template synthesis, if a π-donor is added to the reaction mixture in access, is the so-called π-stacking, which leads to an increase of the yield [178].

For the synthesis with temporary templates no molecular identification is needed. The template gets eliminated at the end of the synthesis and is not part of the final product. There exist also covalently bound templates such as nitrogen or sulfur, which are eliminated from the product via pyrolysis and covalent bound templates which stay permanent in the molecule such as the insertion of a side-chain during the formation of a macro-cycle.

In this work two synthesis methods were tested using temporary templates, more precisely microemulsion templates and cellulose templates.

Microemulsions are colloidal dispersions, which consist of water, oil and a surfactant. These emulsions are macroscopically translucent. In water-in-oil microemulsions the small water droplets (micelles) in the nanometer length scale act as reactors for the material synthesis. Therefore the size of the resulting particles is limited to the size of these water droplets, the micelles are thereby the size-template for the particles because the precipitation of the material takes place only inside of the micelles.

The particle synthesis in microemulsions was already examined extensively in literature [179–182]. An overview over the formation of particles in micelles was given by Erikson and co-workers [179] (Figure 15). Two microemulsions, each containing a reactant, e.g., one with a dissolved metal salt precursor and the other containing a precipitation agent, were mixed together under stirring. The micelles coalesce and thereby the reaction, in the example above the precipitation, can take place in the droplets which limit the size and regulate the shape of the resulting particles.

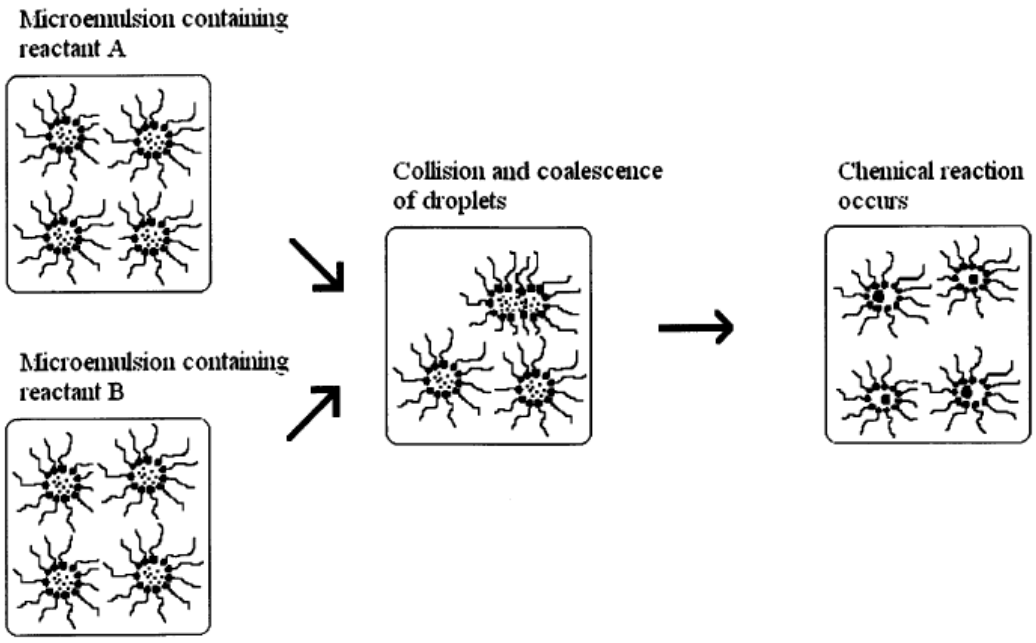

Figure 15. Scheme of the formation of particles in microemulsions [179].

Another approach for a template-precipitation synthesis is the cellulose template method, whereby the particle size and the particle shape are dependent on a template more precisely a cellulose template. This approach is a very simple synthesis method. The cellulose template which is e.g. a filter paper is impregnated with a solution. This solution contains dissolved salts which are basically nitrates, carbonates, hydroxides, acetates, oxalates or other salts with counter ions which decompose residue-free during the calcinations process. The metal cation(s) gets oxidized to the corresponding (mixed-) metal oxide which possesses mainly the morphology of the cellulose template. The template itself should be an ash free burning cellulose material.

Several publications deal with the cellulose template method and found convincing results [183–185]. Shigapov and co-workers examined this method for synthesizing metal oxides and supports. They show interesting results such as SEM images which display the cellulose template and the resulting particles (Figure 16). It can clearly be seen that the resulting metal oxide represents the shape and structure of its template.

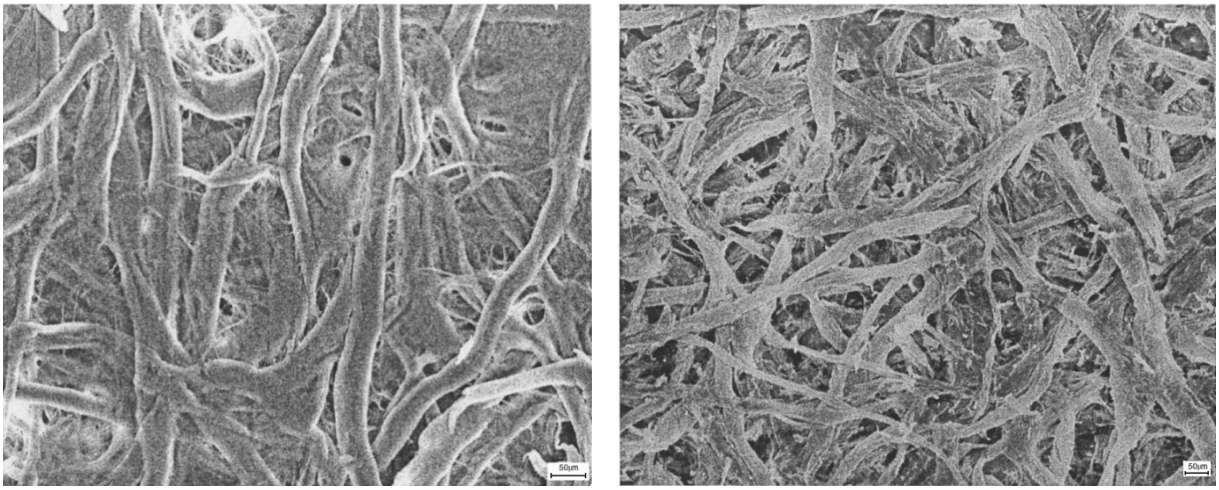

A B

Figure 16. SEM images of Whatman 50 filter paper (A) and Pr-Ce-Zr mixed oxide (B) which was synthesized by the cellulose template method with impregnated Whatman 50 filter paper and subsequent calcinations (1073 K for 2 h) [183]**.**

3 Experimental Methods

3.1 Catalyst Preparation

3.1.1 Materials

The following chemicals were used in this work without further purification. Table 3 shows the stoichiometries, purities and suppliers of the substances.

Table 3. Chemicals used in this work.

Name	Chemical composition	Purity	Supplier
Strontium acetate	$Sr(CH_3COO)_2 \cdot 0.5H_2O$	> 99%	Fluka
Cobalt acetate	$Co(CH_3COO)_2 \cdot 4H_2O$	> 99%	Fluka
Calcium acetate	$Ca(CH_3COO)_2 \cdot xH_2O$	≥ 99%	Sigma-Aldrich
Lanthanum nitrate	$La(NO_3)_3 \cdot xH_2O$	≥ 99.0%	Sigma-Aldrich
Neodymium nitrate	$Nd(NO_3)_3 \cdot 6H_2O$	99.9%	Aldrich
Barium nitrate	$Ba(NO_3)_2 \cdot xH_2O$	≥ 99%	Sigma-Aldrich
Praseodymium nitrate	$Pr(NO_3)_3 \cdot 6H_2O$	99.9%	Aldrich
Samarium nitrate	$Sm(NO_3)_3 \cdot 6H_2O$	99.9%	Aldrich
Manganese nitrate	$Mn(NO_3)_2 \cdot xH_2O$	99.99%	Aldrich
Iron nitrate	$Fe(NO_3)_3 \cdot xH_2O$	99.99%	Aldrich
Chromium nitrate	$Cr(NO_3)_3 \cdot xH_2O$	99%	Sigma-Aldrich
Ammonium heptamolybdate	$(NH_4)_6Mo_7O_{24}$	99.98%	Sigma-Aldrich
Magnesium nitrate	$Mg(NO_3)_2 \cdot 6H_2O$	99.99%	Aldrich
Lithium nitrate	LiNO3	99.99%	Aldrich
Ammonium cerium nitrate	$(NH_4)_2Ce(NO_3)_6$	≥ 98%	Sigma-Aldrich
Lanthanum acetate	$La(CH_3COO)_3 \cdot xH_2O$	99.9%	Aldrich
Neodymium acetate	$Nd(CH_3COO)_3 \cdot xH_2O$	99.9%	Aldrich
Rubidium hydroxide	RbOH	99.8%	Strem Chemicals
Silicium oxide	SiO2	Purum p.a.	Sigma-Aldrich
Ammonium tungstate	$(NH_4)_{10}H_2(W_2O_7)_6$	99.99%	Aldrich
Sodium tungstate	$NaWO_4$	99.995%	Aldrich
Magnesium oxide	MgO	< 99%	Sigma-Aldrich
Lithium carbonate	Li_2CO_3	< 99%	Sigma-Aldrich
Sodium permanganate	$NaMnO_4 \cdot H_2O$	< 97%	Sigma-Aldrich
Strontium carbonate	$SrCO_3$	≥ 99.9%	Aldrich

Yttrium oxide	Y_2O_3	99.99%	Aldrich
Barium fluoride	BaF_2	99.99%	Aldrich
Methane N35	CH_4	≥ 99.95%	Air Liquide
Oxygen	O_2	≥ 99.999%	Air Liquide
Helium N50	He	≥ 99.999%	Air Liquide
Arcal 15	5% ± 0.5% H_2 in Ar	≥ 99.999%	Air Liquide
Oxalic acid	$C_2H_2O_4 \cdot 2H_2O$	99.5%	Merck
Cyclohexane	C_6H_{12}	99.5%	Roth
Ammonia (aq)	NH_3	33 wt% in H_2O	Roth
Methanol	CH_3OH	99.9%	Roth
Marlipal O13/50, O13/100, and O24/50[a]	Alkyl polyglycolethers	Technical grade	Sasol
Triton X-100	*t*-Oct-C_6H_4-$(OCH_2CH_2)_xOH$, x= 9-10	Technical grade	Sasol
Whatman 50 filter paper	Cellulose	< 0.015% Ash	Whatman
[a] The Marlipal surfactants differ in their ethoxylation degree due to their production process. The mean ethoxylation degree is indicated in the surfactant name, e.g. Marlipal O13/50 has a mean ethoxylation degree of five.			

3.1.2 Microemulsion Templating

The composition of the w/o-microemulsion is specified by the weight fraction of oil α in the mixture of water and oil and the weight fraction of surfactant γ in the ternary mixture. Two w/o microemulsions of identical composition were prepared. In the standard recipe, the oil-fraction of both microemulsions is cyclohexane with α = 0.85, the surfactant is Marlipal O13/50 with γ = 0.15, and the total volume of both micro-emulsions is 220 mL. In the water fraction of the first microemulsion (A), 0.24 mol L^{-1} strontium acetate and 0.24 mol L^{-1} cobalt acetate were dissolved. The water fraction of the second microemulsion (B) consisted of a saturated aqueous solution of oxalic acid. Both microemulsions were combined in a semi-batch process (3 mL min^{-1}) at 303 K under vigorous stirring (1,000 min^{-1}). The precipitation of oxalates immediately occurs during the combination of the microemulsions as reported by Schmidt *et al.* [181]. After complete addition of microemulsion A, the reaction mixture was stirred for further 30 min. Subsequently the combined microemulsion was destabilized by adding 100 mL of a methanol–water mixture. The separated water phase was then

centrifuged at 3,000 rpm to obtain the precipitated oxalates. The precursors were subsequently dried for 12 h at 403 K in air, followed by calcination in air at 1,073 K for 5 h. The synthesis procedure is illustrated in Figure 17 and Figure 18.

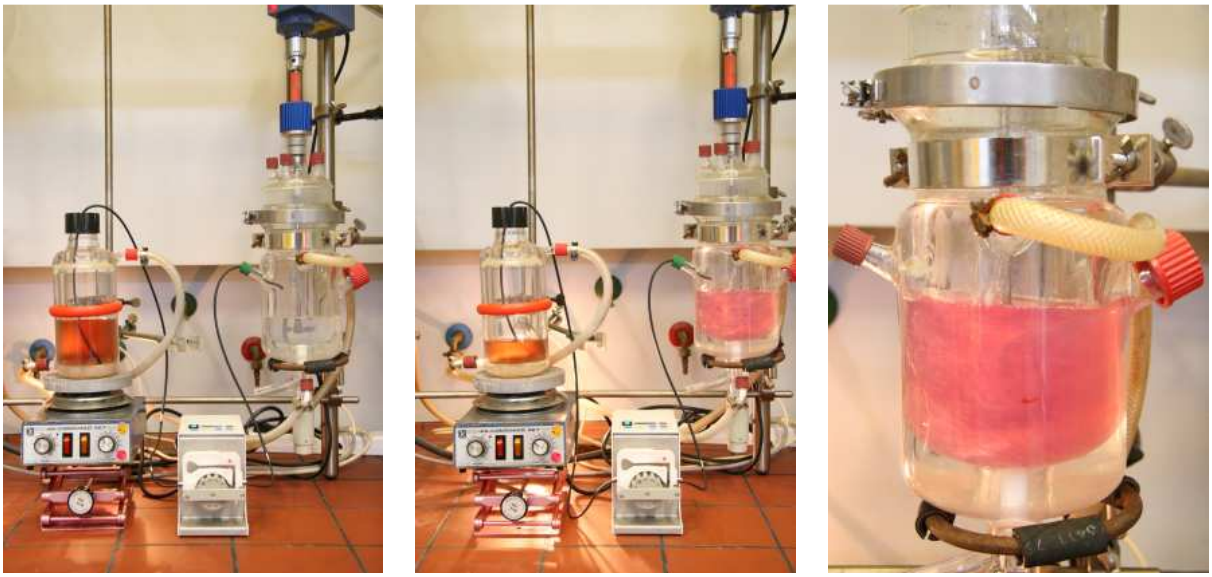

Figure 17. Unification of the microemulsions containing metal cations (brownish solution in stirred glas storage bottle) and oxylic acid (colorless solution in stirred glas reactor with heating jacket). The combined microemulsion turns pink.

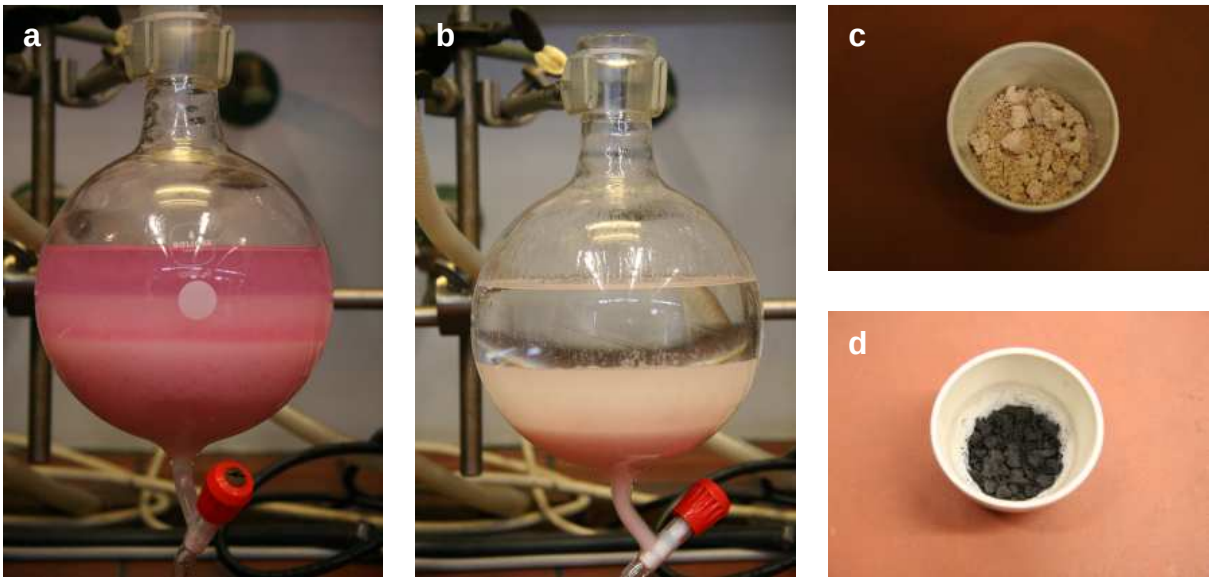

Figure 18. (a,b) Aging of the precipitate after destabilization of the combined microemulsion with methanol in a separatory funnel. (c,d) Color change of the centrifuged and dried precursor during calcination in air.

3.1.3 Cellulose Templating

Metal acetates and nitrates were dissolved in stoichiometric amounts in deionized water. The solution (0.35 mol L^{-1}) was carefully dripped onto filter paper in the ratio of 1.7 mL g^{-1} liquid per filter paper to achieve maximum surface area according to the optimization of cellulose templating (CT) parameters by Shigapov *et al.* [183]. Subsequently, without drying, the impregnated stack of filter papers was transferred into a stainless steel box and then into a preheated muffle oven and calcined for 3 h in air. Precursors and the calcination temperatures for each catalyst prepared by this method are listed in Table 5.

3.1.4 Other Methods

3.1.4.1 Strontium Cobaltate Catalysts

Reference samples of $SrCoO_x$ catalyst precursors were prepared by co-precipitation (CP) and synthesized by dissolving 0.24 mol L^{-1} cobalt acetate and 0.24 mol L^{-1} strontium acetate in water. The same quantity of a saturated aqueous solution of oxalic acid was added to achieve precipitation of the precursors. The mixture was centrifuged at 3,000 rpm, dried at 403 K for 12 h in air, and subsequently calcined in air at different temperatures (1,173 and 1,223 K) and times (5 and 12 h). Furthermore, the citric acid sol-gel (CSAG) method was applied according to Pecchi *et al.* [186]. Aqueous solutions of the metal acetates were mixed with a 1.1 fold excess of an aqueous solution of citric acid and the resulting mixture was stirred for 15 min at room temperature. Gel formation was achieved by water evaporation at 70℃. The resulting precursor was calcined at 1,073 K for 5 h in air.

3.1.4.2 Other Catalysts

Other catalyst samples were prepared by the incipient wetness method or by cellulose templating (see Chapter 3.1.3). Details such as the precursor compounds are listed in Table 4. For incipient wetness preparation the precursor compounds were mixed in the calculated molar ratios and moistened with deionized water. The thick paste was properly ground and dried at 120 ℃ for several hours. For catalysts containing SiO_2 as a support, the other compounds were dissolved in water and then

the solution was dripped on the support followed by drying. With both processes a grained solid was obtained, which was calcined in air at the given temperature.

Table 4. Catalyst precursors and preparation conditions.

Catalyst	Precursor compound	CT	IW	T_{calc}, t_{calc} (CT)	T_{calc}, t_{calc} (IW)
Li/Ce/MgO	$Mg(NO_3)_2 \cdot 6H_2O$ $LiNO_3$ $(NH_4)_2Ce(NO_3)_6$	x	X	120 °C, 16 h	800 °C, 4 h
La/CaO	$La(CH_3CO_2)_3 \cdot xH_2O$ $Ca(CH_3CO_2)_2 \cdot xH_2O$	x	X	120 °C, 12 h	850 °C, 10 h
Nd/CaO	$Nd(CH_3CO_2)_3 \cdot xH_2O$ $Ca(CH_3CO_2)_2 \cdot xH_2O$	x	X	120 °C, 12 h	850 °C, 10 h
Rb_2WO_4/SiO_2	$Rb(OH)_2$, $(NH_4)_2WO_4$, SiO_2		X	120 °C, 8 h	750 °C, 8 h
Na_2WO_4/SiO_2	Na_2WO_4, SiO_2		X	120 °C, 8 h	750 °C, 8 h
0,1 at% Li/MgO	MgO, Li_2CO_3		X	120 °C, 5 h	750 °C, 3 h
$NaMnO_4/MgO$	MgO, $NaMnO_4 \cdot H_2O$	x	X	120 °C, 12 h	850 °C, 16 h
1 at% Sr/La_2O_3	$SrCO_3$, $La_2O_2CO_3$	x	X	120 °C, 12 h	750 °C, 5 h
BaF_2/Y_2O_3	Y_2O_3, BaF_2		X	120 °C, 12 h	800 °C, 5 h
$LaMn_{0,8}Fe_{0,2}O_x$	$La(CH_3CO_2)_3 \cdot xH_2O$ $Mn(NO_3)_2$, $Fe(NO_3)_3 \cdot 9H_2O$	x		120 °C, 12 h	800 °C, 5 h

The following catalysts were prepared according to more complex synthesis routes reported in literature: Na(0,32g)/$BaSrTiO_3$ [59], $BaYSmO_x$ [57], $SrNi_{0.75}Li_{0.25}O_x$, and $Sr_{0.75}Na_{0.25}NiO_x$ [56].

3.2 Physico-Chemical Characterization of the Catalysts

3.2.1 N_2 Physisorption

Specific surface areas of the catalysts were determined by adsorption of nitrogen at 77 K according to the method by Brunauer, Emmet, and Teller (BET). Prior to the measurements, the samples were dried for 2 h at 473 K in vacuum. Nitrogen adsorption was performed using a Quantachrome Autosorb-6B KR sorptometer. The

adsorption branch in the range of p/p_0 = 0.05–0.3 was automatically analyzed using the Autosorb Multistation software by Quantachrome.

3.2.2 X-ray Diffraction

Information about the crystallographic phases and crystallite sizes in the catalyst samples was obtained by X-ray diffraction (XRD). The average particle size was estimated using the Scherrer equation (Eq. 15), which can be applied for crystallites up to 100–150 nm in diameter.

$$\langle d_{hkl} \rangle = \frac{K \lambda}{\beta \cos\theta} \tag{15}$$

$\langle d_{hkl} \rangle$ is the mean length of the crystallite in a direction perpendicular to the reflection planes (hkl), K is the Scherrer constant, β is a measure of the line broadening, λ is the wavelength of the X-ray and θ is the angular position of the reflection peak. A Bruker AXS D5005 diffractometer was applied for XRD measurements on powder samples. $Cu_{K\alpha}$ radiation (λ = 0.154 nm), a scanning speed of 0.04° s^{-1} and a spectral resolution of 0.008° were used.

3.2.3 Temperature-Programmed Reduction

The reducibility pattern of the catalysts was measured by H_2-TPR. 100 mg of the powder catalyst was mixed with 300 mg quartz sand and filled into a tubular quartz glass reactor with an inner diameter of 6 mm. The reactor was flushed at ambient temperature with pre-mixed 5% H_2/Ar (Noxal) until all traces of air and water are removed as followed by online MS. Then the catalyst was heated up to its calcination temperature but not higher than 1,153 K with a heating rate of 5 K min^{-1} in a stream of 50 mL min^{-1} of 5% H_2/Ar. The offgas was analyzed using an online MS (GAM 200, In Process Instruments). The feed components and reaction products were detected at the following m/e values: 2 (H_2), 18 (H_2O), and 40 (Ar).

3.2.4 Scanning and Transmission Electron Microscopy

The visualization of morphology and structural features of the catalyst samples was performed at ZELMI by scanning electron microscopy (SEM) and transmission electron microscopy (TEM). SEM was performed on a Hitachi S-4000 (HHT) instrument. TEM images were taken on a FEI Tecnai G2 20 S-Twin microscope including elemental analysis by energy dispersive X-ray spectroscopy (EDX, EDAX) with a resolution of 134 eV. Specimens were prepared by dripping the catalyst dispersion, which was prepared by ultrasonication in ethanol, onto a carbon TEM grid and drying in air.

3.2.5 Inductively Coupled Plasma Optical Emission Spectroscopy

Inductively coupled plasma optical emission spectroscopy (ICP-OES) measurements were performed on a Jobin-Yvon JY 38 PLUS spectrometer and used to determine the elemental composition of perovskites. The catalyst samples were dissolved in aqua regia and the light emissions at characteristic wavelengths were referred to those of the respective standard solutions of the metal cations.

3.2.6 Thermogravimetry-Differential Thermoanalysis

The thermogravimetry-differential thermoanalyses (TG-DTA) give insight into phase transformation processes and chemical reactions during the calcination processes. Experiments were performed with a Netzsch, STA 409 PC apparatus. In these tests, the precursors were heated from ambient temperature to 1,373 K with a heating rate of 10 K min^{-1} in air. The weight loss and the temperature change as well as the formation of water (m/e = 18) and carbon dioxide (m/e = 44) were determined by on-line mass spectrometry (MS).

3.3 Catalytic Testing

3.3.1 Catalytic Measurements at TU Berlin

Catalytic measurements were performed in a single quartz tubular reactor with an inner diameter of 6 mm operating at atmospheric pressure. The mixture of 100 mg of

the powder catalyst and 300 mg quartz sand was placed on a quartz frit in the isothermal zone of the reactor, which is heated by a surrounding heating jacket. Gases were fed by electronic mass flow controllers. The catalyst was heated up to its calcination temperature but not higher than 1,153 K with a heating rate of 5 K min^{-1} in a CH_4/O_2:He = 20/10/70 atmosphere (50 mL min^{-1} total flow). The product gas mixture was analyzed using an online MS (GAM 200, In Process Instruments). The feed components and reaction products were detected at the following m/e values: 2 (H_2), 4 (He), 15–16 (CH_4), 17–18 (H_2O), 24–27 (C_2H_4, C_2H_6), 28 (C_2H_4, C_2H_6, CO, CO_2), 29–30 (C_2H_6), 32 (O_2), and 44 (CO_2).

3.3.2 Catalytic Measurements at LIKAT

Catalytic tests on the OCM reaction were carried out in parallel in a multi-channel reactor system located at LIKAT (Rostock). This set-up consists of 48 plug flow fixed-bed quartz reactors with an inner diameter of 4 mm (Figure 19). The feed gas mixtures, as introduced one after the other at atmospheric pressure, comprised CH_4/air, $CH_4/N_2O/N_2$, and $CH_4/CO_2/N_2$ mixtures in stoichiometric O/C = 2 ratio with regard to the OCM reaction while keeping the CH_4 concentration constant, i.e., $CH_4:O_2:N_2$ = 1:1:4, $CH_4/N_2O/N_2$ = 1:2:3, and $CH_4:CO_2:N_2$ = 1:2:3. The catalyst grains (250–300 µm) were diluted with quartz sand and filled into each reactor except one empty reactor to account for calibration and the detection of gas phase reactions. An in-house developed flow restrictor equally distributed the total gas flow to the 48 reactors with a constant single reactor flow of 15 mL min^{-1}. A variation of space velocity was realized by using different amounts of catalysts in parallel operating reactors. Thus, using catalyst masses between 50 and 500 mg, gas hourly space velocities (GHSV) of 3,600–100,000 h^{-1} were adjusted. The catalysts were heated in Ar up to 973 K and then brought in contact with the reactant feed. For each oxidizing agent, several reactor temperatures in the range of 973–1073 K with 50 K increments were adjusted. Each temperature was held for approx. 10 h, which corresponds to 3 cycles of GC analyses, to achieve steady state operation conditions.

The feed components and the reaction products were analyzed by an online gas chromatograph (Agilent 7890) equipped with PLOT/Q (for CO_2), AL/S (for hydro-carbons) and Molsieve 5 (for H_2, O_2, N_2, and CO) columns as well as flame ionization

and thermal conductivity detectors. The CH_4 conversion was calculated from the inlet and outlet concentrations of CH_4. The product selectivities were calculated on the feed basis. The GC analysis started after the system had reached reaction temperature and was carried out sequentially for each individual reactor.

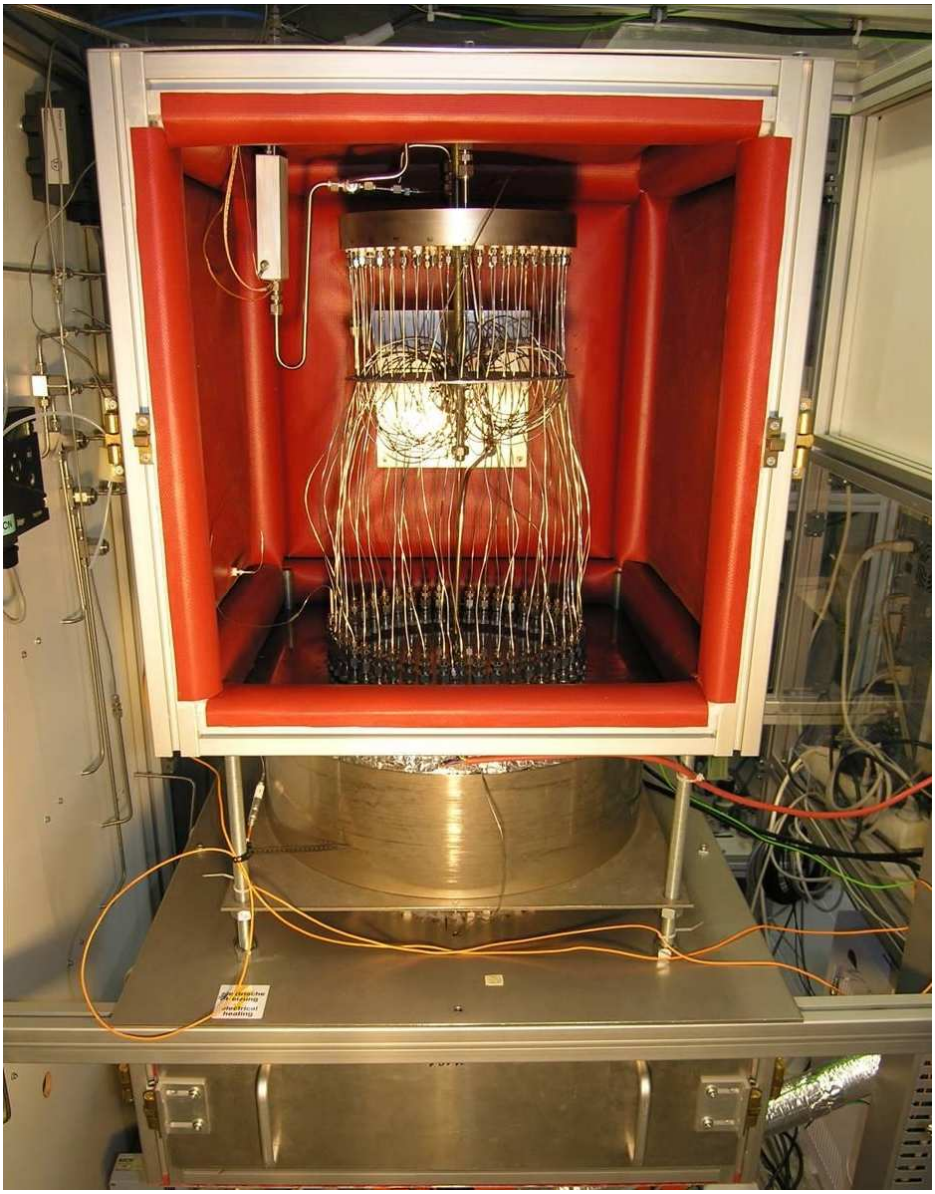

Figure 19. 48-Channel catalytic set-up used for OCM test runs at LIKAT (Rostock).

4 Results and Discussion

4.1 New Synthesis Strategies

4.1.1 Microemulsion Templating

The following chapter is published under the following citation: K. Langfeld, O. Görke, E.V. Kondratenko, R. Schomäcker, Catal. Lett. 141 (2011) 772-778.

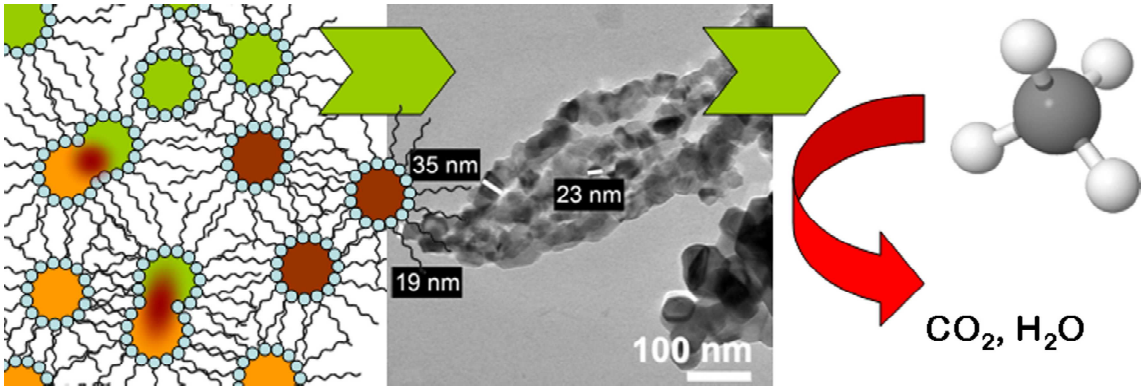

Abstract: Nanostructured perovskite-type $SrCoO_x$ catalysts were prepared using a w/o-microemulsion as a soft template. Conventional co-precipitation and citric acid sol–gel were used as reference methods with regard to surface and bulk physico-chemical properties as well as catalytic performance in methane oxidation. The solids were characterised by XRD, SEM, TEM, EDX, N_2-physisorption, TG-DTA-MS, ICP-OES, and H_2-TPR techniques. The phase transformation temperature of the microemulsion-templated perovskites is by 150 K lower than that in the conventionally prepared ones. Therefore, this material is characterized by smaller crystallite sizes and higher surface areas. As result, it shows a higher activity in oxidative coupling of methane as compared to sol–gel and co-precipitated catalysts. The properties of the catalysts are weakly influenced by changing the specific synthesis parameters of the microemulsions.

4.1.1.1 Specific Introduction

Nanoscience is one of the key branches of modern science [187] and the number of publications dealing with nanosized materials increased rapidly to more than 5,000 publications in 2008. Several routes to prepare nanosized materials are classified as physical, chemical, and physicochemical methods. The synthesis of metal

nanoparticles by microemulsion-templating (MT) was approved to be an interesting and environmentally friendly alternative [188]. Microemulsions are macroscopically homogeneous mixtures of oil, water and surfactant. Water-in-oil (w/o) microemulsions contain nanosized water droplets (reverse micelles) which can act as nanoreactors. Figure 20 shows a schematic overview for nanoparticle formation in reverse micelles. A major advantage of this method is the controllable and narrow particle size distribution of the MT-synthesized particles as compared to particles obtained by co-precipitation, impregnation, or precipitation deposition [179].

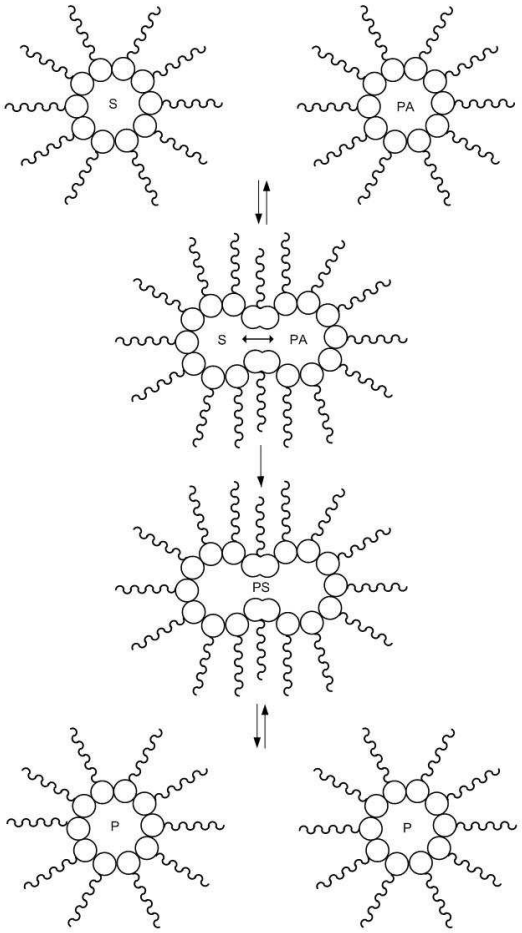

Figure 20. Schematic overview for the formation of nanoparticles in the reverse micelles of w/o-microemulsions; S salt, PA precipitation agent, PS precipitated salt, P particle.

In the present manuscript we apply a MT method to synthesize nanosized mixed metal oxides of the perovskitetype. Perovskites have the general $ABO_{3-\delta}$ formula

where A and B are usually rare earth and transition metal cations. Catalytic properties are often closely related to the type of B-site cation [96, 97]. The oxygen non-stoichiometry δ and its ionic conductivity inside the perovskite lattice are predominantly determined by the A-site cation [98]. Perovskites have been successfully used for many catalytic reactions, e.g., hydrogenation and hydrogenolysis of hydrocarbons, oxidation of carbon monoxide and ammonia, and catalytic combustion [189–192]. A well-studied perovskite system is strontium cobaltate $SrCoO_x$ [131, 133–135]. This composition is known for its wide range of oxygen non-stoichiometry. $SrCoO_x$ was successfully used as cathode material for intermediate-temperature solid oxide fuel cells [137], as oxygen separation membranes [138] and as a catalyst for methane combustion [139] or oxidative coupling of methane (OCM) [54, 140]. Physico-chemical and catalytic properties of $SrCoO_x$ are strongly influenced by its synthesis method [144]. To demonstrate the benefits of MT for perovskite preparation, we compared it with the conventional co-precipitation (CP) and citric acid assisted sol–gel (CASG) methods with regard to physical–chemical properties of $SrCoO_x$ materials and their applicability for oxidative methane conversion via OCM or for catalytic methane combustion. The removal of methane and other hydrocarbons, e.g., from exhaust gases, is important due to its stronger greenhouse effect as compared to carbon dioxide. A particular attention was paid at elucidating the specific parameters of MT, which may influence the properties of the resulting perovskites.

4.1.1.2 Phase Transformation Processes

In the present study, we prepared microemulsions with α = 0.85 and γ = 0.15 at 300 K. A one-phase w/o-microemulsion is formed under these conditions [180], which is required to produce nanoparticles in the nanosized reverse micelles. Marlipal O13/50 was used as the surfactant. The oxalate precipitation in the microemulsion is a rapid process and the resulting calcined particles are free of impurities as proven by EDX analysis. The stoichiometry of the MT-synthesized and calcined perovskite was determined using ICP-OES and EDX. The derived ratio of Sr:Co:O of 1.0:1.0:2.9 is in good agreement with the stoichiometries known from literature [193, 194]. XRD and the TEM examinations showed that the calcined MT mixed metal oxides consist of a

pure perovskite phase whereas both the CP and CASG samples after calcination comprise an additional impurity phase of cobalt oxide.

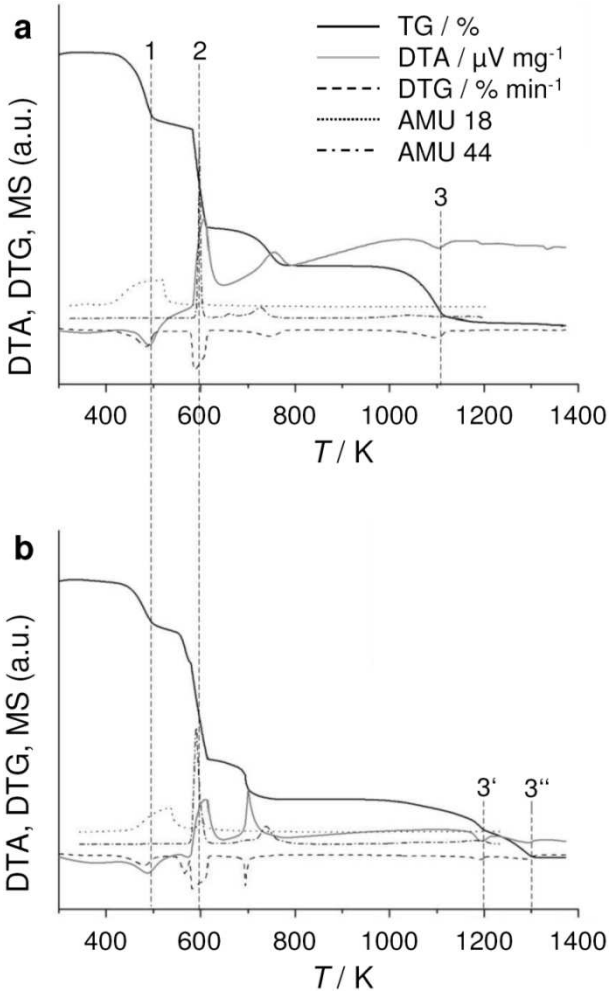

Figure 21. TG-DTA-MS profiles of a the MT-synthesized and b the CP perovskite-precursor

In order to determine the temperature of the phase transformation into the perovskite structure and thereby the optimal (minimum) calcination temperature, the calcinations procedure of perovskite precursors was thoroughly investigated by TG-DTA-MS. Figure 21 compares the TG-DTA-MS profiles of the MT and CP perovskite-precursors. Three different processes can be identified from these profiles. The first one is the endothermic water desorption at about 473 K. This dehydration step is not influenced by the preparation method. The second process is a two-staged oxalate

decomposition to the corresponding carbonates, which starts at about 573 K for both samples. The temperature of the two-staged oxalate decomposition agrees with previous studies [34, 195–197]. The last step is the phase transformation of the carbonates to the corresponding perovskites. The MT precursor showed a homogeneous one-step transformation to the perovskite at about 1,073 K. A similar TG-DTA-MS profile was also obtained, when the perovskite was prepared according to the CASG method. The results are not shown for brevity. In contrast, the corresponding transformation of the CP sample occurred in two steps at 1,173 and 1,273 K. Clearly, the MT precursor forms the perovskite-structure at about 100–200 K lower temperatures as compared to the CP precursor. The presence of the cobalt oxide phase in CP and CSAG samples could serve as an indicator of inhomogeneous precipitation process resulting in the formation of large aggregates of cobalt oxalate/citrate. The larger these aggregates the larger is their resistivity to perovskite-type mixed oxide phase formation. In this way we can interpret the Co oxalate/citrate cluster size in the order CP>CSAG>MT, the latter providing well dispersed microcrystallites with a low barrier to transform into the desired perovskite phase.

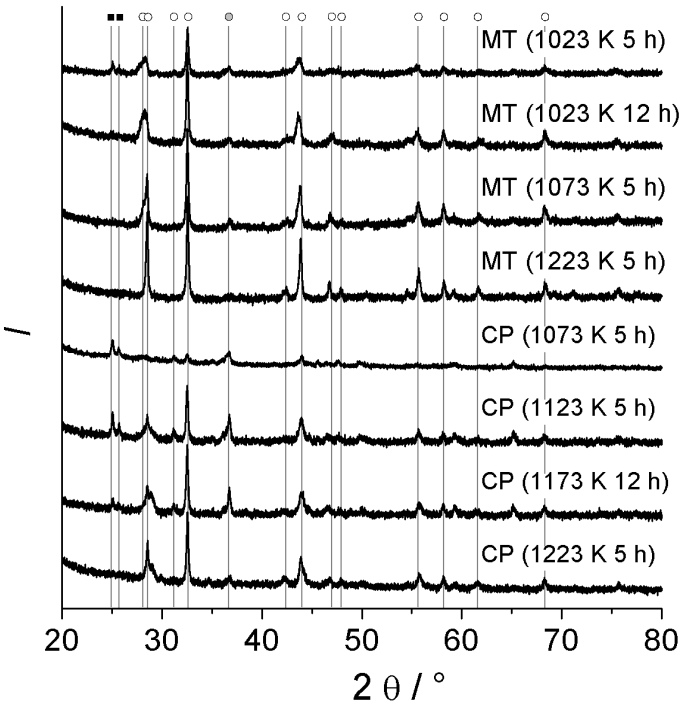

Figure 22. XRD patterns for MT and CP synthesized particles. Markers indicate the reflections of $SrCO_3$ (black squares), $SrCoO_3$ (white circles), and Co_3O_4 (grey circles).

In order to investigate the impact of the preparation method on the crystallinity of the perovskites, the perovskite precursors were calcined at different temperatures and afterwards analyzed by XRD (Figure 22). It is clearly seen that the MT precursor calcined at 1,023 K for 5 h showed nearly complete conversion to the perovskite phase [134] but also some traces of carbonates. These carbonates are completely transformed to the perovskite-structure after 12 h calcination at 1,023 K. A shorter time is required for the transformation at higher temperatures. The CP precursor is not completely transformed to the perovskite below 1,223 K. The XRD pattern of the CP precursor calcined at 1,173 K for 5 h fits to the XRD pattern of the MT precursor calcined only at 1,023 K for 5 h. The CASG precursors showed pure perovskite XRD patterns for calcinations at 1,073 K for 5 h. The results from the XRD experiments agree with those from the TG-DTA-MS measurements and confirm that the MT-synthesized precursors formed the perovskite-structure at 150 K lower temperatures compared to the CP precursor. This is a big advantage of the MT route for preparing nanoparticles because less energy is needed and also less particle growth by sintering effects will occur. The average particle size of perovskites was determined from XRD analysis according to the Scherrer equation (Eq. 15) using the reflection at 32.5° and amounts to about 44 ± 2 nm for all perovskites calcined at or above 1,073 K for 5 h. For the MT perovskite calcined at 1,023 K for 12 h, the crystallite size was determined to be about 38 ± 2 nm. The determination of the crystallite size from the Scherrer equation is not exact because many parameters remain unconsidered but it indicates that the MT perovskite calcined at 1,023 K for 12 h has a smaller average crystallite size than all the other perovskites.

4.1.1.3 Particle Morphology an Reducibility

Specific surface areas of the CP $SrCoO_x$ calcined at 1,173 K for 12 h and at 1,223 K for 5 h amounted to 1.3 and 0.9 $m^2\ g^{-1}$, respectively. The MT $SrCoO_x$ calcined at 1,073 K for 5 h had a surface area of 2.9 $m^2\ g^{-1}$ and the one calcined at 1,023 K for 12 h showed a surface area of 3.1 $m^2\ g^{-1}$. The CASG particles calcined at 1,073 K for 5 h possessed a surface area of 2.9 $m^2\ g^{-1}$. These values are in the range of those previously reported in literature [96]. The differences in specific surface areas

between the MT-synthesized, the CASG synthesized, and CP perovskites are due to the lower temperature of phase transformation in the former method.

Further insights into surface morphology of the synthesized perovskites were derived from TEM and SEM (Figure 23). One can see from the TEM images that the particles of MT-synthesized perovskite exist in different appearances. The MT perovskite consists of nanoparticles varying in their size from about 40–70 nm (Figure 23a). The particle size is in agreement with the average crystallite size determined from the XRD analyzes. Isolated nanoparticles with a size of about 20 nm are also visible (Figure 23b). In addition, there are nanoscaled agglomerated particles (Figure 23c) and sintered particles (Figure 23d). The latter possess nanosized structures at the surface. Compared to the MT perovskite, the TEM-micrographs of the CP precursors show only big sintered particles with plane surfaces. The SEM micrographs evidence also agglomerated and sintered particles for the MT-synthesized sample (Figure 23e). However the sintered particles possess smaller dimensions than the particles of the CP sample (Figure 23f, scale bar).

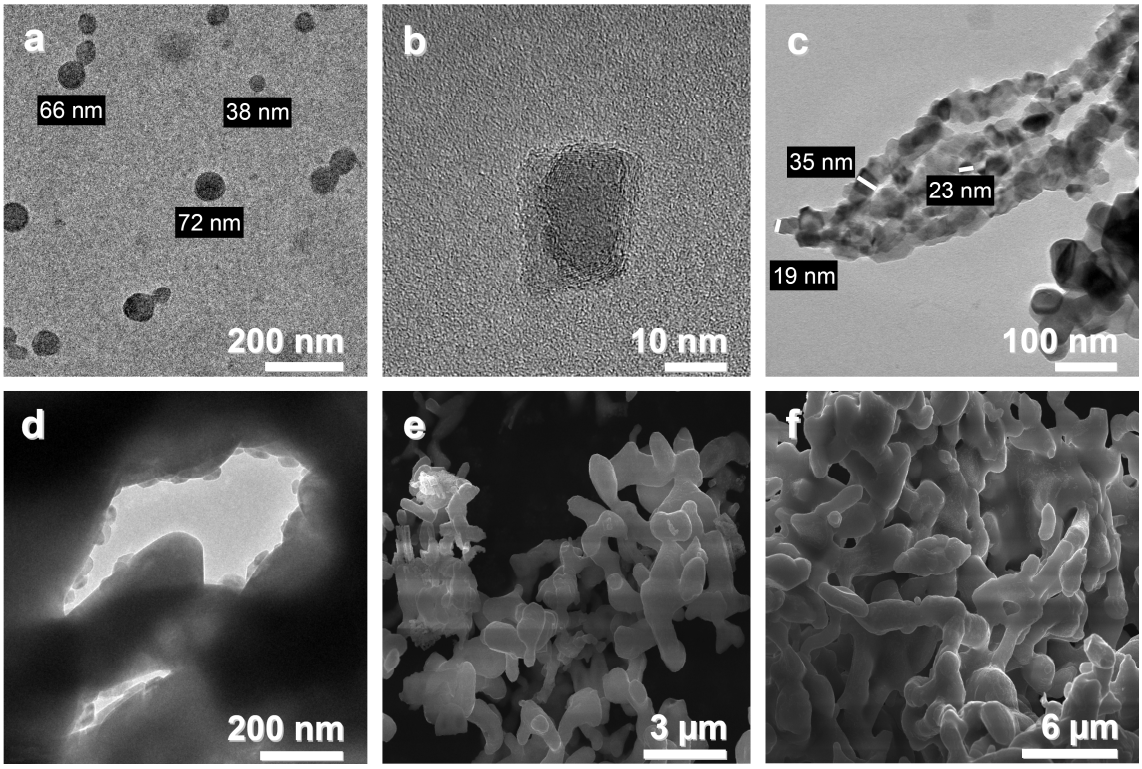

Figure 23. a–c TEM and d–e SEM micrographs of MT-synthesized $SrCoO_x$ particles; f SEM micrograph of CP-synthesized $SrCoO_3$ particles.

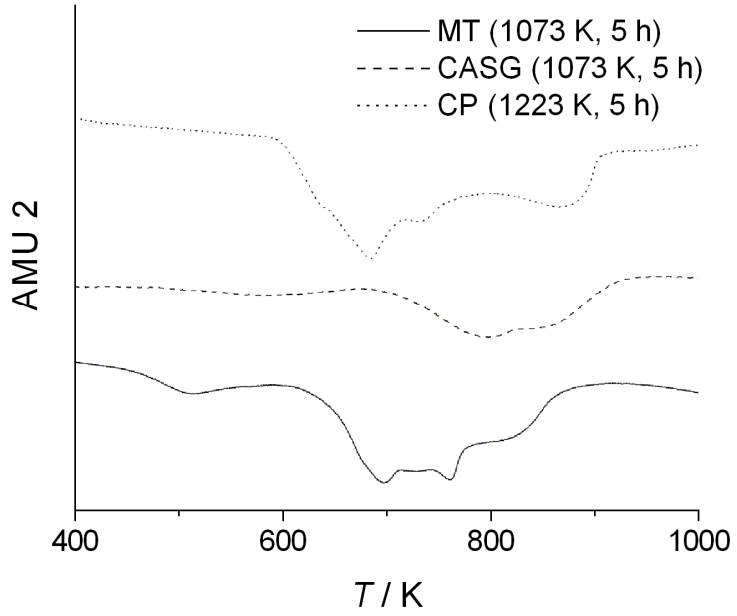

Figure 24. H_2-TPR profiles of CP particles calcined at 1,223 K for 5 h (top), CASG synthesized particles calcined at 1,073 K for 5 h (middle), and MT-synthesized particles calcined at 1,073 K for 5 h (bottom)

In order to derive insights into the influence of the preparation method on redox properties of the perovskites, H_2-TPR measurements were performed. The obtained H_2-TPR profiles of the MT, the CASG and CP perovskites are shown in Figure 24, respectively. $SrCoO_x$ shows a broad peak indicating the presence of different oxygen species and stepwise reduction of cobalt in agreement with literature [54]. The temperature range of H_2 consumption is 500–900 K for the MT perovskites, 600–900 K for the CP perovskites, and 700–900 K for the CASG-synthesized particles. The MT-synthesized, CASG-synthesized, and CP materials had an overall hydrogen consumption of 9.72, 9.37, and 8.75 mmol g^{-1}, respectively. Thus, the MT-synthesized catalyst contains a slightly higher amount of lattice oxygen, which is essentially accessible at lower temperatures. The overall amount of removed oxygen during the TPR corresponds to the reduction of cobalt(IV) to metallic cobalt, that is phase decomposition of the perovskite.

4.1.1.4 Variation of Synthesis Parameters

As demonstrated above the MT method is a promising route to produce nanostructured $SrCoO_x$. Therefore, deeper investigations on the influence of different parameters of this preparation method on the properties of the resulting particles were performed. The following synthesis parameters were varied with the bold written ones as the standard conditions:

(1) Surfactant (**Marlipal O13/50**; Marlipal O13/100; Marlipal O24/50; Triton X100)

(2) Surfactant fraction/c-value (**15**; 17; 20; 30; 55%)

(3) Oil fraction/a-value (75; **80**; 85; 90%)

(4) Phase separation (**methanol-induced**; temperature-induced)

(5) Total salt concentration (**0.24**; 0.12 M)

(6) Precipitation agent (**oxalic acid**, ammonia, ammonium carbonate)

(7) Precipitation temperature (298; **303**; 308 K)

(8) Aging time (**30 min**; 24 h)

(9) Calcination conditions (1023 K/12 h; **1073 K/5 h**; 1223 K/5 h)

The variation of the precipitation agent showed that neither ammonia nor ammonium carbonate is suitable because it rendered impossible to separate the nanoparticles from the microemulsion or produced extremely stable carbonate precursors with a high phase transformation temperature. Further, the surfactant Marlipal O13/50 is the optimum choice. When Triton X100, Marlipal O13/100 and Marlipal 24/50 were the surfactants, the phase transformations to the perovskite structure were shifted to higher temperatures indicating a somewhat higher grain size what is hardly detectable in XRD line shape.

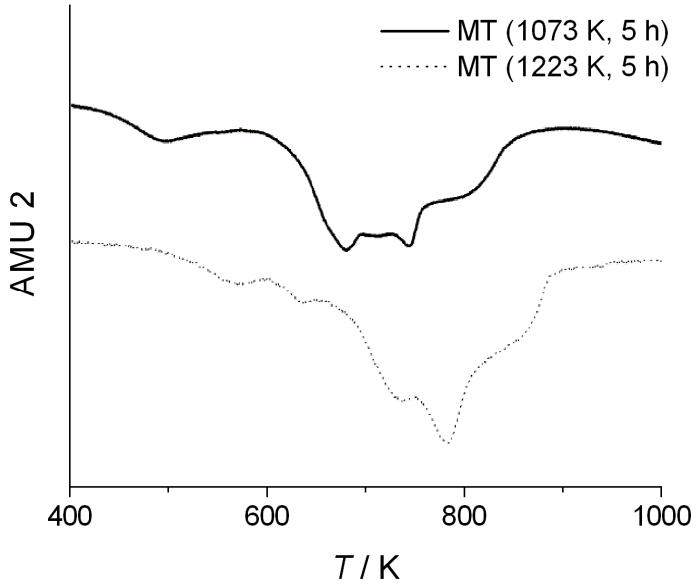

Figure 25. TPR profiles for MT-synthesized $SrCoO_x$ calcined at 1,073 K for 5 h (top) and at 1,223 K for 5 h (bottom).

The variation of other synthesis parameters showed no significant influence on the resulting perovskites according to the results of XRD, SEM, TEM, TG-DTA-MS, or BET analyses. Exceptionally, the calcination procedure influenced the TPR-profiles of the samples (Figure 25). It is observed that the oxygen distribution of the softer calcined sample is more homogeneous and more lattice oxygen is offered at lower temperatures.

4.1.1.5 Catalytic Properties in Oxidative Activation of CH_4

The next step of the characterization was the investigation of the catalytic behavior of the perovskites in methane oxidation. In these experiments, 100 mg of the powdered materials diluted in 300 mg quartz sand were heated at a heating rate of 5 K min^{-1} in a gas feed consisting of 10% O_2 and 20% CH_4 diluted in 70% He. Figure 26 compares the degrees of methane conversion and C_2 selectivity (C_2H_4 + C_2H_6) over the differently prepared $SrCoO_x$ perovskites. This figure clearly demonstrates that the preparation method has significant influence on the catalytic performance. The onset temperature for the CASG prepared catalyst and the CP catalyst is about 800 K, while the MT-synthesized catalyst started to convert methane at about 750 K. It should be noted that very small sized microemulsion droplets adjusted by rather high

avalues (oil fractions from 90%) and high c-values (surfactant fractions from 30%) negatively influenced the activity of the MT-prepared catalysts because of a even stronger sintering during the calcination. Irrespective of reaction temperature and synthesis parameters in the MT method, the following order in the activity for OCM reaction was obtained: MT method>CASG method>CP method. The low impact of reaction parameters on particle properties is in agreement with a previous study [182] on the preparation of alumina ceramics, showing the good suitability of the MT method for scale-up in industrial use due to high process stability and reproducibility of product properties. The reaction rate of methane combustion over the MT-synthesized $SrCoO_x$ at 923 K is 4.1 µmol g^{-1} s^{-1} (Figure 26). This is about 3–4 times higher than reported for $SrCoO_x$ catalysts prepared by co-precipitation [139] confirming the results of the self-prepared reference sample.

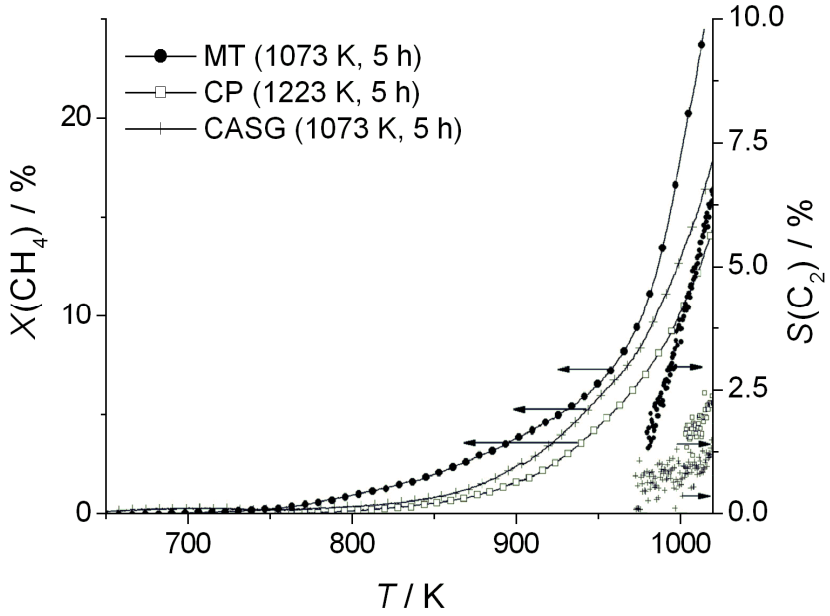

Figure 26. Methane conversions and C_2-selectivities in the OCM for MT, CP, and CASG synthesized $SrCoO_x$.

It is also important to underline that the preparation method influences the C_2-selectivity (C_2H_4 + C_2H_6). Despite the $SrCoO_x$ perovskite is known as a methane combustion catalyst [139] producing mainly CO_2, the MT prepared materials showed 7% C_2-selectivity compared to about 2% obtained over the CASG and CP catalysts.

Higher C_2 selectivities can be achieved over $SrCoO_x$ only in periodic feed mode of O_2 and CH_4 [54, 140, 198]. In this view, the production of small amounts of C_2 products over the MT $SrCoO_x$ in the O_2 and CH_4 co-feed mode indicated better catalytic properties achieved by this preparation technique. In a general sense, the MT method is appropriate for the bulk structuring of mixed oxides and can be employed for a broad variety of perovskites. The main advantage of this method is the lower phase transformation temperature and therefore the resulting higher specific surface areas.

4.1.1.6 Conclusion

Nanoparticles of the $SrCoO_x$ perovskite produced by the MT method are characterized by lower transformation temperatures from the precursor to the perovskite structure than those synthesized by CP. Therefore, softer calcinations conditions are needed to form perovskite structures so that less energy is required in the production process and also less sintering occurs. As a result, the particles show smaller crystallite sizes and higher specific surface areas than the CP particles. The MT nanoparticles possess also higher amount of lattice oxygen available for redox reactions at lower temperatures. Moreover, physico-chemical and catalytic properties of the MT perovskites are hardly influenced by synthesis parameters. Due to the low interference of the synthesis and due to the easy scale-up of this method to higher amounts, the nanoparticle synthesis in microemulsions is also applicable for industrial application.

4.1.2 Cellulose templating

The following chapter is published under the following citation: K. Langfeld, R. Marschner, B. Frank, R. Schomäcker, ChemCatChem 3 (2011) 1354–1358.

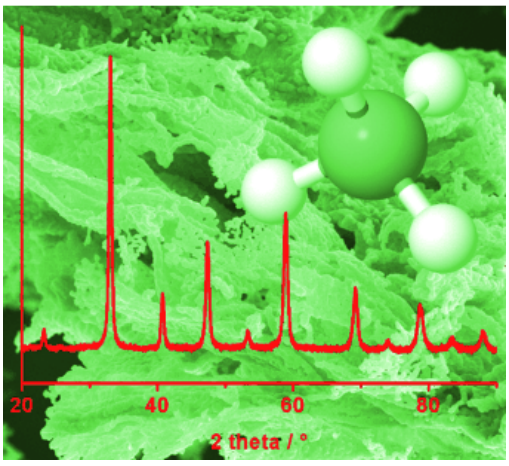

Abstract: A facile and rapid preparation method for a wide variety of medium surface area perovskite-type catalysts on the laboratory scale is presented. The cellulose templating method allows for catalysts with high phase purity, even at the relatively low calcination temperatures. Among the versatile compositions of perovskites based on the $SrCoO_x$ system, straightforward modifications could be performed to optimize the catalytic performance in the oxidation of CH_4. Substitutions in both the A and B positions in the ABO_3 lattice can remarkably affect the catalytic activity. Compared to other preparation methods, the cellulose templating method is a rapid process and the catalytic performances obtained with $SrCoO_x$ and $LaCoO_x$ are at least as good as with materials prepared by conventional methods.

4.1.2.1 Specific Introduction

Currently, a huge stock of natural gas still remains. Methane is the major component of this resource, typically comprising over 90% of the hydrocarbon fraction. Furthermore, a yet untapped reservoir of methane hydrate is located on the ocean floors [199] and could emerge as an important hydrocarbon source for the chemical industry in the future [200]. The effective use of methane as a raw material for industrial processing remains one of the long standing problems in catalysis [201]. Over the past decade, several direct and indirect routes for the methane conversion to value-added products, such as higher hydrocarbons and oxygenates, have been

considered [202–204]. However, due molecular stability, this is a demanding challenge [201]. The activation of at least one C-H bond (435 kJ mol^{-1}) in methane is necessary for different reactions such as steam reforming [205, 206], partial oxidation, or oxidative coupling of methane (OCM) [156, 207–209]. For the latter, many different catalytic materials, supported and nonsupported, were found to be active [207]. A high selectivity was observed, for example, over catalysts composed of alkaline earth oxides, rare earth oxides, and their mixtures [3]. However, for an industrial application C_2 selectivities and yields are too low despite intense research on enhancing them [3, 41, 209, 210].

Furthermore, the elimination of methane and other hydrocarbons from exhaust emissions is of interest due to environmental concerns. With regard to the greenhouse effect, the absorption and reflection of heat radiation from the earth's surface by atmospheric gases [211], the specific global warming potential of methane is more than 100 times higher than that of CO_2 [212]. The contribution of anthropogenic methane emission to radiative forcing is even higher than for chlorofluorocarbons (CFCs) [211], thus an efficient removal by catalytic combustion is highly desired.

Methane is the most stable of all hydrocarbons, challenging the intrinsic activity of the catalyst. Highly active materials of the mixed metal oxide type are perovskites [191]. They are active in many catalytic reactions, for example hydrogenation and hydrogenolysis of hydrocarbons, oxidation of carbon monoxide and ammonia, and catalytic combustion [191, 189, 192, 190]. Due to their variable structure and chemical composition, they are versatile types of catalysts. The compound $SrCoO_x$ is a well studied system known for its nonstoichiometric oxygen atoms. In this work, perovskites with differing compositions on the basis of the $SrCoO_x$ elemental composition were synthesized by the cellulose templating (CT) method.

Syntheses of perovskites with surface areas significantly higher than 10 $m^2\ g^{-1}$ are limited to elaborate multistep hard templating methods. For instance, $LaCoO_3$ compounds with surface areas of up to 100 $m^2\ g^{-1}$ and related high activities in methane combustion have been prepared by a nanocasting technique on mesoporous silica [213]. Also, the defined preparation of three-dimensionally ordered macrostructures can increase the specific surface area of $LaFeO_3$ up to 30 $m^2\ g^{-1}$

[214]. Conversely, CT is a cheap and fast method for preparing homogeneous bulk catalysts with relatively high specific surface areas on the laboratory scale [183]. For instance, Kondratenko et al. showed that highly active catalysts, based on main group metal oxides as well as complex mixed metal oxides with high yield of the crystalline phase, can be obtained [185, 184]. In general, perovskite type materials for catalytic application suffer from a low surface area [96], thus an improvement of activity is expected from this method.

4.1.2.2 Elements, Templating, and Morphology

The present study is based on the $SrCoO_x$ system, and within this ABO_3 lattice the A or the B cations were systematically exchanged by elements fulfilling the Goldschmidt tolerance condition for hexagonal perovskite-type mixed oxides [96].

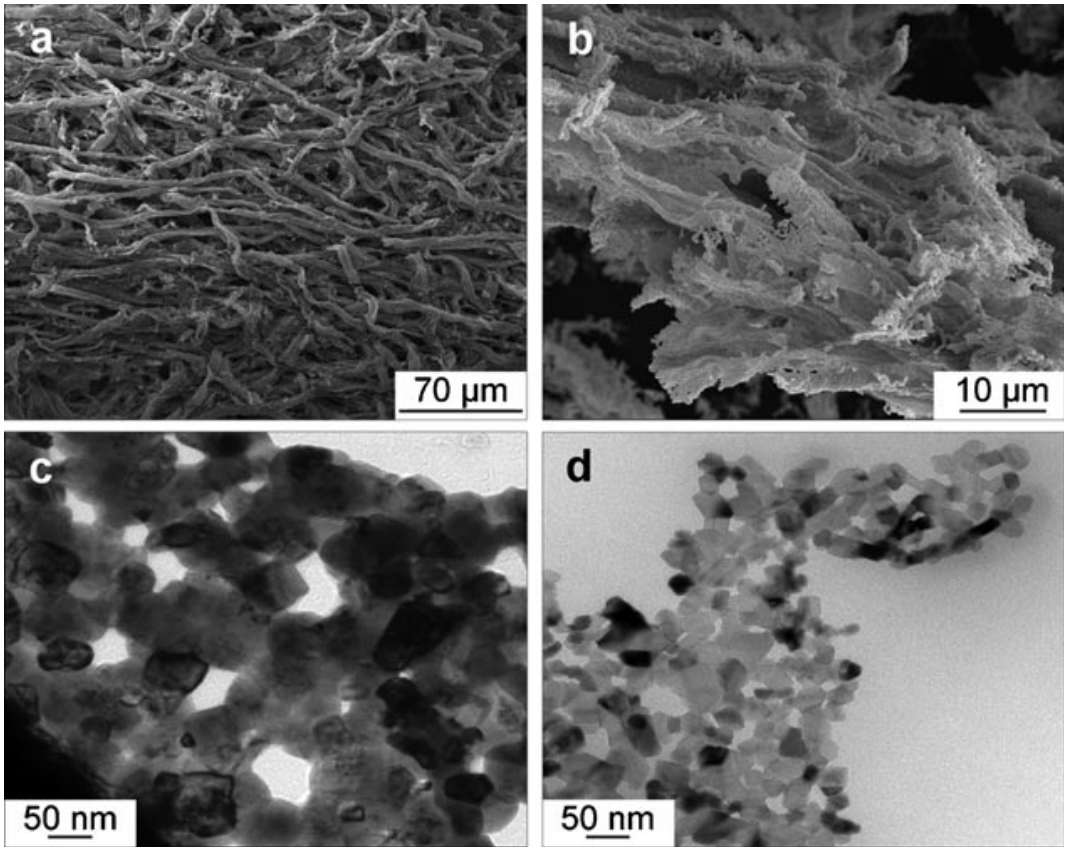

Figure 27. Representative SEM (a, b) and TEM images (c, d) of perovskite-type mixed metal oxides prepared using the CT method. The images show $LaCoO_3$ (a, c) and $Sr_{0.47}Nd_{0.53}MnO_x$ (b, d).

Table 5. Preparation conditions, physicochemical characterization, and catalytic performance of the perovskite catalysts.

Nominal composition	Precursor salts[a]	T_{calc} [K]	S_{BET} [m^2 g^{-1}]	$\langle d_{hkl} \rangle$ [nm]	$X(CH_4)$ [%]		
					723 K	823 K	923 K
$SrCoO_x$[d]	a/a	1123	2.4	134	2.2	3.5	7.1
$LaCoO_x$	n/a	923	4.4	60	2.6	22.5	29.6[c]
$NdCoO_x$	n/a	973	3.4	90	1.8	17.1	29.3[c]
$BaCoO_x$	n/a	1123	1.0	83	0.3	2.1	7.3
$CaCoO_x$[d]	a/a	1123	1.6	133	0.2	0.7	3.2
$PrCoO_x$	n/a	923	6.4	62	1.7	15.9	29.0[c]
$SmCoO_x$	n/a	923	4.6	55	1.1	11.4	28.9[c]
$SrMnO_x$	a/n	1073	10.5	65	2.1	12	26.5
$SrMoO_x$	a/-[b]	1173	<1	154	0	0	0
$SrFeO_x$[d]	a/n	1073	5.9	66	0.7	7	30.4[c]
$SrCrO_x$	a/n	1173	<1	110	0	0	0.2
$Sr_{0.2}La_{0.8}CoO_x$	a/n/a	1073	4.6	49	3.9	27.9	29.3[c]
$Sr_{0.47}Nd_{0.53}MnO_x$	a/n/n	1023	12.0	44	6.7	29.3[c]	29.3[c]
$Sr_{0.3}La_{0.7}MnO_x$	a/n/n	973	12.4	46	6.2	28.5[c]	28.8[c]
$Sr_{0.4}La_{0.6}FeO_x$	a/n/n	1123	8.4	48	2.6	28.3[c]	29.1[c]
$Sr_{0.4}Sm_{0.6}FeO_x$	a/n/n	1173	7.9	49	2.6	29.3[c]	30.0[c]
$Sr_{0.4}La_{0.6}Fe_{0.2}Co_{0.8}O_x$	a/n/n/a	1023	11.9	38	3.9	27.4	29.2[c]

[a] A cation/B cation; a=acetate, n=nitrate. [b] $(NH_4)_2Mo_7O_{24}$. [c] Limited by full O_2 conversion. [d] Presence of nonstoichiometric $A_xB_yO_z$ phases (see Figure 28Figure 29Figure 30).

In particular, with A=Sr, the B cation Co was substituted by Mn, Mo, Fe, and Cr, whereas with B=Co, the A cation Sr was exchanged by La, Nd, Ba, Ca, Pr, and Sm. In addition, partial substitutions of A and/or B cations were performed according to Table 5. Aqueous solutions of the metal nitrates and/or acetates were dripped onto filter paper and calcined for 3 h in air. The morphological analysis of the resulting powders by scanning electron microscopy (SEM, Figure 27a and b) confirms that the crosslinked fibrous structure of the filter paper was successfully transferred to the mixed metal oxide microstructure. In higher resolution, crumpled and furled 2-

dimensional layers of agglomerated particles can be observed. Transmission electron microscopy (TEM, Figure 27c and d) reveals a mean diameter of agglomerated nanoparticles of approximately 50 nm for $LaCoO_x$ and 35 nm for $Sr_{0.47}Nd_{0.53}MnO_x$. A good accessibility of the crystallite surfaces is ensured through interparticle voids of >10 nm.

The specific surface areas (BET) of the perovskites are rather low, in the range of 0.5–12.4 $m^2\ g^{-1}$, which is attributed to the high calcination temperatures required to form the perovskite phase. However, the temperatures given in Table 5 represent the lower limit of pure phase perovskite formation, which was identified by calcination at different temperatures. A surface area of >10 $m^2\ g^{-1}$ can only be observed at temperatures below 1100 K, owing to sintering of the nanoparticles. The presence of rare earth metal cations in the A position apparently tends to keep a higher dispersion resulting in surface areas of at least 3 $m^2\ g^{-1}$. The highest surface areas, however, are observed for the partially substituted perovskites.

4.1.2.3 Phase Analysis by X-ray Diffraction

Crystalline phases within the obtained solids were identified by X-ray diffraction (XRD). Pure phase hexagonal perovskite could be obtained in most cases, depending on the calcination temperature. Typical trace impurities resistant to high temperature treatment are metal (Sr, Ba) carbonates or Co_3O_4, which is formed as a byproduct of Co lean $Sr_6Co_5O_{15}$ and $Ca_3Co_2O_x$ crystallization from the 1:1 stoichiometric salt precursor. The detailed phase identification is given in Figure 28Figure 29Figure 30. The mean crystallite diameter estimated using the Scherrer equation (Eq. 15) is typically around 40–90 nm, in good agreement with the TEM analysis. The higher crystallite size of $SrCoO_x$, $CaCoO_x$, $SrMoO_x$, and $SrCrO_x$ samples of up to 150 nm is caused by the higher calcinations temperatures required. The presence of only one crystallographic phase is attributed to the ideal distribution of cations on a molecular level in the salt solution prior to impregnation of the template. This suppresses the formation of single metal oxide phases as compared to ball-milling or coprecipitation methods.

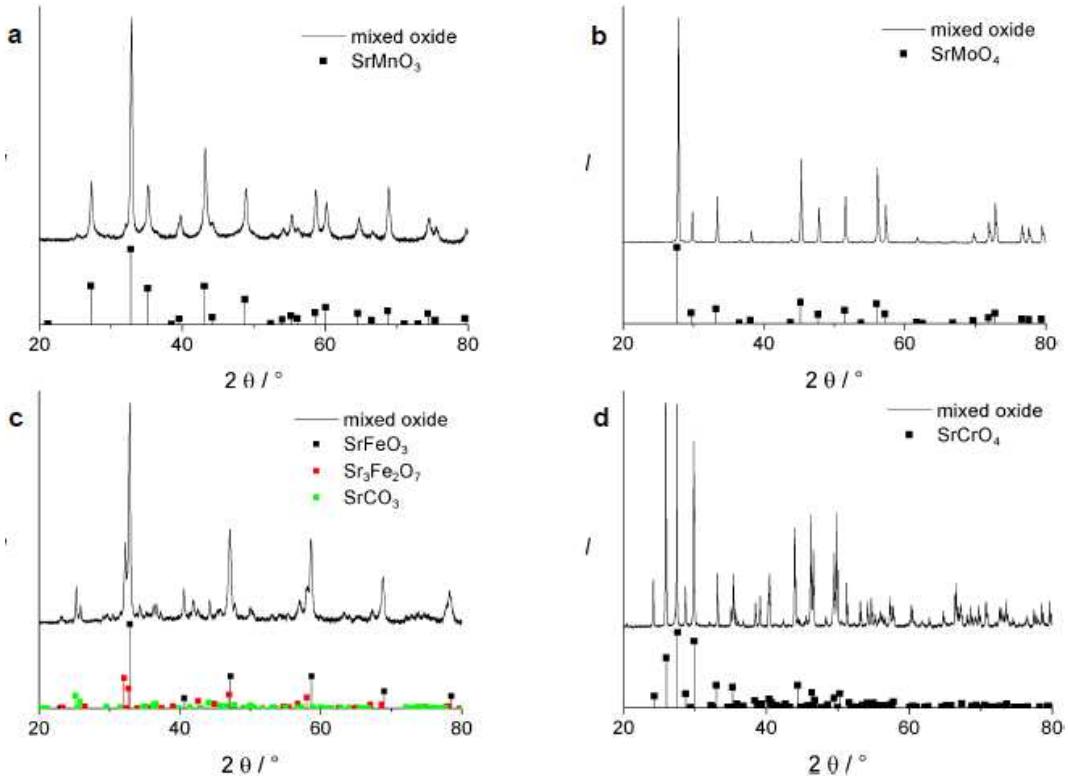

Figure 28. XRD patterns of CT-synthesized (a) $SrMnO_x$, (b) $SrMoO_x$, (c) $SrFeO_x$, and (d) $SrCrO_x$ powders in comparison to the reflections of strontium metallates generated by structural data reported in literature.

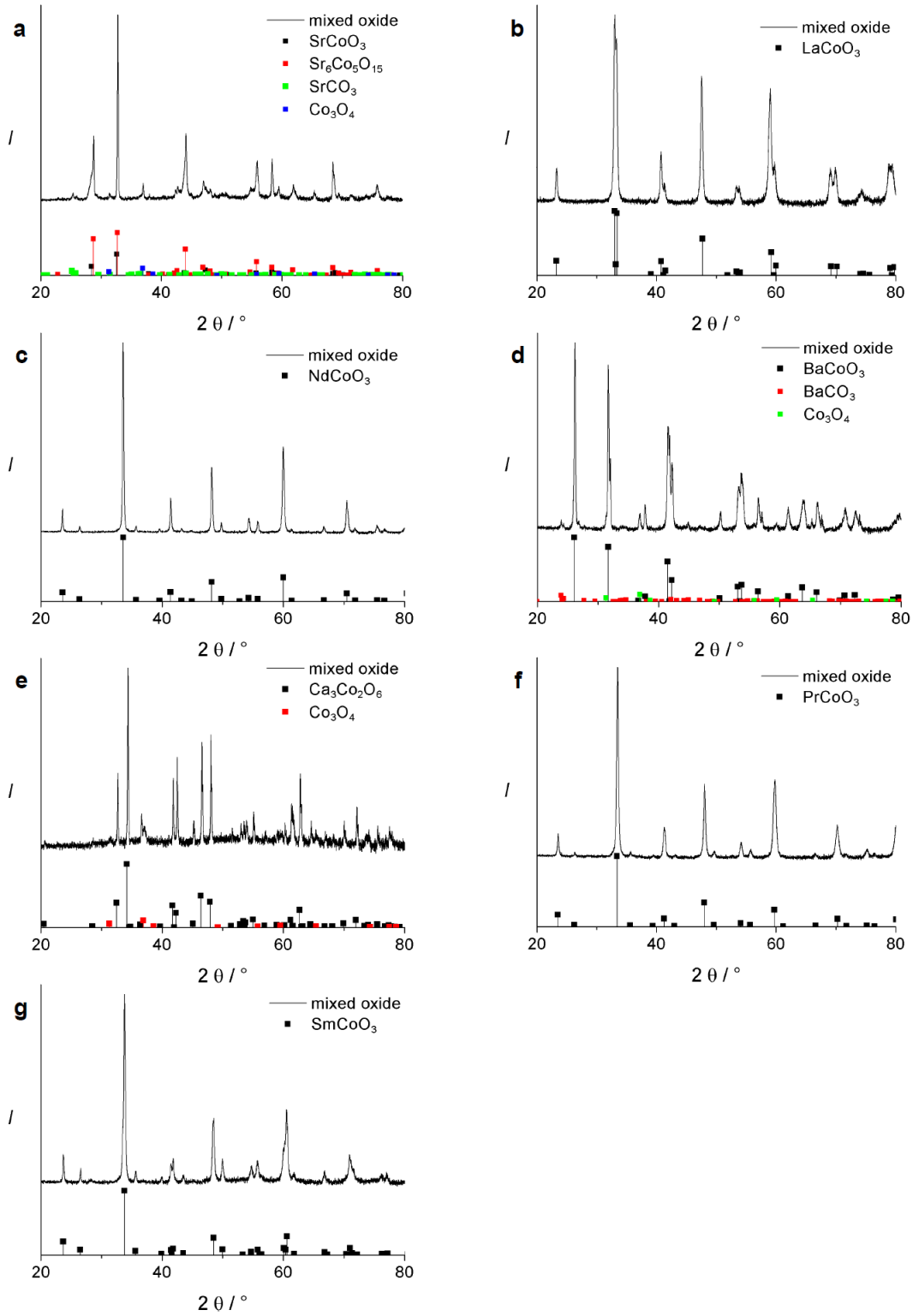

Figure 29. XRD patterns of CT-synthesized (a) $SrCoO_x$, (b) $LaCoO_x$, (c) $NdCoO_x$, (d) $BaCoO_x$, (e) $Ca_3Co_2O_x$, (f) $PrCoO_x$, and (g) $SmCoO_x$ powders in comparison to the reflections of cobaltates and impurities generated by structural data reported in literature.

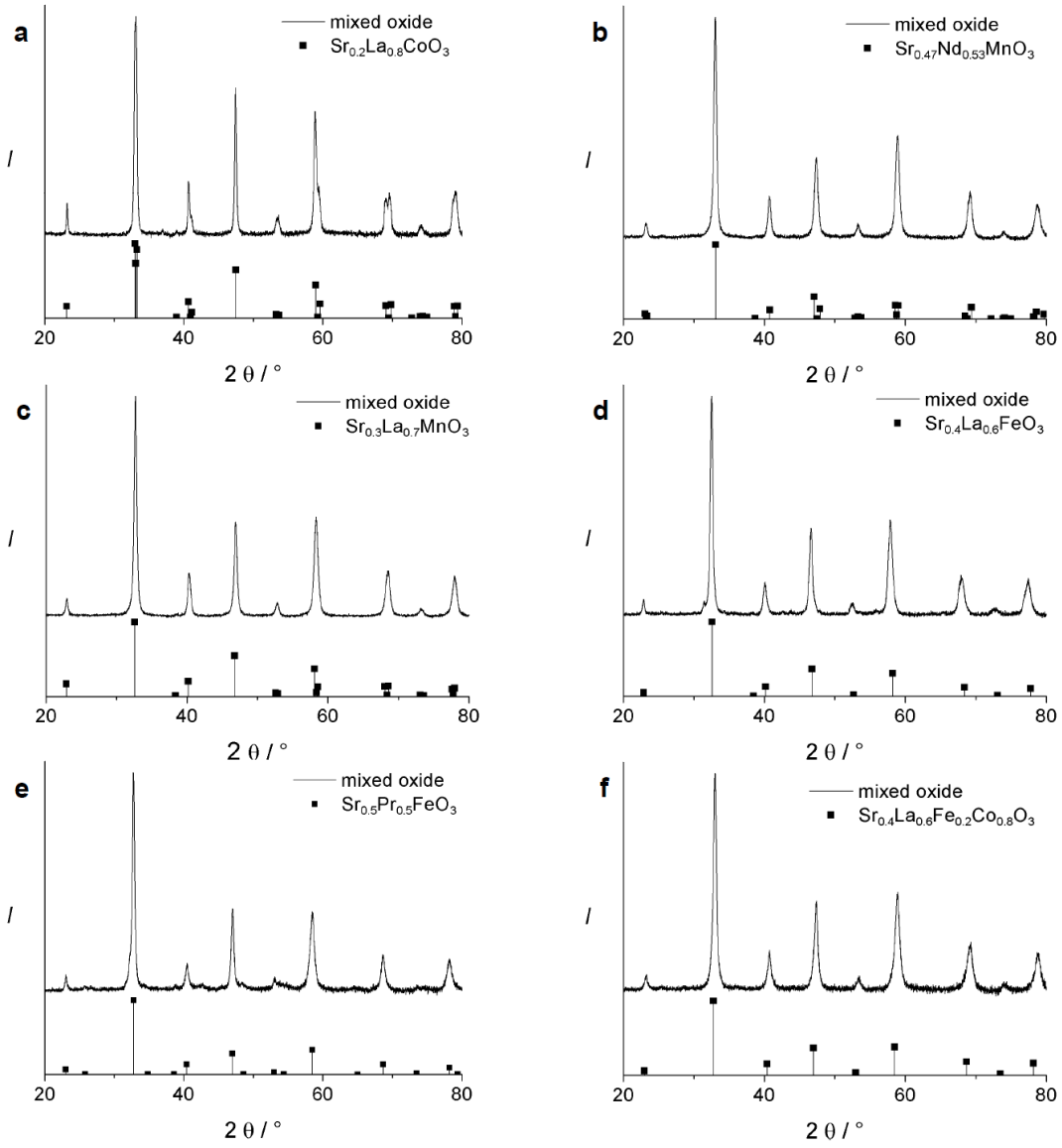

Figure 30. XRD patterns of CT-synthesized (a) $Sr_{0.2}La_{0.8}CoO_x$, (b) $Sr_{0.47}Nd_{0.53}MnO_x$, (c) $Sr_{0.3}La_{0.7}MnO_x$, (d) $Sr_{0.4}La_{0.6}FeO_x$, (e) $Sr_{0.4}Sm_{0.6}FeO_x$, and (f) $Sr_{0.4}La_{0.6}Fe_{0.2}Co_{0.8}O_x$ powders in comparison to the reflections of similar partially substituted $SrCoO_x$ based mixed oxides generated by structural data reported in literature. Due to missing reference, the XRD pattern of $Sr_{0.4}Sm_{0.6}FeO_x$ (e) is compared to the reflections of $Sr_{0.5}Pr_{0.5}FeO_x$.

4.1.2.4 Reducibility of Perovskite-type Materials

Temperature programmed reduction (TPR) of the catalyst samples reveals substantial differences depending on the composition (Figure 31). The basis system

$SrCoO_x$ shows a broad peak, indicating the presence of different oxygen species, and stepwise reduction of cobalt in agreement with literature results [54, 215]. Similar profiles are observed for the substitution of Sr by other alkaline earth metals or by the substitution of the B cation. The reduction of SrMnOx with a major peak at around 700 K and with a shoulder at 790 K follows a similar shape to the profile reported for $LaMnO_x$ [216], suggesting that the A cation in perovskites is difficult to reduce and not redox active in catalysis. Here, Mn^{VI} and Mn^{III} are likely present in the starting material; Mn^{II} is not typically formed below 1000 K [216].

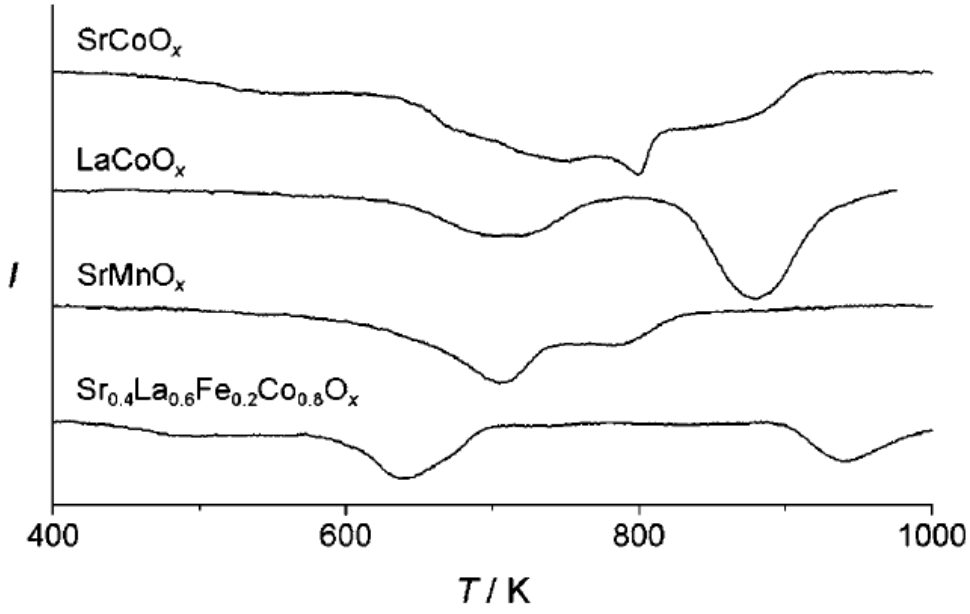

Figure 31. TPR profiles (H_2 consumption) of selected perovskites prepared using the CT method.

The substitution of Sr by lanthanides results in a better defined bimodal H_2 consumption for the stepwise reduction of Co^{III} to Co^{II} at low temperatures and the formation of metallic Co^0 at high temperatures [119, 217, 218], which is also observed for the partially substituted perovskites and confirmed by the quantitative analysis of the TPR experiments. During the first reduction step, the perovskite lattice is preserved, whereas the full reduction at high temperature is accompanied by an irreversible phase separation to metallic cobalt and lanthanide oxide, which is nonreducible under the H_2-TPR conditions applied [119, 217, 218]. Besides the clear

peak assignments based on previously reported studies using XRD or X-ray photoelectron spectroscopy (XPS), broad peaks and frequently observed shoulders in the TPD profiles of other perovskites (Table 5) may also indicate the presence of different oxygen sites within pure phase materials. For this reason, uncertainty, and a lack of the appropriate experiments in the present study, for instance in situ XRD during reduction, further TPD profiles are not discussed.

4.1.2.5 Reactivity Testing in Oxidative Activation of CH_4

The perovskite materials were tested for their catalytic performance in the oxidative activation of methane. Perovskites are known to favor the combustion of methane to form CO_x and H_2O. In principle, the formation of more valuable products, such as formaldehyde, ethylene, or hydrogen, is also possible. However, even though an oxygen lean feed ratio of CH_4:O_2=2:1 was applied as a prerequisite for more selective reaction pathways, the predominant reaction pathway observed for all of the catalysts was combustion. The highest conversions were obtained over the $SrCoO_x$ type perovskites, in which the A cation Sr is (partially) substituted by rare earth metals such as La, Pr, Nd, or Sm. Also, the substitution of the B cation with Mn or Fe resulted in a remarkable rise in activity. Conversely, Ca and Ba in the A position, as well as Mo and Cr in the B position resulted in lower activities, which may partially be explained by the decreased specific surface areas of these materials. Apparently, there is no straightforward, linear dependence of methane activation on physicochemical properties, like ionic radii and electronegativities of the cations, or microstructure, reducibility, and oxygen conductivity of the perovskites. For instance, $SrCoO_x$, $LaCoO_x$, and $SrMnO_x$, which show similar reduction onset temperatures (ca. 650 K (Figure 31), exhibit quite different activities in CH_4 oxidation at 823 K (Table 5). The observed reactivity pattern is likely governed by a complex interplay of all of these factors. Clear tendencies and straightforward interpretations are usually limited to the stepwise substitution of the A or the B cation in a ternary system [191, 219] or tentative modification of a basis system, for instance by alkaline doping [54]. TPR and XRD data obtained for the perovskites in this study revealed fundamental and manifold differences which arose from changing the elemental composition of the perovskite lattice and which are reflected in the catalytic activity.

Based on these results, further perovskite samples were prepared with partial substitution of the A cation by rare earth metals and complete substitution of the B cation by Mn and/ or Fe. As stated above, the resulting materials have with the lowest crystallite sizes and highest specific surface areas. In agreement with the results obtained over the binary perovskites, the highest CH_4 conversions, *X*, were also obtained with these compounds. At the reaction temperature of 823 K, the CH_4 conversion is limited by full O_2 conversion. However, the selectivity to C_2 products did not exceed 5% in all of the experiments, and these materials are better suited for hydrocarbon combustion than for the OCM.

Under the chosen reaction condition, it is difficult to compare the catalytic performance of CT synthesized perovskites with other methods, such as citric acid sol-gel, flame spray pyrolysis, or coprecipitation. Most of the reports found in the literature focus on the elimination of trace amounts of hydrocarbons in excess oxygen. Consequently, the feed in their catalytic studies comprises 0.2–2% CH_4 and 10–20% O_2 [220–223]. High reactivity is observed here; however, the observed rates of CH_4 oxidation do not reach the reaction rate of the CT synthesized catalysts, which is likely due to the lower concentration of CH_4. Thus, the data is not comparable to the reaction conditions applied in this study because the oxidation state of the catalyst would be completely different. A valid comparison can only be obtained under identical reaction conditions or by a kinetic study, which was performed for the $SrCoO_x$ and $LaCoO_x$ catalysts prepared by co-precipitation [139]. Extrapolation of the data presented in this study to the feed comprising 20% CH_4 and 10% O_2 at 923 K gives reaction rates of CH_4 oxidation of 1.15 and 0.2 mmol g^{-1} s^{-1} for $SrCoO_x$ and $LaCoO_x$, respectively. From the data presented in Table 5, the reaction rates of 4.8 and 20.2 mmol g^{-1} s^{-1} can be calculated, the latter being limited by full O_2 conversion, indicating that the CT method drastically increases the catalytic activity of perovskite-type materials compared to conventional coprecipitation. However, it has to be mentioned, that in particular the $LaCoO_x$ catalyst presented in ref. [139] shows a very poor CH_4 oxidation performance compared to other studies [220–222], suggesting that the superiority of the CT method over other synthesis routes with regard to catalytic activity is not that pronounced, whereas its advances clearly combine rapidness and simplicity.

4.1.2.6 Conclusion

The cellulose templating (CT) method is advantageous for the rapid synthesis of laboratory amounts of various perovskitetype materials with surface areas higher than 10 m^2 g^{-1}. Small crystallite sizes are conserved as a result of relatively low calcinations temperatures, which are required to yield pure phase solids. The prepared perovskites are active in CH_4 oxidation. Their activity ranges between conventionally prepared perovskites and well-developed high surface area perovskites exhibiting a good compromise with regard to the facile preparation method. Methane oxidation performance does not singularly depend on factors like ionic radii, electronegativities, acidity/basicity, reducibility, or oxygen conductivity, but is rather a complex interplay among all of these factors.

4.2 Variation of oxidizing agent

The following chapter is published under the following citation: K. Langfeld, B. Frank, V.E. Strempel, C. Berger-Karin, E.V. Kondratenko, R. Schomäcker, *Comparison of Oxidizing Agents for the Oxidative Coupling of Methane over State-of-the-Art Catalysts*, Appl. Catal. A: Gen. (2011) accepted for publication.

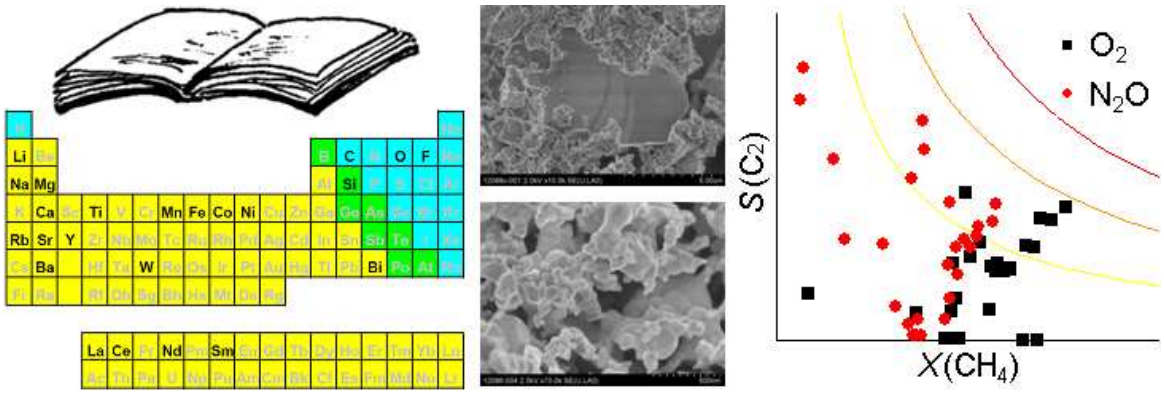

Abstract: The synthesis of selected state-of-the-art catalysts providing high performances in the oxidative coupling of methane (OCM) with O_2 was reproduced according to the respective methods reported in literature. A reference material with identical stoichiometric composition was further synthesized by applying the cellulose templating (CT) method. This method increases the surface area and affects the phase composition and crystallite size of the catalysts as determined by N_2-physisoprtion, X-ray diffraction (XRD), and scanning electron microscopy. This, however, is in most cases detrimental to the catalytic OCM performance due to enhanced global activity resulting in hot spots in the catalyst bed. Prepared catalysts were tested in the OCM under variation of temperature (973–1073 K), GHSV (3,600–100,000 h^{-1}) and oxidizing agent (O_2, N_2O, CO_2). In general, conversions of CH_4 when using N_2O are lower than in the presence of O_2, however, the selectivities to C_2 products ethane and ethylene are higher even at a similar level of CH_4 conversion. This confirms the presence of different oxygen species formed by activation of these oxidizing agents. CO_2 ruled out to be an efficient oxidizing agent since reaction temperatures required are very high (> 1073 K).

4.2.1 Specific Introduction

The use of methane as a chemical feedstock and its transformation into higher hydrocarbons has been the focus of a number of research efforts for several decades. With increasing oil prices especially the Fischer-Tropsch (FT) process via synthesis gas, which is obtained, e.g., by steam reforming of methane, actually retrieves a lot of attractiveness. However, one drawback with regard to process costs is the need for two individual reactors to consecutively produce synthesis gas and higher hydrocarbons or alcohols. Even more complex is the route to high-value olefins via methanol, which is synthesized from synthesis gas. A highly attractive one-step transformation is the oxidative coupling of methane (OCM) to C_2 (C_2H_6 and C_2H_4) hydrocarbons ethane and ethylene discovered in the early 1980's [3]. This reaction, even though extensively investigated and optimized for almost three decades, provides low C_2 selectivities at high industrially relevant methane conversions due to consecutive oxidation of produced hydrocarbons to CO and CO_2. A C_2-yield of 30% is regarded as the economically feasible limit for industrial realization of the process [224].

To improve the OCM selectivity a variety of less active oxidizing agents such as N_2O, CO_2, and H_2O have already been tested. This is not only for environmental reasons – N_2O and CO_2 are important greenhouse gases and their value added chemical transformation is highly desired [152] – but the major intention is the formation of more selective surface oxygen species on the catalyst. Clearly, the formation of electrophilic peroxo-species, which would favor the combustion of adsorbed hydrocarbons during OCM [10, 225], is less probable when using these mild oxidizing agents because N_2O, CO_2, and H_2O, contrarily to O_2, can provide only one O atom for the catalyst reoxidation. The reaction mechanisms proposed for OCM are quite similar for each oxidizing agent and start with generation of surface active oxygen species from the oxidizing agent (Eqs. 16-19). Depending on the oxidizing agent, N_2 [226–229], CO [230–232], or H_2 [158] are formed as the by-product in these reaction steps. The reaction of O_2 (Eq. 16) is reported to pass a peroxo intermediate [10, 233].

$$½\ O_2 + (\ ) \rightarrow (O) \qquad (16)$$

$$N_2O + (\ ) \rightarrow (O) + N_2 \qquad (17)$$

$$CO_2 + (\ ) \rightarrow (O) + CO \qquad (18)$$

$$H_2O + (\ ) \rightarrow (O) + H_2 \qquad (19)$$

The following (selective) reaction pathway is the oxygen-assisted CH_4 activation to form a methyl radical and a surface OH group [8, 234]. The latter recombines to form gaseous H_2O and a vacancy to be reoxidized. Methyl radicals also recombine to form C_2H_6 which dehydrogenates to C_2H_4. Unselective pathways include the interaction of hydrocarbons and intermediates with electrophilic surface and gas phase species [45], such as mentioned surface peroxo-species [225], or gas phase O_2 [8].

One of the most promising and probably the best investigated [75] catalyst for OCM is Li-doped MgO [8, 235–237]. However, a recent review [238] reveals numerous wellperforming and promising catalyst compositions reported in literature so far. In the cofeed mode (simultaneously introducing CH_4 and O_2 into the reactor) C_2-yields up to 25–27% have been reported over $RbWO_4/SiO_2$ and $Bi_{1.5}Y_{0.3}Sm_{0.2}O_{3-\delta}$ catalysts, respectively [60, 57]. High yields on less selective catalysts can also be obtained by improved reaction engineering [239]. For example, yields in the range of 17-23% were reported when operating in a membrane reactor with an oxygen-ion conducting $La_{0.8}Sr_{0.2}Co_{0.6}Fe_{0.4}O_{3-\delta}$ membrane separating the CH_4 and O_2 gas streams [240], or by alternating feed mode of CH_4 and O_2, e.g., over $Sr_{0.75}Na_{0.25}NiO_{3-\delta}$ or $SrNi_{0.75}Li_{0.25}O_{3-\delta}$ [56], even though applied perovskite-type and/or Ni-containing catalysts are commonly used for catalyzing partial or total oxidation pathways of methane. However, a major lack of so far published catalytic data is the poor comparability among studies by different authors. For instance, as can be seen in Table , reaction temperatures, CH_4/O_2 ratios, and space velocities cover a broad range and make assembled data difficult to compare. Other important data such as conversion of O_2 or stability with time-on-stream are often not given.

Besides the chemical composition, also the preparation method could provide a certain potential for optimizing the catalyst activity and C_2-yields. In recent studies, we could show that synthesis methods utilizing w/o-microemulsions [241] (see Chapter 4.1.1) or cellulose filter papers [242] (see Chapter 4.1.2) as structural templates for mixed metal oxides can significantly improve the catalytic properties of perovskite-type catalysts for oxidative methane activation as compared to conventional co-precipitation or sol-gel methods. The overall activity as well as the selectivity to C_2 products can be influenced.

Table 6. Catalysts investigated in the present study and their performances in the OCM under different reaction conditions as reported in literature.

Catalyst	*T* [K]	CH_4:O_2 :inert	GHSV [mL g^{-1} h^{-1}]	*X*(CH_4) [%]	*S*(C_2) [%]	Ref.
BaF_2(95 mol%)/Y_2O_3	1023	2.5:1:11	6,000	36.1	62.1	[58]
Rb_2WO_4(0.3 mmol g^{-1})/SiO_2	1123	4.5:1	2,000[a]	32	78	[60]
Na_2WO_4(0.3 mmol g^{-1})/SiO_2	1123	4.5:1	2,000[a]	44	52	[60]
$NaMnO_4$(12.5 wt%)/MgO	1073	5:1:4	4,800	28[b]	69	[62]
Na(0.32 g)/$BaSrTiO_3$	1073	2:1:2	6,000[a]	47	51	[59]
Li(0.2 wt%)/MgO	923	21:1:28	6,000	3.0	17.7	[8]
$SrCO_3$/$La_2(CO_3)_3$ (La:Sr = 2)	1153	10:1:0	219,800	15.8[b]	80.8	[243]
La(5 mol%)/CaO	1073	8:1:0	51,360	19.8	67.2	[63]
Nd(5 mol%)/CaO	1073	8:1:0	51,360	19.5	70.8	[63]
Li(5 mol%)/Ce(0.5 mol%)/MgO	1073	5:1:44	6,000	21.7	64.0	[64]
$Bi_{1.5}Y_{0.3}Sm_{0.2}O_{3-\delta}$	1223	2:1:3	8,955	42.4[b]	62.7	[57]
$Bi_{1.5}Y_{0.3}Sm_{0.2}O_{3-\delta}$	1173	membrane reactor, 21% O_2/N_2 (O_2 side), 2% CH_4/He (CH_4 side)		65.0	54.7	[244]
$Sr_{0.75}Na_{0.25}NiO_{3-x}$	973	alternating mode, pure gases		17.4	99.8	[56]
$SrNi_{0.75}Li_{0.25}O_{3-x}$	973	alternating mode, pure gases		22.5	99.7	[56]
$Sr_{0.3}La_{0.7}MnO_x$	823	2:1:7	30,000	28.5[b]	< 5	[242]
$Sr_{0.4}La_{0.6}Fe_{0.2}Co_{0.8}O_x$	823	2:1:7	30,000	27.4	< 5	[242]
[a] h^{-1}; [b] limited by full O_2 conversion; *X*(O_2) > 90%.						

The present study aims at the improvement of C_2 yields in the OCM reaction. Based on the elemental compositions and preparation recipes of best performing catalysts reported in literature this is intended to be realized by variation of the oxidizing agent and by applying cellulose templating (CT) as an alternative synthesis method to the respective method reported in literature. This study furthermore provides a direct comparison of catalytic performances of state-of-the-art catalysts reported in past literature.

4.2.2 Catalyst Characterization

4.2.2.1 N_2 Physisorption and X-ray Diffraction

Characterization results presented herein were selected according to the catalysts OCM behavior by employing the criteria as mentioned in section 4.2.4. Briefly, during OCM with O_2 at 1073 K, NaWSi(lit), LiMg(lit), and BaY(lit) provide highest C_2 selectivities around 40% at different degrees of methane conversion in the range of 30–50%. Contrarily, LiMg(CT) shows a C_2 selectivity of only 16% at the similar level of CH_4 conversion. The perovskite SrLaFeCo(CT) provides a methane conversion of 30%, which is limited by full O_2 conversion, at almost zero C_2 selectivity. Specific surface areas of these catalysts are listed in Table 7. The comparison with literature data shows that all catalysts provide a low surface area after long term catalytic tests in OCM reaction. Especially for LiMg(lit), LiMg(CT), and SrLaFeCo(lit) a dramatic difference is observed. For BaY(lit), low surface areas are explained by sintering effects during high temperature treatment [58] and it is assumed that this is also the reason for structural collapse of other catalysts investigated. Accordingly, the high surface area of LiMg(lit) was measured after a reaction time of 3 h at the low temperature of 923 K [8]. However, even though showing a lower C_2-selectivity in comparison to LiMg(lit), the structural stability of LiMg(CT) is remarkable and the sample keeps the relatively high surface area of > 12 $m^2\ g^{-1}$ even after long term reaction conditions.

Table 7. Specific surface areas of selected catalysts.

Catalyst	S_{BET} [$m^2\ g^{-1}$]	$S_{BET,lit}$ [$m^2\ g^{-1}$]	Ref.
NaWSi(lit)	1.2	-[a]	[60]
BaY(lit)	2.0	1.1	[58]
LiMg(lit)	0.1	37	[8]
LiMg(CT)	12.7	16[b]	[183]
SrLaFeCo(CT)	1.7	11.9	[242]
[a] not published, [b] pure MgO, T_{calc} = 1323 K.			

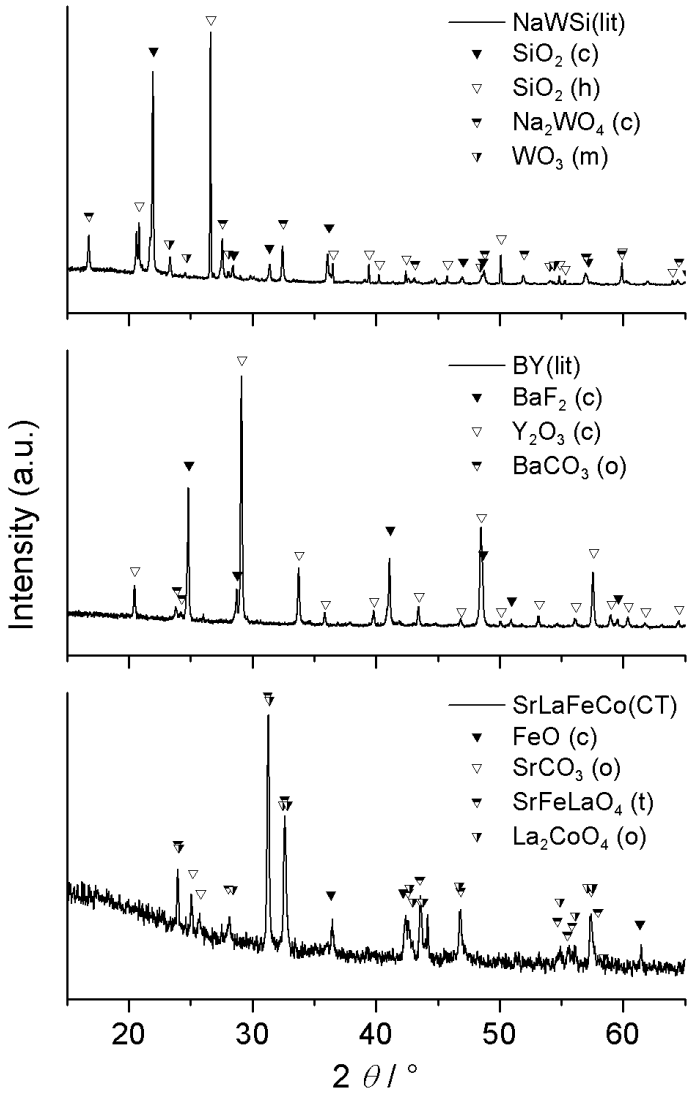

Figure 32. XRD patterns of NaWSi(lit), BaY(lit), and SrLaFeCo(CT) catalysts after use in OCM for 40 h on stream, reaction conditions as listed in section 3.3.2. Modifications are given in parenthesis: cubic (c), hexagonal (h), monoclinic (m), orthorhombic (o), tetragonal (t).

Comparing the crystallographic data gained from XRD analysis over fresh and used catalysts reveals significant restructuring induced by being applied to OCM reaction for 40 h on stream; solely the LiMg samples are phase stable under the above conditions. Owing to the low Li loading the diffractograms of LiMg(lit) and LiMg(CT) (not shown) disclose phase-pure MgO according to powder diffraction file PDF 00-043-1022. The peak analysis according to Scherrer [245] gives an estimate of the mean crystallite sizes of 188 and 114 nm for LiMg(lit) and LiMg(CT), respectively.

Note that this is only a rough estimate as the Scherrer equation (Eq. 15) is valid only for crystallite diameters below 100 nm. This correlates well with the higher surface area of the CT sample and underlines the advantages of the cellulose template method for the synthesis of highly dispersed and structurally stable oxidic structures [183]. The BaY(lit) sample (Figure 32) comprises BaF_2 (PDF 00-085-1342) and Y_2O_3 (PDF 00-041-1105) phases and a small amount of $BaCO_3$ (PDF 00-044-1487). The stability of the precursor phases is reported in literature [58], however, the presence of a carbonate phase indicates the slow transformation of BaF_2 to $BaCO_3$ in the presence of CO_2, which is a by-product of OCM. This questions the stability of BaY(lit) at extended OCM reaction periods, although the formation of $BaCO_3$ could also be accelerated by the experiments using CO_2 in high concentration.

The NaWSi(lit) catalyst comprises two different modifications of the SiO_2 support, namely cubic cristobalite (PDF 00-001-0438) and tetragonal quartz (PDF 00-033-1161), whereas in the original report only the christobalite phase is detected [60]. More importantly, a small amount of WO_3 (PDF 00-030-1387) can be identified by XRD, suggesting that Na_2WO_4 (PDF 00-012-0772) is unstable under the reaction conditions applied. The least structurally stable catalyst is SrLaFeCo(CT), which completely decomposes into FeO (PDF 00-001-1223), $SrCO_3$ (PDF 00-005-0418) as well as several binary and ternary mixed oxide phases, which are difficult to identify in detail. Although the ICSD database [246] provides numerous similar patterns containing the elements of the perovskite, the typical reflexes of $SrFeLaO_4$ (PDF 00-029-1305) and La_2CoO_4 (PDF 00-034-1081) are given as references. The signal-to-noise ratio detected in the diffraction patterns of the fresh SrLaFeCo(CT) (as can be taken from [242]) is lower compared to that of used SrLaFeCo(CT) depicted in Figure 32. This may demonstrate a loss of crystallinity, which is in line with the structural collapse of the material.

4.2.2.2 Scanning Electron Microscopy

The SEM and EDX analyses of the used catalysts are shown in Figure 33. The porous structure of NaWSi(lit) (Figure 33a) is conserved from the porous SiO_2 support used for impregnation even after 40 h on OCM conditions. The elements are macroscopically well dispersed over the catalyst particles as pointed out by EDX

analysis and backscattered SEM (Figure 33b). Na_2WO_4 is dispersed on the smooth SiO_2 surface in 50–500 nm sized clusters (Figure 33c). Traces of C are mainly located on the SiO_2 surface, whereas the Wand Na-rich areas are almost free of C. BaY(lit) (Figure 33d) remains a physical mixture of plain shaped BaF_2 crystals (Figure 33e) and Y_2O_3 (Figure 33f), which provides a rough surface. In agreement with the phase analysis by XRD, the elemental mapping reveals the coherence of Ba and F, as well as Y and O. Traces of C can be detected on both BaF_2 and Y_2O_3 materials.

The LiMg catalysts show clear differences in their microstructure. LiMg(lit) conserved the ~5 µm sized spherical MgO particles with smooth surfaces (Figure 33g and h), whereas LiMg(CT) appears less ordered and provides rough surfaces (Figure 33j-l) in agreement with the higher specific surface area owing to the CT method (Table 7). However, the latter misses the typical cellulose templated structure observed for other mixed oxides [242], which is probably due to sintering processes during reaction. On both samples Li cannot be detected by EDX due to the low loading of 0.2 wt% and the low atomic mass of Li. However, both samples provide a strong C signal, which is even more pronounced on the LiMg(CT) sample. It is also confirmed by optical analysis of used catalysts, whose colors are grey and white for LiMg(CT) and LiMg(lit) samples, respectively. On LiMg(lit) carbon is present in the form of bigger flakes (Figure 33g and h, arrows), whereas on the CT sample it appears to be more homogeneously distributed. The latter fact may hint towards C to be partly present as an artifact of the cellulose template. The primary particle size of MgO crystallites in both samples is in the range of 100–200 nm (Figure 33i and l) in agreement with XRD analysis.

The most drastic structural collapse is observed for the SrLaFeCo(CT) catalyst, as indicated by the XRD analysis. The nicely adapted cellulose structure (as had been observed in [242]) is completely destroyed and sintered to form a less porous microstructure (Figure 33m and n). The metallic constituents of the homogeneously substituted perovskite segregated to form crystallites and clusters of varying composition, mainly oxides and carbonates as illustrated in the element map (Figure 33o). The average chemical composition as determined by EDX, however, still represents the stoichiometry of the perovskite (Sr: 21.6 at%, La: 30.6 at%, Fe: 9.6 at%, Co: 38.2 at%). Only small amounts of C can be detected on the SrLaFeCo(CT) sample.

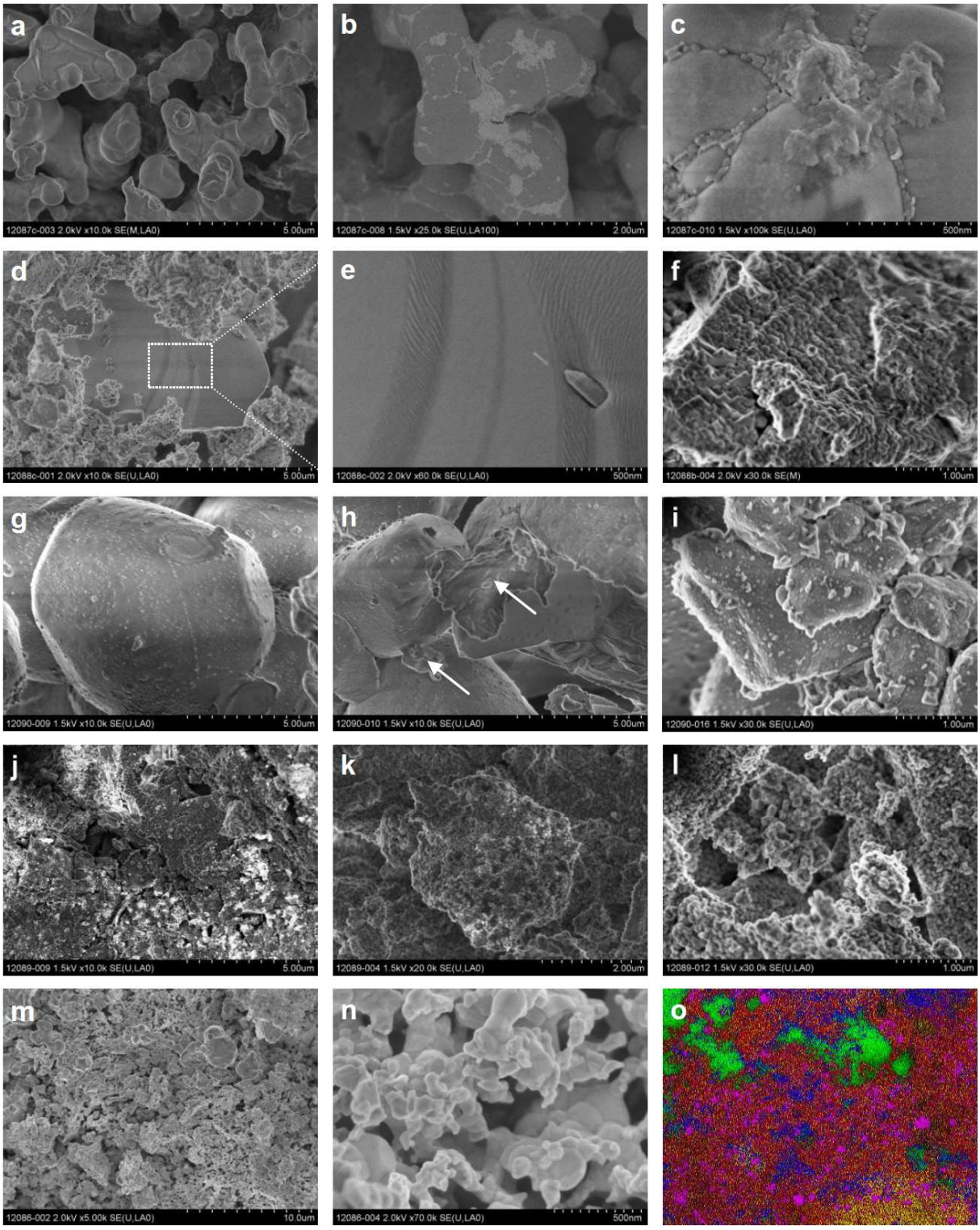

Figure 33. SEM images of NaWSi(lit) (a-c), BaY(lit) (d-f), LiMg(lit) (g-i), LiMg(CT) (j-l), and SrLaFeCo(CT) (m-n) catalysts after use in OCM for 40 h on stream under varying reaction conditions. The elemental mapping of SrLaFeCo(CT) (o) shows section (m) and indicates enrichment of Sr (green), La (red), Fe (yellow), Co (magenta), and O (blue).

4.2.3 Catalytic Testing

4.2.3.1 Thermodynamic Considerations

Gibbs enthalpies of the OCM reaction to ethylene using O_2, N_2O, CO_2, and H_2O as the oxidizing agents are displayed in Figure 34. From a general point of view, H_2O cannot directly be regarded as an oxidation agent in the OCM reaction, because the O atom recombines with H atoms from CH_4 molecules and the net reaction in this case would be the non-oxidative coupling of methane with H_2 as the by-product. However, it appears plausible that the addition of steam to the reactant mixture affects the catalyst properties or influences the thermodynamic equilibrium of gas phase and surface species. In numerous catalytic processes, steam is added to the reaction, mostly to reduce catalyst deactivation by coking. Furthermore, with regard to downstream refining processes, H_2O is by far easier to separate from the product gas mixture than inert gases like N_2.

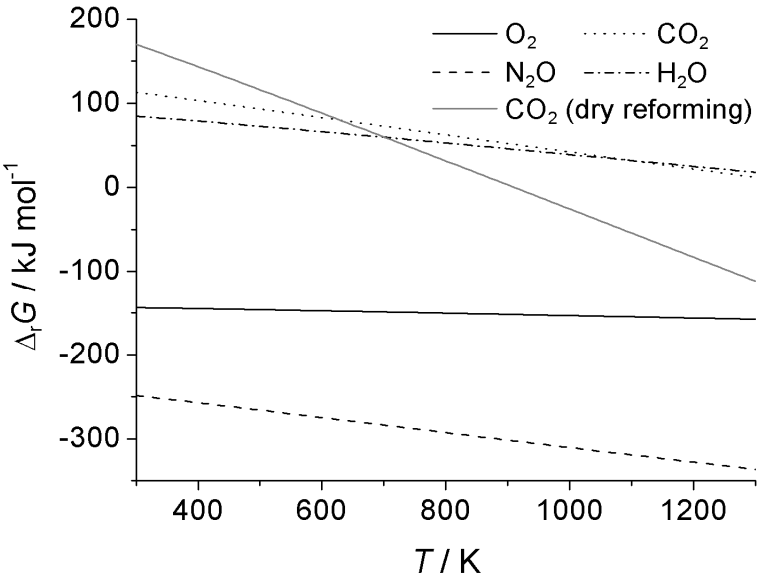

Figure 34. Temperature dependency of Gibbs enthalpies of OCM to C_2H_4 with different oxidizing agents and of CH_4 dry reforming.

Figure 34 shows that from thermodynamic point of view the OCM with O_2 or N_2O is free of limitations. The reaction with N_2O is even more favoured due to the instability of nitrous oxide ($\Delta_f G$ = 104 kJ mol^{-1}). The OCM reactions with CO_2 or H_2O is prohibited in the low temperature regime, however, they become possible at >

1000 K, where relevant CH_4 conversions can preferentially be obtained at a molar excess of the oxidizing agent. For example, at 1073 K and starting from a CH_4:CO_2 molar ratio of 1:2 at atmospheric pressure without dilution, an equilibrium CH_4 conversion of 32% to C_2H_4 can be calculated, which is in good agreement to previously reported data [247]. Under the reaction conditions applied in this work (973–1073 K, CH_4:O_2:N_2 = 2:2:3) the maximum conversion amounts to 14–25%. However, when using CO_2 as the oxidizing agent the possibility of dry reforming of CH_4 has to be taken into account (Figure 34), which is thermodynamically preferred over the OCM reaction at > 630 K.

4.2.3.2 Ni-Containing Catalysts and CO_2 as Oxidizing Agent

Ni-containing perovskite type catalysts were reported to catalyze the OCM with almost 100% C_2 selectivity in the alternating feed mode (Table 6) [56]. Nevertheless, in the cofeed mode as carried out in the current study almost full selectivity to synthesis gas is obtained, since Ni is generally known to catalyze CH_4 reforming reactions [121, 248]. Traces of C_2 products are observed only at very short contact times in the reactions of CH_4 with O_2 and N_2O, respectively. For SrNaNi and SrNiLi the full selectivity to CO_2 at low conversions of CH_4 is observed, suggesting that the reaction starts with CH_4 oxidation to intermediately form CO_2 (Eqs. 20 and 21). The subsequent increase of the CO selectivity indicates consecutive dry reforming of remaining CH_4 (Eq. 8). The H_2/CO ratio is finally adjusted by water-gas shift and Boudouard reactions (Eqs. 11 and 22) [248].

$$CH_4 + O_2 \rightarrow 2\ H_2 + CO_2 \quad (20)$$

$$CH_4 + 2\ N_2O \rightarrow 2\ H_2 + CO_2 + 2\ N_2 \quad (21)$$

$$CH_4 + CO_2 \rightarrow 2\ CO + 2\ H_2 \quad (8)$$

$$CO_2 + H_2 \leftrightarrows CO + H_2O \quad (11)$$

$$2\ CO \leftrightarrows CO_2 + C(s) \quad (22)$$

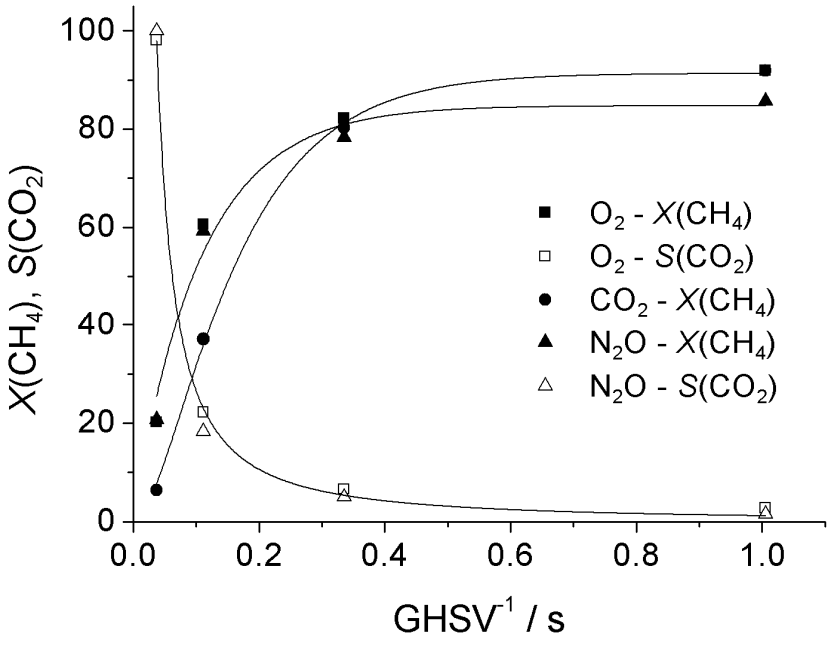

Figure 35. Conversions of CH_4 and selectivities to CO_2 in the reactions of CH_4 with O_2, CO_2, and N_2O, respectively, over SrNaNi(CT) at 1073 K.

Table 8. Catalytic performances of Ni-containing catalysts in the reactions of CH_4 with O_2, CO_2, and N_2O, respectively, (O/C = 1) at 1073 K and GHSV 3,600 h^{-1}.

Catalyst	Oxidizing agent	$X(CH_4)$ / %	$S(CO)$ / %	H_2/CO
SrNaNi(lit)	O_2	96.7	81.8	2.1
	N_2O	79.5	78.4	0.0
SrNaNi(CT)	O_2	91.9	97.2	2.1
	CO_2	91.9	97.1	2.0
	N_2O	85.8	100	1.8
SrNiLi(lit)	O_2	38.5	38.0	1.5
	N_2O	55.2	81.8	0.0
SrNiLi(CT)	O_2	40.9	49.5	3.3
	CO_2	57.0	83.7	1.8
	N_2O	80.5	100	1.8

The almost congruent evolution of conversions of CH_4 and selectivities to CO_2 in the CH_4 reaction with O_2, CO_2, and N_2O as shown for the SrNaNi(CT) catalyst (Figure 35) suggests that the initial oxidation step is fast and the subsequent dry reforming with CO_2 is rate determining in the overall reaction network. The slower activation of CH_4 as compared to CO_2, which is observed over a Ni/SiO_2 catalyst by isotope studies [249], could also contribute to this observation.

Conversions and selectivities of all Ni-containing catalysts are assembled in Table 8. In general, SrNaNi is more active than SrNiLi, which might be related to its higher Ni content. The DRM performance of SrNiLi even exceeds its POM activity. Due to the close-to-equilibrium conversions over SrNaNi this is hardly to be estimated. At sufficiently high conversions the H_2/CO ratios range around 2 in experiments applying O_2 and CO_2 as oxidants. Under identical reaction conditions, the CO yield obtained over SrNaNi almost as high as over a Rh/La_2O_3 catalyst obtained from a La-Rh-O mixed oxide precursor [121] encouraging further investigations on this catalyst system. It is observed that even after 40 h time-on-stream some catalysts are still not operating in steady state, but gain in activity. This behavior can be explained in view of the active species for the POM reaction: metallic Ni [121]. Although the catalysts are exposed to the CH_4-O_2 feed in their oxidized state, the high Ni content leads to higher reducibility in the presence of CH_4 compared to lower loaded materials. This reduction process continues with time on stream providing a steadily increasing number of POM active sites over more than 40 h on stream.

Unfortunately, the entirety of other catalysts tested in the OCM with CO_2 as the oxidizing agent at temperatures below 1123 K provided methane conversions below 3% and a noteworthy C_2 yield was hardly observed.

4.2.3.3 Li_2O/MgO based Catalysts

The catalytic performances of pure as well as Zr and Ce doped Li_2O/MgO catalysts are shown in Table 9. The stability is given as the temporal change of absolute activity in terms of CH_4 conversion dX/dt within 10 h on stream under the respective reaction conditions. In general, the use of O_2 as the oxidizing agent leads to higher conversions of CH_4 than N_2O except for LiMgZr(CT). Full conversion of O_2 and N_2O, respectively, at the GHSV of 3600 h^{-1} is observed in each case. N_2O is totally

converted except over LiMg(lit). It is seen that the CT catalysts provide lower conversions of CH_4 than the catalysts prepared by recipes from literature [8, 64]. With regard to the full conversion of O_2, this can be directly correlated to the lower selectivity because the total oxidation of CH_4 consumes more O_2 than the selective OCM. The doped CT catalysts provide a higher C_2 selectivity and also a higher stability over the pure LiMg(CT). ZrO_2 and CeO_2 are known as red-ox promotors and structural stabilizers, which can enhance the catalytic performance of active components [250].

Table 9. Catalytic performances of Li_2O/MgO-based catalysts in the reactions of CH_4 with O_2 and N_2O, respectively, (O/C = 1) at 1073 K and GHSV 3,600 h^{-1}.

Catalyst	Oxidizing agent	$X(CH_4)$ / %	$S(C_2)$ / %	$\Delta X/\Delta t$ / % h^{-1}
LiMg(lit)	O_2	41.4	37.3	– 0.33
	N_2O	9.0	55.2	– 0.08
LiMg(CT)	O_2	28.1	12.9	– 0.45
	N_2O	27.0	9.7	+ 0.02
LiMgZr(CT)	O_2	27.4	15.2	– 0.38
	N_2O	30.6	41.7	– 0.03
LiMgCe(lit)	O_2	43.0	37.0	– 0.01
	N_2O	34.3	41.9	– 0.01
LiMgCe(CT)	O_2	40.3	28.6	– 0.08
	N_2O	33.7	36.4	+ 0.04

Also the oxidizing agent has a remarkable impact on the stability of the samples. O_2 leads to a rapid activity loss in most cases, which is well-known for Li_2O/MgO catalysts [75, 235]. Contrarily, the use of N_2O apparently prevents the deactivation by O_2. In some cases even an increase in activity with time on stream was observed observed ($\Delta X/\Delta t > 0$). The lower oxidation strength of N_2O also lowers the areal rate of CH_4 conversion (Table 9). Moreover, the formation of more selective O species on the catalyst surface when using N_2O as the oxidizing agent lowers the local heat production since the reaction enthalpy for selective OCM reaction is lower than that of the CH_4 combustion. Thus it is assumed that the hot spot in the catalyst bed is

more pronounced in the OCM with O_2, which could be one reason for the differences in deactivation behavior. Accordingly, the thermally induced deactivation of the LiMg(CT) catalyst in OCM with O_2, i.e., sintering and/or evaporation of Li [75], is only 0.04% h^{-1} at 1023 K and 0.002% h^{-1} at 973 K, even though full O_2 conversion is obtained in each case.

In this view the origin of the lower stabilities and the lower C_2 selectivities obtained over the CT catalysts are assumed in their relatively high surface area leading to heat transfer limitations, which could favor secondary combustion of formed C_2 products [251] and thus explain the lower selectivity observed on these samples. The conversions of O_2 at 1073 K are compared in Figure 36 and it is seen that the global rates are by a factor of approx. 2 higher on the CT catalysts irrespective of the doping, which apparently only affects the product selectivities.

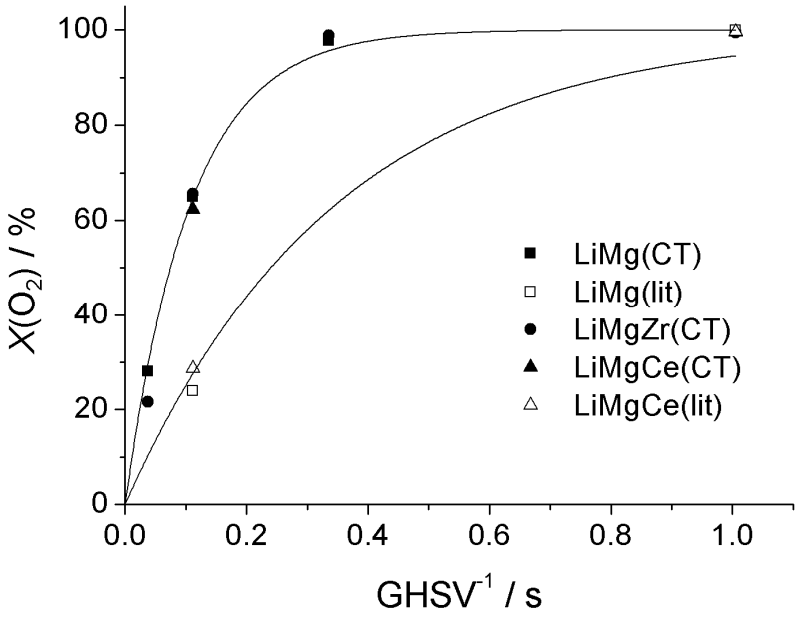

Figure 36. Conversions of O_2 in the OCM over LiMg-based catalysts at 1073 K.

4.2.3.4 Tungstate Catalysts

Methane conversions, C_2 selectivities as well as catalytic stability of NaWSi and RbWSi samples are shown inTable 10. The CT method leads to slightly higher conversions in the OCM with O_2. Generally, OCM activity with N_2O as the oxidizing agent is exceeding that of OCM with O_2. The higher activity of CT prepared catalysts

is attributed to the fine dispersion of tungstate ions over the catalyst bulk and surface as a result of the CT method. This provides an ideal distribution of the metal cations on a molecular level in the salt solutions prior to the impregnation of the template [185]. Instead, the incipient wetness impregnation reported in literature [60] yields agglomerates of alkaline tungstates on the SiO_2 surface (Figure 33b and c).

Table 10. Catalytic performances of alkaline tungstate catalysts in the reactions of CH_4 with O_2 and N_2O, respectively, (O/C = 1) at 1073 K and GHSV 3,600 h^{-1}.

Catalyst	Oxidizing agent	$X(CH_4)$ / %	$S(C_2)$ / %	$\Delta X/\Delta t$ / % h^{-1}
NaWSi(lit)	O_2	4.9	14.2	– 0.05
	N_2O	4.3	83.4	– 0.16
NaWSi(CT)	O_2	32.1	25.5	+ 0.19
	N_2O	21.3	49.5	– 0.05
RbWSi(lit)	O_2	29.7	45.3	– 0.12
	N_2O	3.8	73.5	– 0.12
RbWSi(CT)	O_2	31.8	29.9	+ 0.06
	N_2O	27.0	42.1	– 0.03

Contrarily to the Li_2O/MgO based catalysts, the tungstates tend to be more stable in the O_2 containing feed and deactivate in the OCM feed with N_2O. Especially for the CT catalysts, a gain in activity is observed for the reaction with O_2. Even more importantly the C_2 selectivity also increases with time-on-stream indicating that the maximum performance of these catalysts is not equilibrated even after 40 h reaction time. The loss of activity of the NaWSi(lit) sample can possibly be attributed to the decomposition of the Na_2WO_4 phase to WO_3 (Figure 32).

4.2.3.5 Earth alkaline and Lanthanide Oxides

The catalytic performance of earth alkaline and lanthanide oxide catalysts tested in this study is assembled in Table 11. At 1073 K and GHSV of 3,600 h^{-1}, all catalysts showed full O_2 conversion as it is also valid for the almost tenfold lower contact time (GHSV 32,000 h^{-1}). The CH_4 conversion is lower for N_2O than O_2 as the oxidizing

agent and almost unaffected by contact time in this regime free of oxidative compounds. However, the C_2 selectivity significantly increases with decreasing contact times. From that, we suggest that the catalytic performance shown in Table 11 is far from optimum conditions. As shown in Table 6, a CH_4:O_2 feed ratio > 2 is frequently observed for this class of catalysts. The catalysts of this group are very stable under the reaction conditions applied.

Table 11. Catalytic performances of earth alkaline and lanthanide oxides in the reactions of CH_4 with O_2 and N_2O, respectively, (O/C = 1) at 1073 K and GHSV 3,600 h^{-1}.

Catalyst	Oxidizing agent	$X(CH_4)$ / %	$S(C_2)$ / %	$S(C_2)$[a] / %	$\Delta X/\Delta t$ / % h^{-1}
SrLa(lit)	O_2	32.6	18.9	22.1	– 0.19
	N_2O	26.7	20.0	28.5	– 0.01
SrLa(CT)	O_2	37.5	22.2	29.1	– 0.07
	N_2O	29.8	26.8	31.1	+ 0.02
LaCa(lit)	O_2	35.9	16.7	21.4	– 0.01
	N_2O	29.9	24.3	32.1	– 0.01
LaCa(CT)	O_2	28.8	1.07	9.4	+ 0.06
	N_2O	27.5	18.5	19.9	– 0.01
NdCa(lit)	O_2	32.9	12.0	20.9	– 0.05
	N_2O	30.2	28.4	28.6	+ 0.02
NdCa(CT)	O_2	33.5	13.4	21.1	$\pm$ 0
	N_2O	29.8	30.6	35.0	+ 0.02
[a] GHSV 32,000 h^{-1}					

Although full conversion of the oxidizing agent is also observed in all experiments with N_2O, the conversions of CH_4 are higher in the presence of O_2 regardless the same C/O feed ratio in these comparative experiments and the higher C_2 selectivities obtained with N_2O. However, with regard to the secondary degradation of C_2 products as mentioned above, the latter might be the result of a slower overall reaction and not necessarily points at a different (more selective) O species formed by N_2O. In each case it is assumed that even at the short contact times significant coking occurs on these highly active catalysts. Unfortunately, shorter contact times

have not been realized in the experimental program. The CT method provides slight advantages in terms of CH_4 conversion and C_2 selectivity for SrLa and NdCa samples, whereas the preparation method reported in literature [63] appears to be the better choice in case of the LaCa catalyst.

4.2.3.6 BiYSm, NaMnMg, and Halogenide Containing Catalysts

Catalytic data of halogenide containing catalysts as well as the NaMnMg and BiYSm samples are listed in Table 12. In general, the reaction with N_2O is slower as compared to O_2. However, for the BiYSm catalysts C_2 selectivities are lower at the lower conversions of CH_4 indicating that active sites (re)generated by N_2O are less selective than those (re)generated by O_2. A very poor performance is observed for the NaMnMg(CT) sample, which provides lowest C_2 selectivities. It suggests that highly oxidizing permanganate ions are reduced to $Mn^{II/III}$ during the CT synthesis and released oxygen is consumed for the combustion of the cellulose template. Instead the impregnated NaMnMg(lit) catalyst [62] provides drastically improved conversions of CH_4 and higher selectivities to C_2 products in the OCM with O_2. The BaY samples show highest yields observed in this study and the use of N_2O increases the C_2 selectivity, however, at lower conversion of CH_4 making it difficult to distinguish whether this effect is due to secondary combustion of C_2 products or due to catalyst improvement. Full conversion of the oxidizing agent is observed in each experiment listed in Table 12 except for CO_2, which appears to be inappropriate to reoxidize the active site. BiYSm(lit), BaY(lit), and NaMnMg catalysts increase in activity with time-on-stream whereas all other samples show a stable catalytic performance or deactivate. BaY catalysts are unstable in N_2O suggesting that a high oxidative potential is required to maintain the catalytic activity similar to the observation of the low C_2 selectivity over the reduced NaMnMg(CT) sample.

A very poor catalytic performance in terms of OCM is observed for the NaBaSrTi catalysts. Zero selectivity to C_2 products is found in a broad range of reaction conditions, the low C_2 selectivity of NaBaSrTi(lit) in O_2 is overshadowed by a rapid activity loss. Regarding the poor performance of these catalysts in the present study, the high C_2 yield reported [59], however, under slightly different reaction conditions, is

difficult to comprehend. Instead, the high selectivities to CO_2 observed are in full agreement with the expected product spectrum for a perovskite-type catalyst [96].

The preparation method appears to be highly important for this group of catalysts. BiYSm and BaY catalysts provide a lower conversion of CH_4 when prepared via CT, which is a result of the drastically lowered C_2 selectivity as found for the Li_2O/MgO type catalysts. Similarly, the higher activity as a result of higher surface areas of CT samples is assumed to induce hot spots in the catalyst bed, which lower the C_2 selectivity and also the catalyst stability. For NaBaSrTi this effect is most obvious and the amenity of the CT method over citric acid sol gel synthesis is clearly visible [242] when C_2 selectivity is no object.

Table 12. Catalytic performances of halogenide containing catalysts in the reactions of CH_4 with O_2 and N_2O, respectively, (O/C = 1) at 1073 K and GHSV 3,600 h^{-1}.

Catalyst	Oxidizing agent	$X(CH_4)$ / %	$S(C_2)$ / %	$\Delta X/\Delta t$ / % h^{-1}
BiYSm(lit)	O_2	34.7	23.5	+ 0.12
	N_2O	27.0	23.0	± 0
BiYSm(CT)	O_2	27.5	5.0	– 0.03
	N_2O	23.5	3.3	– 0.01
NaMnMg(lit)	O_2	33.7	22.4	+ 0.09
	N_2O	16.7	29.3	– 0.28
NaMnMg(CT)	O_2	28.6	0.7	+ 0.19
	N_2O	22.6	1.4	– 0.01
BaY(lit)	O_2	45.4	40.7	+ 0.05
	N_2O	22.9	67.0	– 0.25
BaY(CT)	O_2	27.4	8.7	– 0.01
	N_2O	21.8	9.3	– 0.18
NaBaSrTi(lit)	O_2	6.7	9.3	– 0.73
	N_2O	2.9	0.0	– 0.17
NaBaSrTi(CT)	O_2	28.1	0.0	– 0.09
	N_2O	26.4	0.0	– 0.02

4.2.3.7 Perovskite Reference Samples

Perovskite-type oxides is a class of catalysts covering excellent materials for total oxidation of hydrocarbons with high selectivity to CO_2 [96]. In the present study selected samples showing a high CH_4 combustion performance with O_2 [242] were additionally tested in the reaction with N_2O. Although the lattice structure is not stable under the reaction conditions applied as shown for SrLaFeCo(CT) in the catalyst characterization section the catalysts tested show a very high and stable catalytic performance (Table 13) with a high selectivity to CH_4 combustion. The full conversion of O_2 and N_2O is found even at the lower reaction temperature of 750 °C and higher GHSV of 32,000 h^{-1}. Lower conversions of CH_4 when using N_2O are a result of higher selectivities to CO_2 obtained over these catalysts.

Table 13. Catalytic performances of perovskite catalysts in the reactions of CH_4 with O_2 and N_2O, respectively, at 800 °C and GHSV 3,600 h^{-1}.

Catalyst	Oxidizing agent	$X(CH_4)$ / %	$S(C_2)$ / %	dX/dt / % h^{-1}
SrLaMn(CT)	O_2	28.8	0.0	– 0.01
	N_2O	24.6	0.7	± 0
SrLaFeCo(CT)	O_2	30.7	0.0	– 0.03
	N_2O	24.3	0.1	– 0.03

Furthermore, it is very interesting to note that trace amounts of C_2 products are detected when using this mild oxidizing agent. The amounts of C_2 products are even higher at the initial period of reaction and decrease with time-on-stream in parallel to the degradation of the perovskite lattice. It suggests that the initial well ordered structure, which brings up C_2 selectivities of up to 2%, has a certain, however limited, potential for OCM catalysis.

4.2.4 Relationship between Catalyst Composition and Catalytic Performance

The comparison of oxidizing agents for the OCM over state-of-the-art catalysts indicates that N_2O could contribute to the solution of the C_2 selectivity problem. The total activities are lower when using N_2O as the oxidizing agent, however,

accompanied by higher selectivities to ethylene and ethane (Figure 37). It is in agreement with the fact that N_2O is a mild and less reactive oxidizing agent, whereas O_2 is highly reactive and more rapidly reoxidizes the catalyst surface. The higher selectivities observed at the lower conversions when using N_2O, however, can also be explained by reaction kinetics. Decreasing *S*/*X* trajectories are an indicator for a Wheeler type III reaction network of product formation and consecutive product degradation [252] as it is suggested for the OCM [45]. An increased microkinetic selectivity can only be determined at iso-conversion, i.e., by variation of GHSV. Unfortunately, several catalysts turned out to be too reactive thus providing full conversion of O_2 and N_2O in the whole range of GHSVs adjusted (e.g., SrLa, LaCa, NdCa). *S*/*X* data obtained in this regime is hard to compare. The statistical analysis of the entire dataset, however, reveals a remarkable improvement of the C_2 selectivity. In the range of CH_4 conversions between 25–35%, which comprises roughly 120 experimental data points of the entire dataset and corresponds to the upper limit of N_2O reactivity data, the increase of the average C_2 selectivity is + 11.1%. Thus it is concluded that the reoxidation of the catalyst by O_2 and N_2O provides different oxygen species as the final oxide species or as reactive intermediates, which substantially affect the overall selectivity in the OCM. On the other hand, disappointing results were obtained when using CO_2 as the oxidizing agent. Although thermodynamically allowed, conversions of CH_4 hardly exceed 1% and, if any, C_2 selectivities are very low. One reason could be that catalysts selected were chosen on the basis of best catalytic performance in the OCM with O_2 and the activation of CO_2 requires substantially different active sites, i.e. chemical compositions. But then a recent review points out that commonly used earth alkaline and lanthanide oxides are capable for CO_2 activation in the OCM reaction and also tungstates show a good performance [232]. However, even at 1123 K the highest conversions of CH_4 reported are around 5–7%. With regard to the maximum temperature of 1073 K in the present study this might be the most important reason for low performances observed.

With regard to the CT method as an alternative approach for catalyst preparation it turns out that these catalysts in most cases are in parts drastically inferior to the samples prepared via the respective methods reported in literature. One reason could be the higher surface areas obtained, which increase the global reactivity to

create hot spots in the catalyst bed and finally accelerate the combustion of C_2 reactants and products. Another reason could be the phase composition and hierarchical structure, which is, e.g, not BaF_2/Y_2O_3 in the BaY(CT) sample and not Na_2WO_4/SiO_2 in the NaWSi(CT) sample. Instead, various highly dispersed bulk mixed oxide phases are formed from the homogeneous mixture of precursor ions used for cellulose impregnation, which apparently is detrimental to the catalytic performance.

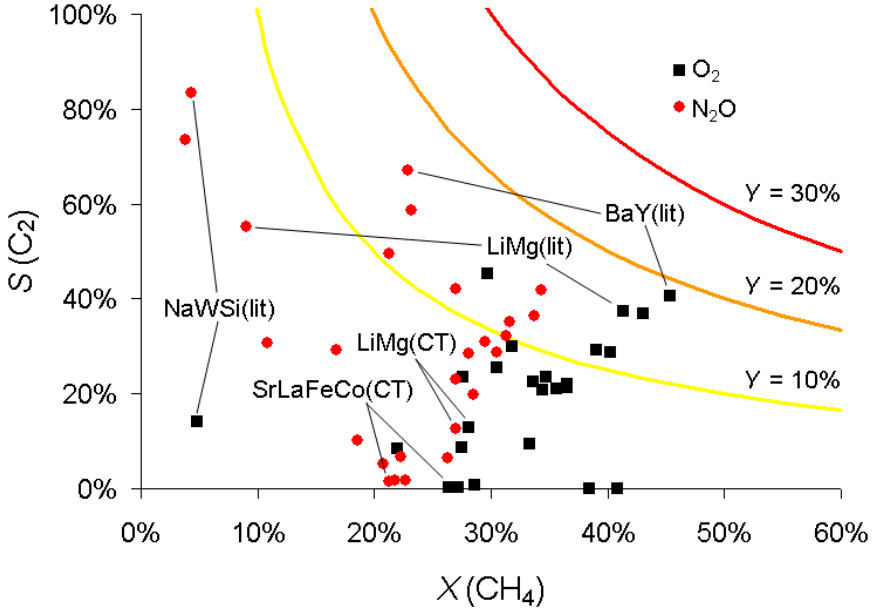

Figure 37. *S*/*X*-plot of catalytic performances obtained for all catalysts in the OCM with O_2 and N_2O at 1073 K. The plot contains data representing the highest C_2 yields obtained by variation of GHSV.

The last point to be mentioned is that the recipes reported in literature not in each case produce a valuable OCM catalyst. Especially for NaBaSrTi(lit), which is reported to provide a C_2 yield of almost 25% under reaction conditions similar to those applied in the present study [59], a poor catalytic performance with almost zero C_2 selectivity is found, which agrees with the typically observed high total oxidation performance of perovskite type catalysts [96]. The best catalyst identified under similar reaction conditions are BaY(lit), LiMg(lit), and LiMgCe(lit) giving yields of C_2 products close to 20%. The fact that the industrially relevant range of 30% is not attained must be referred to nonoptimized reaction conditions, i.e., molar composition of the feed. As can be seen from Table 6, the molar ratio of CH_4:O_2 often exceeds the stoichiometric

value of 2, whereas the addition of an inert diluting agent is frequently omitted. Both factors could contribute to an improved catalytic performance.

4.2.5 Conclusion

The present study underlines that besides the chemical composition also the synthesis strategy is a crucial factor for success in terms of high C_2 yields in the OCM reaction. High surface areas obtained with the cellulose templating method can favor nonisothermicity thus are detrimental to the C_2 selectivity. Catalyst recipes and trends in catalytic performances reported in literature could be reproduced in most cases. Compared to commonly used molecular oxygen as the oxidizing agent for OCM, nitrous oxide is a milder reactant leading to lower CH_4 conversions and higher C_2 selectivities even at iso-conversion of methane. CO_2 activation requires high temperatures although thermodynamically favored.

5 Conclusion

Polyethylene is one of the most important polymers. Thus it is not surprising that the ethylene demand is huge and expected to continuously increase within the next years and decades. Due to the declining resources of crude oil new synthesis strategies for olefins have to be explored. There are multiply bigger resources of natural gas than crude oil on earth. Natural gas mainly consists of methane, which can be converted to ethylene in energy consuming multiple process steps. The direct conversion of methane to ethylene via the Oxidative Coupling of Methane (OCM) is a challenging alternative. Since the early 80's research has been done on that reaction and many studies have been published, which dealt with its optimization and exploring new catalytic materials. However, a C_2-yield of 30%, which was determined to be the lower limit for an efficient industrial application of the OCM has not been achieved so far.

The aim of the present work was to examine the application of alternative oxidizing agents instead of O_2, which has a high risk potential. Furthermore, O_2 tends to promote the total oxidation of methane and C_2-products to CO and CO_2. A group of high-temperature stable catalysts with promising performance for the OCM with CO_2 are perovskites. To prepare active and stable mixed metal oxides of the perovskite type, different synthesis strategies and metal constituents were examined. Especially the template-assisted synthesis strategies such as the microemulsion templating and the cellulose templating were tested and the prepared materials were characterized with different methods such as XRD, SEM, TEM, N_2-BET, H_2-TPR, and others. For comparison, selected materials were also synthesized with more common methods such as sol-gel method or co-precipitation. As a result of variation of synthesis strategies, the materials prepared via microemulsion templating possess a lower perovskite phase transformation temperature as compared to the reference materials. This leads to smaller average crystal sizes in the nanometer scale combined with large specific surface areas. Furthermore, the microemulsion-templated materials possess a larger capacity for storage of lattice oxygen, which is available for surface redox processes at lower temperatures.

$SrCoO_x$ was chosen as the basis perovskite system because numerous publications are available on the characterization of this material. The $SrCoO_x$-perovskite

synthesized in microemulsions turned out to be a highly active methane combustion catalyst und rather unselective in the OCM with oxygen, which was an expected result. However, the microemulsion-templated materials showed higher activities and at least up to 5% C_2-selectivity compared to the reference materials prepared by co-precipitation and the sol-gel method.

Another synthesis strategy applied in this work is the cellulose templating method in which a usual filter paper gets impregnated with salt solutions and consecutively burned. Based on $SrCoO_x$ different compositions of mixed metal oxides were synthesized and accordingly tested in the OCM reaction. Here, the perovskite A-position (Sr) respectively the B-position (Co), were substituted systematically by different ions. The materials obtained were examined using scanning electron microscopy (SEM) and transmission electron microscopy (TEM). All materials showed a cellulose-like structure with highly cross-linked fibers. In the high magnification of the TEM the cellulose-like structure was found to consist of agglomerated nanoparticles of 40 to 150 nm in diameter. The specific surface areas of the perovskite oxides were determined to be in the range of 1 to 12 $m^2\ g^{-1}$, which is higher than those typically found in literature. The X-ray diffraction examinations revealed that all materials consist of pure hexagonal perovskite-phases and only some samples formed traces of carbonates, especially Sr and Ba containing perovskites. H_2-TPR examinations showed many different reduction profiles for the different perovskite compositions. The temperature range, the number of peaks and also the reduction onset temperatures were very different. A correlation of the profiles was not possible because the insertion of new ions in the perovskite lattice leads to other oxygen species and possibly to different reduction mechanisms. The $SrCoO_x$-based perovskites were also examined on their capability to activate methane and they showed very good activities towards total oxidation.

Those materials, which were substituted with rare earth metals such as La, Pr, Nd, or Sm at the A-position, showed the highest activities. However, also the substitution of Mn or Fe at the B-position of the $SrCoO_x$ led to higher activities as compared to the basis system. The exchange of Sr with Ca and Ba, but also the exchange at the B-position with Mo and Cr resulted in worse methane activation properties. The latter provide smaller specific surface areas, which could explain the lower activities.

Although the perovskites were tested in an oxygen-lean atmosphere, C_2-selectivities above 5% at a reaction temperature of 823 K could not be observed. The methane activation rates were increased as compared to the basis system $SrCoO_x$ and also to perovskites synthesized with other methods. However, the chosen reaction conditions were not optimal because almost all catalysts showed complete oxygen conversion due to the high selectivity to the oxygen consuming methane combustion pathway. In summary, a comparison with literature data is very demanding because the gas compositions commonly tested strongly differ from the one used in this work. This is because perovskite materials are known to be hydrocarbon combustion catalysts. Anyway, on selected catalysts it could be proven that the cellulose templating method leads to materials with improved structural and catalytic properties compared to other synthesis strategies.

The final part of this work was to select well-performing OCM catalysts from previous work packages and from literature and to compare their catalytic performances under the same reaction conditions. These different materials were prepared according to the synthesis recipes reported in literature but also with the cellulose templating method. Selected samples were structurally analyzed after the long term catalysis run. All samples showed smaller specific surface areas as reported in literature, which can be explained by the sintering of the catalysts during OCM reaction at elevated temperature. After long-term catalysis the LiMgO catalyst synthesized with the cellulose templating method provides a higher specific surface area as compared to the sample synthesized according to literature (incipient wetness impregnation), which indicates a more stable structure of the first. This is a big advantage of the cellulose templating method because LiMgO is known for its poor structural stability. Regarding the high-performance catalysts, XRD analyses showed that BaF_2/Y_2O_3 and Na_2WO_4/SiO_2 are relatively stable during catalysis, however, $BaCO_3$ and WO_3 were found, respectively, after 40 h time-on-stream, possibly leading to a deactivation of the catalysts. The catalyst with the most pronounced deactivation was the perovskite $Sr_{0.4}La_{0.6}Fe_{0.2}Co_{0.8}O_x$. Here, many different mixed metal oxide phases arised, which means that the material was completely decomposed. SEM and EDX examinations supported the results from the XRD analysis. This is in contradiction to the previously mentioned advantage of the high temperature stability of the perovskites. Based on thermodynamic calculations the different catalysts were tested

in the OCM with O_2, CO_2, and N_2O. In the OCM with CO_2 the catalysts showed no or only minor activity and almost no C_2-selectivity under the reaction conditions applied in this work. In contrast N_2O is an efficient oxidizing agent. The general trend is, that in comparison to O_2 a lower overall activity at a higher C_2-selectivity is observed. These results are in good agreement with the fact that N_2O in several other applications turned out to be a milder and less reactive oxidizing agent than O_2. Unfortunately, some of the tested catalysts provided such high reactivity that complete O_2 and N_2O conversions were observed under almost all the reaction conditions adjusted. In summary, the comparison of the literature methods with the cellulose templating method illustrates that the cellulose templated catalysts in average showed worse catalytic results. A reason could be the higher specific surface areas, which were obtained as a result of cellulose templating. Higher global activities obtained this way could lead to hot spots in the catalyst bed, promoting total combustion of the hydrocarbons.

As an outlook to future studies on this topic the next step could be to repeatedly assort the materials and identify the most active and selective ones. These catalysts should be tested again in the OCM with O_2 and N_2O, whereby the reaction conditions should be adapted to the results of this work. That could include, e.g., lower GHSVs or a molar excess of the oxidizing agent with respect to methane in the feed gas. This way a better comparison between the materials should be possible. In addition the best materials should further be structurally analyzed in more detail. To identify the processes, which lead to catalyst deactivation, and the facts that make a good OCM catalyst fresh and used catalyst samples should be taken after different times-on-stream to be analyzed. Temporal analysis of products (TAP) experiments could give a more precise idea about the difference between O_2 and N_2O as the oxidizing agent in OCM and on the consequences for conversion and selectivity. The approach to find an alternative oxidizing agent for O_2 in the OCM should to be continued with N_2O and further materials should be tested. Furthermore, CO_2 as the cheapest and environmentally most friendly oxidizing agent should be repeatedly tested at higher temperatures above 950 K.

6 References

[1] F. Geldsetzer, U. Jahn, in: Römpp Chemie-Lexikon, Thieme, 2006.
[2] Erdgas - Wikipedia, (2011).
[3] G.E. Keller, M.M. Bhasin, J. Catal., 73 (1982) 9-19.
[4] Ullmann's Encyclopedia of Industrial Chemistry, (2003) 774.
[5] P.F. van den Oosterkamp, *Encyclopedia of Catalysis*, 6. Aufl., Wiley-VCH Weinheim, 2003.
[6] H. Aritani, H. Yamada, T. Nishio, T. Shiono, S. Imamura, M. Kudo, S. Hasegawa, T. Tanaka, S. Yoshida, J. Phys. Chem., 104 (2000) 10133-10143.
[7] J.H. Lunsford, Angew. Chem. Int. Ed., 34 (1995) 970-980.
[8] T. Ito, J. Wang, C.H. Lin, J.H. Lunsford, J. Am. Chem. Soc., 107 (1985) 5062-5068.
[9] E.V. Kondratenko, D. Wolf, M. Baerns, Catal. Lett., 58 (1999) 217-223.
[10] E.V. Kondratenko, O.V. Buyevskaya, M. Soick, M. Baerns, Catal. Lett., 63 (1999) 153-159.
[11] P.C.T. Au, Y.W. Liu, C.F. Ng, J. Catal., 176 (1998) 365-375.
[12] J.H. Lunsford, Catal. Rev.-Sci. Technol., 8 (1973) 135.
[13] H. Yamashita, Y. Machida, A. Tomita, Appl. Catal. A, 79 (1991) 203-214.
[14] N.-B. Wong, J.H. Lunsford, J. Chem. Phys., 56 (1972) 2664.
[15] T. Ito, M. Kato, K. Toi, T. Shirakawa, I. Ikemoto, T. Tokuda, J. Chem. Soc., Faraday Trans. 1, 81 (1985) 2835.
[16] C. Louis, T. Lin Chang, M. Kermarec, T. Le Vana, J. Michel Tatibouët, M. Chea, Catal. Today, 13 (1992) 283-289.
[17] J.X. Wang, J.H. Lunsford, J. Phys. Chem., 90 (1986) 5883-5887.
[18] W. Weng, M. Chen, H. Wan, Y. Liao, Catal. Lett., 53 (1998) 43-50.
[19] D.J. Driscoll, W. Martir, J.X. Wang, J.H. Lunsford, J. Am. Chem. Soc., 107 (1985) 58-63.
[20] O.V. Buyevskaya, M. Rothaemel, H.W. Zanthoff, M. Baerns, J. Catal., 146 (1994) 346-357.
[21] D. Dissanayake, J.H. Lunsford, M.P. Rosynek, J. Catal., 146 (1994) 613-615.
[22] S.C. Street, G. Liu, D.W. Goodman, Surf. Sci., 385 (1997) L971-L977.
[23] K.D. Campbell, E. Morales, J.H. Lunsford, J. Am. Chem. Soc., 109 (1987) 7900-7901.
[24] Y. Feng, J. Niiranen, D. Gutman, J. Phys. Chem., 95 (1991) 6558-6563.
[25] O. Buyevskaya, D. Wolf, M. Baerns, Recl. Trav. Chim. Pays-Bas, 113 (1994) 459-464.
[26] J.G. McCarty, A.B. McEwen, M.A. Quinlan, in: New Developments in Selective Oxidation, Elsevier, New York, 1992, S. 405-415.
[27] C. Shi, M. Hatano, J.H. Lunsford, Catal. Today, 13 (1992) 191-199.
[28] K. van der Wiele, J.W.M.H. Geerts, J.M.N. van Kasteren, in: Methane Conversion by Oxidative Processes, New York, 1992, S. 259-319.
[29] R. Auer, F.C. Thyrion, Ind. Eng. Chem. Res., 41 (2002) 680-690.
[30] P.M. Couwenberg, Q. Chen, G.B. Marin, Ind. Eng. Chem. Res., 35 (1996) 3999-4011.
[31] M. Daneshpayeh, N. Mostoufi, A. Khodadadi, R. Sotudeh-Gharebagh, Y. Mortazavi, Energy & Fuels, 0 (0).
[32] Y.K. Kao, L. Lei, Y.S. Lin, Ind. Eng. Chem. Res., 36 (1997) 3583-3593.
[33] M. Kilo, M.A. Taylor, C. Argirusis, G. Borchardt, R.A. Jackson, O. Schulz, M. Martin, M. Weller, Solid State Ionics, 175 (2004) 823-827.
[34] S. Majumdar, I.G. Sharma, A.C. Bidaye, A.K. Suri, Thermochim. Acta, 473 (2008) 45-49.
[35] S.C. Reyes, C.P. Kelkar, E. Iglesia, Catal. Lett., 19 (1993) 167-180.
[36] S.C. Reyes, E. Iglesia, C.P. Kelkar, Chem. Eng. Sci., 48 (1993) 2643-2661.
[37] J.A. Roos, S.J. Korf, R.H.J. Veehof, J.G. van Ommen, J.R.H. Ross, Appl. Catal., 52 (1989) 131-145.
[38] C.T. Tye, A.R. Mohamed, S. Bhatia, Chem. Eng. J., 87 (2002) 49-59.
[39] C.A. Jones, J.J. Leonard, J.A. Sofranko, J. Catal., 103 (1987) 311-319.
[40] C.H. Lin, K.D. Campbell, J.X. Wang, J.H. Lunsford, J. Phys. Chem., 90 (1986) 534-537.
[41] J.A. Labinger, Catal. Lett., 1 (1988) 371-375.
[42] C.A. Mims, R. Mauti, A.M. Dean, K.D. Rose, J. Phys. Chem., 98 (1994) 13357-13372.
[43] J.A. Roos, A.G. Bakker, H. Bosch, J.G. van Ommen, J.R.H. Ross, Catal. Today, 1 (1987) 133-145.
[44] G.J. Hutchings, M.S. Scurrell, in: Methane Conversion by Oxidative Processes, 1992, S. 201-258.
[45] L. Mleczko, M. Baerns, Fuel Proc. Technol., 42 (1995) 217-248.
[46] M. Hatano, K. Otsuka, J. Chem. Soc., Faraday Trans. 1, 85 (1989) 199.
[47] Z. Kalenik, E.E. Wolf, Catal. Today, 13 (1992) 255-264.
[48] D.J. Statman, J.T. Gleaves, D. McNamara, P.L. Mills, G. Fornasari, J.R.H. Ross, Appl. Catal., 77

(1991) 45-53.
[49] K.P. Peil, J.G. Goodwin, G. Marcelin, J. Catal., 131 (1991) 143-155.
[50] W. Hinsen, M. Baerns, Chem. Z., 107 (1983) 223.
[51] T. Ito, J.H. Lunsford, Nature, 314 (1985) 721-722.
[52] O.V. Krylov, Catal. Today, 18 (1993) 209-302.
[53] V.D. Sokolovskii, E.A. Mamedov, Catal. Today, 14 (1992) 415-465.
[54] Y.I. Pyatnitsky, N.I. Ilchenko, L.Y. Dolgikh, N.V. Pavlenko, Top. Catal., 11-12 (2000) 229-237.
[55] A.I. Bostan, Y.I. Pyatnitskii, L.N. Raevskaya, V.G. Pryanikova, S.A. Nedil'ko, A.G. Dzyaz'ko, E.G. Zen'kovich, Theor. Exp. Chem., 41 (2005) 32-36.
[56] Y.I. Pyatnitskii, A.I. Bostan, L.N. Raevskaya, S.A. Nedil'ko, A.G. Dzyaz'ko, E.G. Zen'kovich, Theor. Exp. Chem., 41 (2005) 117-121.
[57] Y. Zeng, F.T. Akin, Y.S. Lin, Appl. Catal. A, 213 (2001) 33-45.
[58] C.T. Au, X.P. Zhou, Y.W. Liu, W.J. Ji, C.F. Ng, J. Catal., 174 (1998) 153-163.
[59] Z. Fakhroueian, F. Farzaneh, N. Afrookhteh, Fuel, 87 (2008) 2512-2516.
[60] A. Palermo, J.P. Holgado Vazquez, R.M. Lambert, Catal. Lett., 68 (2000) 191-196.
[61] J.M. DeBoy, R.F. Hicks, Ind. Eng. Chem. Res., 27 (1988) 1577-1582.
[62] J.A. Sofranko, J.J. Leonard, C.A. Jones, A.M. Gaffney, H.P. Withers, Catal. Today, 3 (1988) 127-135.
[63] V.H. Rane, S.T. Chaudhari, V.R. Choudhary, J. Chem. Technol. Biotechnol., 81 (2006) 208-215.
[64] R.L.P. Gonçalves, F.C. Muniz, F.B. Passos, M. Schmal, Catal. Lett., 135 (2010) 26-32.
[65] J.M. Thomas, W. Ueda, J. Williams, K.D.M. Harris, Faraday Discuss. Chem. Soc., 87 (1989) 33.
[66] Z.C. Jiang, C.J. Yu, X.P. Fang, S.B. Li, H.L. Wang, J. Phys. Chem., 97 (1993) 12870-12875.
[67] R. Mariscal, M.A. Pen[small tilde]a, J.L.G. Fierro, Appl. Catal. A, 131 (1995) 243-261.
[68] L. Lietti, S.T. Brandao, P. Villa, S. Rossini, Catal. Lett., 36 (1996) 151-157.
[69] I. Matsuura, Y. Utsumi, T. Doi, Y. Yoshida, Appl. Catal., 47 (1989) 299-306.
[70] S.J. Korf, J.A. Roos, N.A. de Bruijn, J.G. van Ommen, J.R.H. Ross, Catal. Today, 2 (1988) 535-545.
[71] V. Choudhary, S. Mulla, M. Pandit, S. Choudhari, V. Rane, J. Chem. Technol. Biotechnol., 75 (2000) 828-834.
[72] J.S.. Hargreaves, G.. Hutchings, R.W. Joyner, C.J. Kiely, Catal. Today, 13 (1992) 401-407.
[73] J.A. Roos, S.J. Korf, A.G. Bakker, N.A. De Bruijn, J.G. Van Ommen, J.R.H. Ross, in: Methane Conversion, Proceedings of a Symposium on the Production of Fuels and Chemicals from Natural Gas, Elsevier, 1988, S. 427-432.
[74] X.D. Peng, D.A. Richards, P.C. Stair, J. Catal., 121 (1990) 99-109.
[75] S. Arndt, PhD thesis, TU Berlin, 2011.
[76] S.J. Korf, J.A. Roos, N.A. De Bruijn, J.G. Van Ommen, J.R.H. Ross, Appl. Catal., 58 (1990) 131-146.
[77] J.M.N. van Kasteren, J.W.M.H. Geerts, K. van der Wiele, in: New Developments in Selective Oxidation, Elsevier, 1990, S. 343-349.
[78] J. Wu, S. Li, J. Niu, X. Fang, Appl. Catal. A, 124 (1995) 9-18.
[79] D.J. Wang, M.P. Rosynek, J.H. Lunsford, J. Catal., 155 (1995) 390-402.
[80] S. Pak, P. Qiu, J.H. Lunsford, J. Catal., 179 (1998) 222-230.
[81] A. Palermo, J.P. Holgado Vazquez, A.F. Lee, M.S. Tikhov, R.M. Lambert, J. Catal., 177 (1998) 259-266.
[82] R. Andorf, M. Baerns, Catal. Today, 6 (1990) 445-452.
[83] S. Becker, M. Baerns, J. Catal., 128 (1991) 512-519.
[84] J.A.S.P. Carreiro, M. Baerns, J. Catal., 117 (1989) 396-403.
[85] T. Grzybek, M. Baerns, J. Catal., 129 (1991) 106-113.
[86] K.D. Campbell, J.H. Lunsford, J. Phys. Chem., 92 (1988) 5792-5796.
[87] V.R. Choudhary, S.T. Chaudhari, A.M. Rajput, V.H. Rane, Catal. Lett., 3 (1989) 85-87.
[88] K. Otsuka, Q. Liu, M. Hatano, A. Morikawa, Chem. Lett., (1986) 903-906.
[89] A.N. Shigapov, M.A. Novoshilova, S.N. Vereshchagin, A.G. Anshits, V.D. Sokolovskii, React. Kinet. Catal. Lett., 37 (1988) 397-402.
[90] R. Burch, G.D. Squire, S.C. Tsang, Appl. Catal., 43 (1988) 105-116.
[91] B.K. Warren, Catal. Today, 13 (1992) 311-320.
[92] Y. Osada, S. Koike, T. Fukushima, S. Ogasawara, T. Shikada, T. Ikariya, Appl. Catal., 59 (1990) 59-74.
[93] Y. Erarslanoglu, I. Onal, T. Dogu, S. Senkan, Appl. Catal. A, 145 (1996) 75-84.
[94] S. Liu, X. Tan, K. Li, R. Hughes, Catal. Rev.-Sci. Eng., 43 (2001) 147.

[95] M. Stoukides, Catal. Rev.-Sci. Eng., 42 (2000) 1.
[96] V.L.G. Tejuca, J.L.G. Fierro, *Properties and Applications of Perovskite-type Oxides*, New York, 1993.
[97] H. Tanaka, I. Tan, M. Uenishi, M. Kimura, K. Dohmae, Top. Catal., 16-17 (2001) 63-70.
[98] Y. Nishihata, J. Mizuki, T. Akao, H. Tanaka, M. Uenishi, M. Kimura, T. Okamoto, N. Hamada, Nature, 418 (2002) 164-167.
[99] R.H. Buttner, E.N. Maslen, Acta Crystallogr. B, 48 (1992) 644-649.
[100] V.M. Goldschmidt, Naturwiss., 14 (1926) 477-485.
[101] Perowskit – Wikipedia, http://de.wikipedia.org/wiki/Perowskit, Mai 2011.
[102] M.J. Sayagués, M. Vallet-Regí, A. Caneiro, J.M. González-Calbet, J. Solid. State Chem., 110 (1994) 295-304.
[103] B.C. Tofield, W.R. Scott, J. Solid. State Chem., 10 (1974) 183-194.
[104] L.G. Tejuca, J.L.G. Fierro, J.M.D. Tascón, Academic Press, 1989, S. 237-328.
[105] D. Fino, N. Russo, G. Saracco, V. Specchia, Progress in Solid State Chemistry, 35 (2007) 501-511.
[106] R.J.H. Voorhoeve, D.W. Johnson, J.P. Remeika, P.K. Gallagher, Science, 195 (1977) 827 -833.
[107] C.H. Kim, G. Qi, K. Dahlberg, W. Li, Science, 327 (2010) 1624 -1627.
[108] P.R. Watson, G.A. Somorjai, J. Catal., 74 (1982) 282-295.
[109] G.A. Somorjai, Chem. Soc. Rev., 13 (1984) 321.
[110] M.A. Ulla, R.A. Migone, J.O. Petunchi, E.A. Lombardo, J. Catal., 105 (1987) 107-119.
[111] N. Yamazoe, N. Miura, Components, Packaging, and Manufacturing Technology, Part A, IEEE Transactions on, 18 (1995) 252-256.
[112] H. Obayashi, T. Kudo, Mater. Res. Bull., 13 (1978) 1409-1413.
[113] E.C. Subbarao, *Solid electrolytes and their applications*, Plenum Press, 1980.
[114] G. Kremenic, J.M.L. Nieto, J.M.D. Tascon, L.G. Tejuca, J. Chem. Soc., Faraday Trans. 1, 81 (1985) 939.
[115] T. Nakamura, M. Misono, Y. Yoneda, Bull. Chem. Soc. Japan, 55 (1982) 394-399.
[116] T. Nitadori, M. Misono, J. Catal., 93 (1985) 459-466.
[117] H. Arai, T. Yamada, K. Eguchi, T. Seiyama, Appl. Catal., 26 (1986) 265-276.
[118] D. Ferri, L. Forni, Appl. Catal. B, 16 (1998) 119-126.
[119] R. Lago, G. Bini, M.A. Peña, J.L.G. Fierro, J. Catal., 167 (1997) 198-209.
[120] T. Hayakawa, A.G. Andersen, M. Shimizu, K. Suzuki, K. Takehira, Catal. Lett., 22 (1993) 307-317.
[121] Å. Slagtern, U. Olsbye, Appl. Catal. A, 110 (1994) 99-108.
[122] T. Hayakawa, H. Harihara, A.G. Andersen, K. Suzuki, H. Yasuda, T. Tsunoda, S. Hamakawa, A.P.E. York, Y.S. Yoon, M. Shimizu, K. Takehira, Appl. Catal. A, 149 (1997) 391-410.
[123] H. Provendier, C. Petit, C. Estournes, A. Kiennemann, in: NATURAL GAS CONVERSION V, Proceedings ofthe 5th International Natural Gas Conversion Symposium,, Elsevier, 1998, S. 741-746.
[124] J.W. Nam, H. Chae, S.H. Lee, H. Jung, K.-Y. Lee, in: NATURAL GAS CONVERSION V, Proceedings ofthe 5th International Natural Gas Conversion Symposium,, Elsevier, 1998, S. 843-848.
[125] S. Suzuki, T. Hayakawa, S. Hamakawa, K. Suzuki, T. Shishido, K. Takehira, in: NATURAL GAS CONVERSION V, Proceedings ofthe 5th International Natural Gas Conversion Symposium,, Elsevier, 1998, S. 783-788.
[126] J.E. ten Elshof, H.J.M. Bouwmeester, H. Verweij, Appl. Catal. A, 130 (1995) 195-212.
[127] T. Hibino, T. Sato, K.-ichi Ushiki, Y. Kuwahara, J. Chem. Soc., Faraday Trans., 91 (1995) 4419.
[128] W. Wang, Y.S. Lin, J. Membr. Sci., 103 (1995) 219-233.
[129] S. Hamakawa, T. Hibino, H. Iwahara, J. Electrochem. Soc., 141 (1994) 1720-1725.
[130] G. Marnellos, O. Sanopoulou, A. Rizou, M. Stoukides, Solid State Ionics, 97 (1997) 375-383.
[131] A. Nemudry, P. Rudolf, R. Schollhorn, Chem. Mater., 8 (1996) 2232-2238.
[132] A. Nakatsuka, A. Yoshiasa, N. Nakayama, T. Mizota, H. Takei, ChemInform, 35 (2004).
[133] K.-W. Lee, W.E. Pickett, Phys. Rev. B, 73 (2006) 174428-8.
[134] Z. Gaoke, L. Ying, Y. Xia, W. Yanping, O. Shixi, L. Hangxing, Mater. Chem. Phys., 99 (2006) 88-95.
[135] T. Nagai, W. Ito, T. Sakon, Solid State Ionics, 177 (2007) 3433-3444.
[136] L. Karvonen, S. Räsänen, H. Yamauchi, M. Karppinen, Chem. Lett., 36 (2007) 1176.
[137] P. Zeng, R. Ran, Z. Chen, W. Zhou, H. Gu, Z. Shao, S. Liu, J. Alloy Comp., 455 (2008) 465-470.
[138] V.V. Kharton, A.A. Yaremchenko, A.V. Kovalevsky, A.P. Viskup, E.N. Naumovich, P.F. Kerko, J.

Membr. Sci., 163 (1999) 307-317.
[139] Z.-B. Chen, T.-R. Ling, M.-D. Lee, React. Kinet. Catal. Lett., 62 (1997) 185-190.
[140] K. Omata, O. Yamazaki, K. Tomita, K. Fujimoto, J. Chem. Soc., Chem. Commun., (1994) 1647-1648.
[141] J.-C. Grenier, S. Ghodbane, G. Demazeau, M. Pouchard, P. Hagenmuller, Mater. Res. Bull., 14 (1979) 831-839.
[142] P. Zhu, J. Li, Q. Huang, S. Yan, M. Liu, R. Zhou, J. Nat. Gas Chem., 18 (2009) 346-353.
[143] S.S.-Y. Lin, H. Daimon, S.Y. Ha, Appl. Catal. A, 366 (2009) 252-261.
[144] L. Ge, Z. Zhu, Z. Shao, S. Wang, S. Liu, Ceram. Int., 35 (2009) 3201-3206.
[145] G.I. Golodets, *Heterogeneous Catalytic Reaction*, Elsevier, Amsterdam, 1983.
[146] O. Ovsitser, M. Cherian, E.V. Kondratenko, J. Phys. Chem., 111 (2007) 8594-8602.
[147] J.H. Lunsford, J.P. Jayne, J. Phys. Chem., 70 (1966) 3464-3469.
[148] O.V. Krylov, L.Y. Margolis, Int. Rev. Phys. Chem., 3 (1983) 305.
[149] P. Meriaudeau, C. Naccache, A.J. Tench, J. Catal., 21 (1971) 208-211.
[150] P.D.F. Vernon, M.L.H. Green, A.K. Cheetham, A.T. Ashcroft, Catalysis Letters, 6 (1990) 181-186.
[151] A.P.E. York, T. Xiao, M.L.H. Green, J.B. Claridge, Catalysis Reviews, 49 (2007) 511-560.
[152] E.V. Kondratenko, O. Ovsitser, Angew. Chem. Int. Ed., 47 (2008) 3227-3229.
[153] X. Rozanska, E.V. Kondratenko, J. Sauer, J. Catal., 256 (2008) 84-94.
[154] E.V. Kondratenko, A. Brückner, J. Catal., 274 (2010) 111-116.
[155] E.V. Kondratenko, M. Cherian, M. Baerns, D. Su, R. Schlögl, X. Wang, I.E. Wachs, J. Catal., 234 (2005) 131-142.
[156] E.V. Kondratenko, N.G. Maksimov, G.E. Selyutin, A.G. Anshits, Catal. Today, 24 (1995) 273-275.
[157] J.B. Kimble, J.H. Kolts, Energy Prog., 6 (1986) 226.
[158] X. Li, K. Tomishige, K. Fujimoto, Catal. Lett., 36 (1996) 21-24.
[159] A.M. Maitra, C. Sacchetta, R.J. Tyler, in: Natural Gas Conversion II - Proceedings of the Third Natural Gas Conversion Symposium, Elsevier, 1994, S. 261-263.
[160] P. Pereira, S.H. Lee, G.A. Somorjai, H. Heinemann, Catal. Lett., 6 (1990) 255-262.
[161] T. Nishiyama, K.-I. Aika, J. Catal., 122 (1990) 346-351.
[162] K. Asami, T. Fujita, K.-ichi Kusakabe, Y. Nishiyama, Y. Ohtsuka, Appl. Catal. A, 126 (1995) 245-255.
[163] L. Yuliati, H. Yoshida, Chem. Soc. Rev., 37 (2008) 1592.
[164] J. Raskó, F. Solymosi, Catal. Lett., 46 (1997) 153-157.
[165] J. Raskó, F. Solymosi, Catal. Lett., 54 (1998) 49-54.
[166] .
[167] C.L. Thomas, in: Catalyst Manufacture, Academic Press, New York, 1995, S. 291.
[168] G. Ertl, H. Knözinger, F. Schüth, J. Weitkamp, Hrsg., *Handbook of Heterogeneous Catalysis*, Wiley-VCH Verlag GmbH & Co. KGaA, Weinheim, Germany, 2008.
[169] P. Peshev, A. Toshev, G. Gyurov, Mater. Res. Bull., 24 (1989) 33-40.
[170] L.L. Hench, *Kirk-Othmer Encyclopedia of Chemical Technology*, John Wiley & Sons, 2007.
[171] C.J. Brinker, G.W. Scherer, in: The Physics and Chemistry of Sol-Gel Processing, Academic Press, Boston, 1990, S. 908.
[172] M. Schneider, A. Baiker, Catal. Rev.-Sci. Eng., 37 (1995) 515.
[173] A.C. Pierre, G.M. Pajonk, Chem. Rev., 102 (2002) 4243-4266.
[174] A.C. Pierre, *Introduction to sol-gel processing*, Springer, 1998.
[175] D.H. Busch, J. Incl. Phenom. Macrocycl. Chem., 12 (1992) 389-395.
[176] D. Wöhrle, G. Meyer, Kontakte Darmstadt, 3 (1985) 38.
[177] F. Vögtle, *Supramolekulare Chemie.: Eine Einführung.*, Teubner, 1992.
[178] M. Bühner, W. Geuder, W. Gries, S. Hünig, M. Koch, T. Poll, Angewandte Chemie, 100 (1988) 1611-1614.
[179] S. Eriksson, U. Nylén, S. Rojas, M. Boutonnet, Appl. Catal. A, 265 (2004) 207-219.
[180] A. López-Trosell, R. Schomäcker, Mater. Res. Bull., 41 (2006) 333-339.
[181] J. Schmidt, C. Guesdon, R. Schomäcker, J. Nanopart. Res., 1 (1999) 267-276.
[182] G. Schinkel, I. Garrn, B. Frank, U. Gernert, H. Schubert, R. Schomäcker, Mater. Chem. Phys., 111 (2008) 570-577.
[183] A.N. Shigapov, G.W. Graham, R.W. McCabe, H.K. Plummer, Appl. Catal. A, 210 (2001) 287-300.
[184] A. Simon, E.V. Kondratenko, Chem. Eur. J., 16 (2010) 1765-1767.

[185] E.V. Kondratenko, V. Gölden, S. Sokolov, ChemCatChem, 2 (2010) 633-635.
[186] G. Pecchi, P. Reyes, R. Zamora, C. Campos, L.E. Cadús, B.P. Barbero, Catal. Today, 133-135 (2008) 420-427.
[187] C.A. Mirkin, Small, 1 (2005) 14-16.
[188] J.M. Campelo, D. Luna, R. Luque, J.M. Marinas, A. Romero, ChemSusChem, 2 (2009) 18-45.
[189] D. Kießling, R. Schneider, P. Kraak, M. Haftendorn, G. Wendt, Appl. Catal. B, 19 (1998) 143-151.
[190] M. O'Connell, A.K. Norman, C.F. Hüttermann, M.A. Morris, Catal. Today, 47 (1999) 123-132.
[191] M.A. Peña, J.L.G. Fierro, Chem. Rev., 101 (2001) 1981-2018.
[192] K. Stephan, M. Hackenberger, D. Kießling, G. Wendt, Chem. Eng. Technol., 27 (2004) 687-693.
[193] N.E. Trofimenko, J. Paulsen, H. Ullmann, R. Müller, Solid State Ionics, 100 (1997) 183-191.
[194] R. Le Toquin, W. Paulus, A. Cousson, C. Prestipino, C. Lamberti, J. Am. Chem. Soc., 128 (2006) 13161-13174.
[195] E. Knaepen, J. Mullens, J. Yperman, L.C. Van Poucke, Thermochim. Acta, 284 (1996) 213-227.
[196] E. Ingier-Stocka, L. Rycerz, J. Therm. Anal. Calorim., 56 (1999) 547-552.
[197] F. Al-Newaiser, S. Al-Thabaiti, A. Al-Youbi, A. Obaid, M. Gabal, Chem. Pap., 61 (2007) 370-375.
[198] N. Il'chenko, N. Pavlenko, L. Raevskaya, A. Bostan, Theor. Exp. Chem., 36 (2000) 48-53.
[199] A.V. Milkov, Earth Sci. Rev., 66 (2004) 183-197.
[200] T.S. Collett, AAPG Bulletin, 86 (2002) 1971-1992.
[201] . A. Labinger, J.E. Bercaw, Nature, 417 (2002) 507-514.
[202] J.R. Rostrup-Nielsen, Catal. Today, 63 (2000) 159-164.
[203] J.H. Lunsford, Catal. Today, 63 (2000) 165-174.
[204] T.V. Choudhary, E. Aksoylu, D.W. Goodman, Catal. Rev.-Sci. Eng., 45 (2003) 151.
[205] J.P. Van Hook, Catal. Rev.-Sci. Eng., 21 (1980) 1.
[206] D.L. Trimm, in: Methane Conversion, Proceedings of a Symposium on the Production of Fuels and Chemicals from Natural Gas, Elsevier, 1988, S. 39-50.
[207] M. Baerns, E.V. Kondratenko, in: Handbook of Heterogeneous catalysis, VCH, 2008, S. 3010-3023.
[208] H. Zanthoff, M. Baerns, Ind. Eng. Chem. Res., 29 (1991) 2-10.
[209] M. Baerns, K. van der Wiele, J.R.H. Ross, Catal. Today, 4 (1989) 471-494.
[210] J.S. Lee, S.T. Oyama, Catal. Rev., 30 (1988) 249.
[211] J. Feichter, U. Schurath, R. Zellner, Chem. unserer Zeit, 41 (2007) 138-150.
[212] D.T. Shindell, G. Faluvegi, D.M. Koch, G.A. Schmidt, N. Unger, S.E. Bauer, Science, 326 (2009) 716 -718.
[213] Y. Wang, J. Ren, Y. Wang, F. Zhang, X. Liu, Y. Guo, G. Lu, J. Phys. Chem. C, 112 (2008) 15293-15298.
[214] M. Sadakane, T. Horiuchi, N. Kato, K. Sasaki, W. Ueda, J. Solid. State Chem., 183 (2010) 1365-1371.
[215] L.Y. Dolgikh, N.I. Il'chenko, N.V. Pavlenko, Y.I. Pyatnitskii, L.A. Staraya, Theor. Exp. Chem., 38 (2002) 43-48.
[216] L. Lisi, G. Bagnasco, P. Ciambelli, S. De Rossi, P. Porta, G. Russo, M. Turco, J., 146 (1999) 176-183.
[217] J.L.G. Fierro, M.A. Pen[small tilde]a, L. González Tejuca, J. Mater. Sci., 23 (1988) 1018-1023.
[218] M. Crespin, W.K. Hall, J. Catal., 69 (1981) 359-370.
[219] A.A. Leontiou, A.K. Ladavos, P.J. Pomonis, Appl. Catal. A, 241 (2003) 133-141.
[220] K.S. Kim, S.B. Kim, W.J. Choi, T.O. Kim, H.S. Hahm, J. Ind. Eng. Chem., 7 (2001) 110-115.
[221] C.-Q. Chen, W. Li, C.-Y. Cao, W.-G. Song, Journal of Materials Chemistry, 20 (2010) 6968.
[222] G.L. Chiarello, I. Rossetti, L. Forni, Journal of Catalysis, 236 (2005) 251-261.
[223] L. Marchetti, L. Forni, Appl. Catal. B, 15 (1998) 179-187.
[224] J.C.W. Kuo, C.T. Kresge, R.E. Palermo, Catalysis Today, 4 (1989) 463-470.
[225] U. Zavyalova, M. Geske, R. Horn, G. Weinberg, W. Frandsen, M. Schuster, R. Schlögl, ChemCatChem, 3 (2011) 949-959.
[226] E.N. Voskresenskaya, L.I. Kurteeva, G.G. Pervyshina, A.G. Anshits, Catal. Today, 24 (1995) 277-279.
[227] G.M. Pajonk, T. Manzalji, Appl. Catal. A, 108 (1994) 41-51.
[228] H. Yamamoto, H.Y. Chu, M.T. Xu, C.L. Shi, J.H. Lunsford, J. Catal., 142 (1993) 325-336.
[229] K. Otsuka, T. Nakajima, J. Chem. Soc., Faraday Trans. I, 83 (1987) 1315-1321.
[230] K.-ichi Aika, T. Nishiyama, Chem. Commun., (1988) 70-71.
[231] C. Chen, Y. Xu, G. Li, X. Guo, Catal. Lett., 42 (1996) 149-153.

[232] S. Wang, Z.H. Zhu, Energy Fuels, 18 (2004) 1126-1139.
[233] N.-X. Lu, G. Fu, X. Xu, H.-L. Wan, J. Chem. Phys., 128 (2008) 034702.
[234] L.M. Aparicio, S.A. Rossini, D.G. Sanfilippo, J.E. Rekoske, A.A. Trevino, J.A. Dumesic, Ind. Eng. Chem. Res., 30 (1991) 2114-2123.
[235] S. Arndt, U. Simon, S. Heitz, A. Berthold, B. Beck, O. Görke, J.-D. Epping, T. Otremba, Y. Aksu, E. Irran, G. Laugel, M. Driess, H. Schubert, R. Schomäcker, Top. Catal., 54 (2011) 1266-1285.
[236] Y. Kuo, F. Behrendt, M. Lerch, Z. Phys. Chem., 221 (2007) 1017-1037.
[237] P. Myrach, N. Nilius, S.V. Levchenko, A. Gonchar, T. Risse, K. Dinse, L.A. Boatner, W. Frandsen, R. Horn, H. Freund, R. Schlögl, M. Scheffler, ChemCatChem, 2 (2010) 854-862.
[238] E.V. Kondratenko, M. Baerns, in: G. Ertl, H. Knözinger, F. Schüth, J. Weitkamp (Hrsg.), Handbook of Heterogeneous Catalysis, Wiley-VCH, 2008, S. 3010-3023.
[239] H.R. Godini, H. Arellano-Garcia, M. Omidkhah, R. Karimzadeh, G. Wozny, Ind. Eng. Chem. Res., 49 (2010) 3544-3552.
[240] Y. Zeng, Y.S. Lin, S.L. Swartz, J. Membr. Sci., 150 (1998) 87-98.
[241] K. Langfeld, E.V. Kondratenko, O. Görke, R. Schomäcker, Catal. Lett., (2011).
[242] K. Langfeld, R. Marschner, B. Frank, R. Schomäcker, ChemCatChem, 3 (2011) 1354-1358.
[243] H. Mimoun, A. Robine, S. Bonnaudet, C.J. Cameron, Appl. Catal., 58 (1990) 269-280.
[244] F.T. Akin, Y.S. Lin, Catal. Lett., 78 (2002) 239-242.
[245] P. Scherrer, Gött. Nachr., 2 (1918) 98-100.
[246] Inorganic Crystal Structure Database, URL: http://icsd.fkf.mpg.de/., .
[247] Y. Wang, Y. Takahashi, Y. Ohtsuka, J. Catal., 186 (1999) 160-168.
[248] M.C.J. Bradford, M.A. Vannice, Catal. Rev.-Sci. Eng., 41 (1999) 1-42.
[249] H.-Y. Wang, C.-T. Au, Catal. Lett., 38 (1996) 77-79.
[250] A. Mastalir, B. Frank, A. Szizybalski, H. Soerijanto, A. Deshpande, M. Niederberger, R. Schomäcker, R. Schlögl, T. Ressler, J. Catal., 230 (2005) 464-475.
[251] B. Frank, A. Dinse, O. Ovsitser, E.V. Kondratenko, R. Schomäcker, Appl. Catal. A, 323 (2007) 66-76.
[252] A. Wheeler, Academic Press, 1951, S. 249-327.